ROBERT RAAD

OVERLAPPED CDMA SYSTEM IN OPTICAL PACKET NETWORKS: RESOURCE ALLOCATION AND PERFORMANCE EVALUATION

Thèse de doctorat présentée
à la Faculté des études supérieures de l'Université Laval
dans le cadre du programme de doctorat en génie électrique
pour l'obtention du grade de Philosophiæ Doctor (Ph. D.)

DÉPARTEMENT DE GÉNIE ÉLECTRIQUE ET DE GÉNIE INFORMATIQUE
FACULTÉ DES SCIENCES ET DE GÉNIE
UNIVERSITÉ LAVAL
QUÉBEC

2009

To whom I love and I respect,
to my parents Joseph and Souheila,
brother and sisters Mounir, Lina and Rita,
to my fiancée Josiane Abdallah.

Résumé

Dans cette thèse, la performance du système CDMA à chevauchement optique (OV-CDMA) au niveau de la couche de contrôle d'accès au support (MAC) et l'allocation des ressources au niveau de la couche physique (PHY) sont étudiées. Notre but est d'apporter des améliorations pour des applications à débits multiples en répondant aux exigences de délai minimum tout en garantissant la qualité de service (QoS). Nous proposons de combiner les couches PHY et MAC par une nouvelle approche d'optimisation de performance qui consolide l'efficacité potentielle des réseaux optiques. Pour atteindre notre objectif, nous réalisons plusieurs étapes d'analyse.

Tout d'abord, nous suggérons le protocole S-ALOHA/OV-CDMA optique pour sa simplicité de contrôler les transmissions optiques au niveau de la couche liaison. Le débit du réseau, la latence de transmission et la stabilité du protocole sont ensuite évalués. L'évaluation prend en considération les caractéristiques physiques du système OV-CDMA, représentées par la probabilité de paquets bien reçus. Le système classique à traitement variable du gain (VPG) du CDMA, ciblé pour les applications à débits multiples, et le protocole MAC « round-robin » récepteur/émetteur (R^3T), initialement proposé pour les réseaux par paquets en CDMA optique sont également pris en compte. L'objectif est d'évaluer comparativement la performance du S-ALOHA/OV-CDMA en termes de l'immunité contre l'interférence d'accès multiple (MAI) et les variations des charges du trafic. Les résultats montrent que les performances peuvent varier en ce qui concerne le choix du taux de transmission et la puissance de transmission optique au niveau de la couche PHY.

Ainsi, nous proposons un schéma de répartition optimale des ressources pour allouer des taux de transmission à chevauchement optique et de puissance optique de transmission dans le système OV-CDMA comme des ressources devant être optimalement et équitablement réparties entre les utilisateurs qui sont regroupés dans des classes de différentes qualités de service. La condition d'optimalité est basée sur la maximisation de la capacité par utilisateur

de la couche PHY. De ce fait, un choix optimal des ressources physiques est maintenant possible, mais il n'est pas équitable entre les classes.

Par conséquent, pour améliorer la performance de la couche liaison tout en éliminant le problème d'absence d'équité, nous proposons comme une approche unifiée un schéma équitable et optimal pour l'allocation des ressources fondé sur la qualité de service pour des multiplexages temporels des réseaux par paquets en CDMA à chevauchement optique. Enfin, nous combinons cette dernière approche avec le protocole MAC dans un problème d'optimisation d'allocation équitable des ressources à contrainte de délai afin de mieux améliorer le débit du réseau et le délai au niveau de la couche liaison avec allocation équitable et optimale des ressources au niveau de la couche PHY.

Abstract

In this dissertation, the performance of the optical overlapped CDMA (OV-CDMA) system at the medium access control (MAC) layer of the optical packet network and the resource allocation at the physical (PHY) layer are investigated. Our purpose is to bring improvements for the multi-rate applications meeting minimum delay requirements and quality of service (QoS) guarantee. The proposal consists of combining the PHY and the MAC layers through a novel approach of performance optimization which consolidates the potential efficiency of optical networks. To achieve our objective, we carry out several steps of analysis.

First, we suggest optical S-ALOHA/OV-CDMA protocol for its simplicity to control the optical transmissions from the link layer. The network throughput, the transmission latency and the stability of the protocol are then evaluated. The evaluation takes into consideration the physical characteristics of the OV-CDMA system represented by the correct packet probability. The classical variable processing gain (VPG) CDMA system for multi-rate applications and the round robin receiver/transmitter (R^3T) MAC protocol, originally proposed for optical CDMA packet networks are also considered. The aim is to comparatively assay the performance of S-ALOHA/OV-CDMA in terms of multiple-access interference (MAI) immunity and traffic load variations. The results show that the performance can vary with respect to the choice of the transmission rate and the optical transmission power at the PHY layer.

Thus, we propose an optimal resource allocation scheme for allocating overlapping transmission rates and optical transmission powers in the OV-CDMA system as resources required to be fairly and optimally distributed among users clustered in different classes of QoS. The optimality condition is based on maximizing the PHY layer capacity per user. As a result, an optimal choice of the physical resources is now possible, but it is unfair among the classes.

Consequently, to improve the link layer performance while overwhelming the unfairness problem, we suggest a fair QoS-based optimal resource allocation scheme for time-slotted OV-CDMA packet networks as a unified approach. Finally, we combine the latter approach with the MAC protocol under delay-constraint fair resource allocation optimization problem in order to optimally improve the network's throughput and delay at the link layer with fair and optimal resource allocation at the PHY layer.

Acknowledgement

How much exhilarating the harvest season is? Indeed, it is the great moment which recapitulates years of hardworking. Obtaining a Ph.D. degree is a great honor to me. However, this achievement wouldn't have been realized without the considerable support and encouragement of my co-supervisor Dr. Elie Inaty and my supervisor Dr. Paul Fortier. I would like to thank them a lot for their valuable efforts and sacrifices. Also, I would like to express my gratitude to Dr. Hossam M. H. Shalaby for his appreciable collaboration.

I would like to thank Dr. Jean-Yves Chouinard and Dr. Martin Maier for accepting to be members of the jury. It is an honor to me to have them as evaluators for my thesis.

Of course my parents and my fiancée, they deserve a vast appreciation for their momentous role of consolidating me in the hard moments. Besides, my colleagues and friends are always in memory; I thank them all for their standing by me during the studying period, especially Mr. Ziad El-Sahn and Mr. Pascal Djiknavorian.

I would like to thank Laval University for sustaining me and satisfying me an appropriate environment for studying, references and logistic matters necessary for facilitating my research. Finally, I am grateful to the Natural Science and Engineering Research Council (NSERC) of Canada for supporting and funding this scientific research.

Table of Contents

List of Figures

Acronyms

- **CDMA**: Code Division Multiple Access
- **CSMA**: Carrier Sense Multiple Access
- **EHC**: Extended Hyperbolic Congruantial
- **FBG**: Fiber Bragg Grating
- **FET**: First Exit Time
- **FFH-CDMA**: Fast Frequency Hopping CDMA
- **FTTX**: Fiber-To-The-something (Curb, Home, etc.)
- **FSV**: Frequency Shifted Version
- **MAC**: Medium Access Control
- **MAI**: Multiple Access Interference
- **NET**: Network Layer
- **OCDMA**: Optical CDMA
- **O-FFH-CDMA**: Overlapped FFH-CDMA
- **OOK**: On-Off Keying
- **OV-CDMA**: Optical Overlapped CDMA
- **PG**: Processing Gain
- **PHY**: Physical Layer
- **QoS**: Quality of Service
- R^3T : Round Robin Receiver/Transmitter
- **S-ALOHA**: Slotted ALOHA
- **SIR**: Signal-To-Interference Ratio
- **SNR**: Signal-To-Noise Ratio
- **VPG-FFH-CDMA**: Variable Procession Gain FFH-CDMA

Chapter 1

Introduction

Optical code-division multiple-access (OCDMA) becomes a fundamental technique to exploit the large bandwidth of the optical fiber medium in optical networks [1]-[3]. First, it enables a large number of users to access the optical medium simultaneously by assigning them different codes. Second, by means of coding, OCDMA fairly partitions the bandwidth among the large number of users. Hence, the bandwidth allocation problems, imposed on other network types, can be solved. Since each user now gains benefit from the huge optical bandwidth offered by the optical medium, high-speed connectivity can be achieved. As a result, bandwidth-hungry applications with differentiated quality of service (QoS) can be easily supported [3]. Besides, other attractive characteristics are attributed to OCDMA systems. For example, it is flexible in such a way that new users can be added by simply assigning them new codes without additional circuitry. Also, because the number of OCDMA users is limited to codebook cardinality, it is sufficient to use simple protocols to control and manage the channel contention in OCDMA networks [2]-[4]. In real situations, however, the true number of active users at a particular instant is smaller than the available ones due to the multiple-access interference (MAI) effect [4] which limits the network capacity.

Reducing the MAI effect has impelled the researchers' interest toward effective coding techniques and system designs that can achieve a high autocorrelation property of a matching transmitter-receiver pair, and a very low cross-correlation property of non-matching pairs. Abundant research is found in the literature [5]-[17], attempting to solve the problem from the PHY layer perspective. The objective is always to improve the OCDMA network capacity and to enhance its potential of handling various communication services.

On the other hand, another perspective has been extensively proposed in the literature to tackle this issue through the use of higher layers to alleviate the distortion-prone effects of MAI. In particular, the focus is on the medium access control (MAC) layer owing to its critical role for providing error-free data to the other higher layers of the network, a factor which increases the capacity and the network performance [18]-[27]. This can be achieved by dynamically controlling the packet arrivals of the OCDMA users whenever the MAI level varies in the optical network; whereas, the error packets are managed by means of retransmission [23] or forward error correction [27]. The idea of using the MAC layer to improve the OCDMA network performance comes from the fact that the optical channel is intensity medium [3], [28]. Thus, controlling the burstiness of arrivals influences the MAI intensity level.

Thus, managing the MAI intensity has emerged the optical power control in OCDMA networks as an alternative perspective to improve the OCDMA performance again from the PHY layer. The intention behind is to optimally allocate optical transmission power to the users with multi-rate variation, subject to some constraint requirements for limiting MAI. Few analyses are however recorded in this area [58]-[61]. Most of them do not consider any optimal criterion for controlling transmission rate, simultaneously.

1.1 Motivation

Due to the massive growth in today's communication applications and services which entail high transmission bit rates, low delay and critical power management mechanism, OCDMA integrated-networks offer an ideal solution to cover such requirements [1]-[3]. In this trend, the overlapped OCDMA (OV-CDMA) system had been proposed [7]-[9], [13] to deal with this issue in terms of satisfying the highest transmission rate possible, by allowing the bit transmission to go beyond the physical limit of the optical channel, with no considerations for the upper layers of the protocol stack (Fig. 1.1).

The layered architecture of the protocol stack divides the overall networking task into layers and defines a hierarchy of services to be provided by the individual layers.

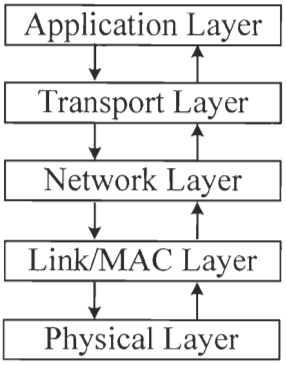

Fig. 1.1: The Protocol stack model.

The services at the layers are realized by designing protocols for the different layers. The architecture forbids direct communication between nonadjacent layers; communication between adjacent layers is limited to procedure calls and responses. This architecture has greatly simplified network design and led to the robust scalable protocols in the Internet [29]. However, this inflexibility and sub-optimality of the strict layered architecture can result in poor performance of the communication system [77]. This is due to the fact that a higher-layer protocol design only makes use of the services at the lower layers and is not concerned about the details of how the service is being provided. Thus, we believe that a kind of interrelation between protocol layers would bring improvement to the communication system.

In this trend, in order to assess the feasibility of the OV-CDMA system for a practical implementation, the system performance has to be investigated at the upper layers of the optical packet networks. Since the link layer forms the interface between the PHY layer and the other layers of the protocol stack, it has a critical task of reliably controlling the flow of correct information between the two sides, especially when a large number of users share the channel. To handle this issue, slotted MAC protocols ought to be imposed at the link layer. The reason is that in the OV-CDMA packet network, several packets are expected to be transmitted simultaneously, carrying an excess number of bits induced by the overlapping process. If the actual number of transmitting terminals exceeds the value of the maximum

channel capacity in terms of MAI, then all packets are destroyed. Hence, this suggests the use of a certain MAC protocol to resolve such contention in the shared media [28].

As a result, a new methodology of collaboration between the two layers (i.e. PHY and MAC) should be set up to respond to the proper services provided by the OV-CDMA system at the PHY layer while this system is operating in the packet access network.

1.2 Optical OV-CDMA System

In OCDMA system, each user is assigned a unique code sequence, called user's signature, used to encode its message signal. Normally, the user signature is independent of the information signal. The encoding process consists of multiplying the user's message signal by its corresponding signature [1], [2]. The resultant is a coded signal wide-spread in time domain, wavelength domain or in both time-wavelength domains as illustrated in Fig. 1.2.

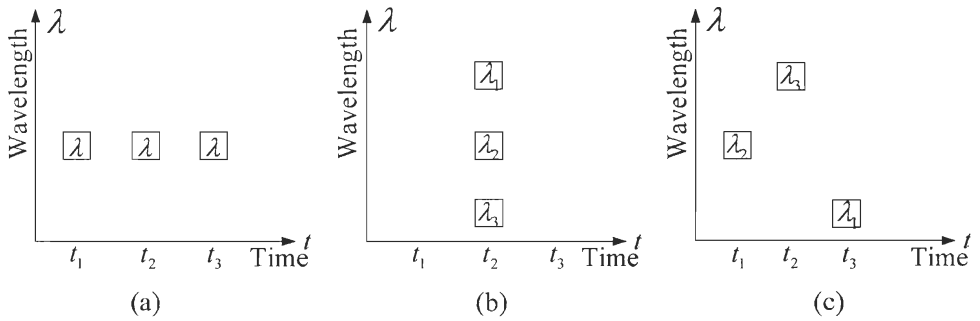

Fig. 1.2: Spreading sequence: (a) Time domain, (b) Wavelength domain, (c) Time-Wavelength domain.

The power of the information message is spread over the channel as a background noise usually known as MAI. As the number of the simultaneous users grows up above a certain limit, the spreading power of their signatures increases the background noise, hence the interference level, to certain threshold at which the OCDMA channel degrades rapidly. Therefore, the main source of noise is MAI, and often OCDMA is recognized as MAI-

limited system. The beat noise is considered mitigated. At the receiver, a reverse operation is applied to the received intended signal to decode the message signal. The desired signal power is aggregated over the decoded signal interval. This message signal is correctly detected when its power level is greater than the interference level, or the ratio of the signal power to interference is greater than a predefined threshold. The latter is known as signal-to-interference ratio (SIR) and it is considered as an important metric in evaluating the performance of such systems. OCDMA system design principle is represented in Fig. 1.3.

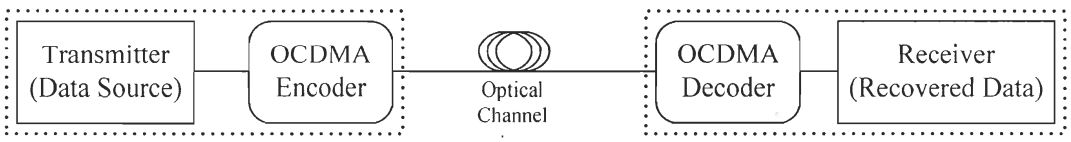

Fig. 1.3 OCDMA system design principle.

Although optimal coding techniques are employed to allow large number of users to utilize the optical channel and at the same time to reduce as much as possible MAI [5], [6], [9]-[15], the maximum achievable rates attained by those users are still restricted to the physical limit of the channel. OV-CDMA system [8] was suggested as a novel idea to permit variable data rates of different traffic classes to go beyond the nominal physical rates tolerable by the optical channel and the constraints imposed by the encoder/decoder set.

OV-CDMA is an OCDMA system that uses time-wavelength spreading as two-dimensional coding technique with a bit overlapping process. The electrical data bits modulate an optical broadband source at the encoder. Passing through a fiber Bragg grating (FBG) array, the optically modulated signal is spectrally and temporally sliced according to the two-dimensional coding pattern (also known as fast frequency hopping (FFH) pattern) of a given family of code [13]. The overlapping process is achieved simultaneously with the encoding process. Hence, the OV-CDMA system is also called optical overlapped fast frequency hopping CDMA (O-FFH-CDMA). Thus, the overlapping concept is that in passive OCDMA varying the bit duration will not affect the processing gain (PG) at the output of the optical encoder. Hence, for a fixed PG increasing the link transmission rate

beyond a given value, known as nominal rate, will produce a bit overlap at the encoder output. The boundary limit of bit overlap of a given class rate is defined as the cutoff rate which is the maximum achievable bit rate beyond the nominal rate. The concept of bit overlapping is illustrated in Fig. 1.4.

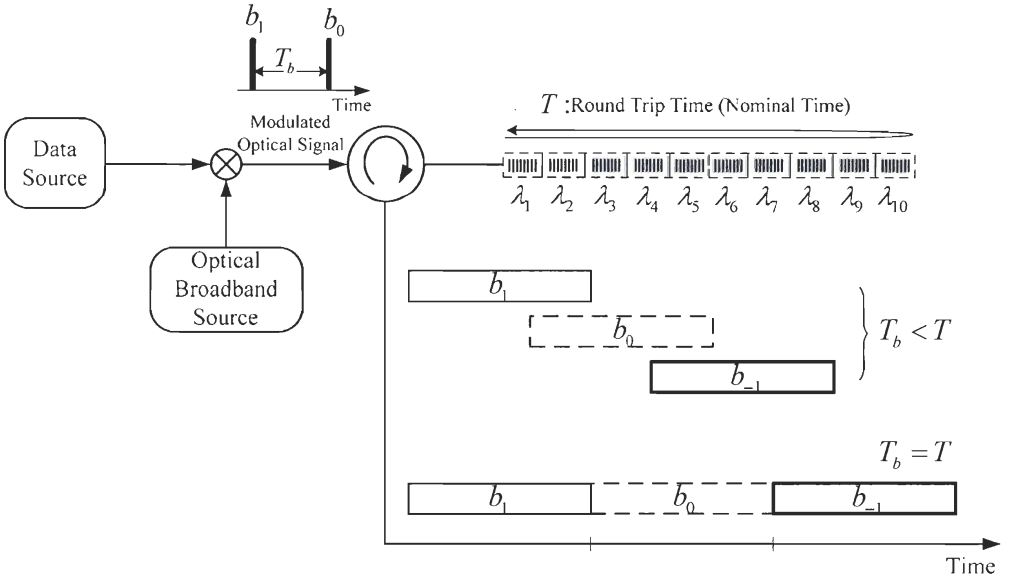

Fig. 1.4: Optical OV-CDMA system.

The array of FBG encodes the optical signal according to the FFH pattern. A nominal time (T) is required for a bit to pass the FBG. For example, two data bits are transmitted, and optically modulated by the optical broadband source as two optical pulses (b_0 and b_1). The delay time (T_b) between them is the same as before modulation. When the second optical pulse (b_1) is fed into the FBG right after the first (b_0) leaves it, the two optical pulses are adjacent to each other. In this case, the delay time between the two consecutive optical pulses is equal to the round trip time of the FBG (i.e. $T_b = T$). Now, when the second optical pulse (b_1) is fed into the FBG before the first (b_0) leaves it, the two optical pulses are overlapped in time (i.e. $T_b < T$). The optical encoded signal observed at the decoder of a

given receiver as multi-codes delayed according to the transmission rate of the source. Thus, a user transmitting at a rate greater than the nominal rate (i.e. $R > R_n$), introduces a bit overlap coefficient representing the number of overlapping chips between two consecutive bits.

Before stating the general problem of our dissertation, it is worth to go back to the literature to review what was proposed in this context.

1.3 Retrospective View

In this section, we present a literature review of some MAC protocols and their integration in CDMA systems in general and in OCDMA systems in particular. In addition, some approaches of resource allocations are also covered in this review.

Since its invention, S-ALOHA [30], [31] was seen an attractive protocol to cope with channel access management in the presence of multiple users competing to share their information over a local area network (LAN). However, the protocol efficiency in terms of channel throughput was inadequate as the networks' traffics grew [30]. In S-ALOHA protocol, the time axis is divided into time slots of length the size of a packet. When a user has packets ready for transmission during a given time slot, he has to wait for the beginning of the next time slot to transmit. If another user is attempting transmission simultaneously at the same time slot, then collision occurs. Consequently, both transmissions are lost, and the users have to wait for a random time for transmitting at the beginning of the next slots. The vulnerable period has duration of one time slot. Because the user has no knowledge whether the transmission will succeed or not, the occurrence of the successful transmission is treated as a random process. If we assume that a large number of users are accessing the communication channel simultaneously, then the number of transmissions is very large and the chance of successful transmission to take place is relatively rare. For Poisson-distributed transmitted arrivals, the system throughput is 36.8% of the total arrivals rate [30].

Since then, diverse versions of ALOHA-like protocols have come into existence as the so-called carrier sense multiple-access (CSMA) protocols to ameliorate the network performance by improving the protocol's throughput while keeping the average packet delay as low as possible [32]-[37]. Briefly, in CSMA protocols, the user first senses the channel before transmitting its packets. If the sensed channel is busy, the sensing user defers and reschedules its transmissions based on pre-defined strategies in order to avoid collision with the user accessing the channel simultaneously. On the other hand, if the sensed channel is idle, the sensing user proceeds on its transmission. Although the throughput improvement offered by CSMA protocols is significant [33], [37], this protocol is more complex.

S-ALOHA is thoroughly studied in the literature about random access packet networks. For instance, Carleial and Hellman [38] and Kleinrock and Lam [39] provided a trading relation among channel stability, throughput and average packet delay of an S-ALOHA random access system. They showed in their analysis that S-ALOHA is characterized by a bistable behavior, and the locus of the system stability is in the light-load region where the channel throughput is less than or equal to the maximum achievable throughput and the delay is fairly acceptable. Raychaudhuri [40] suggested the possibility of using CDMA with S-ALOHA with an appropriate choice of channel coding technique to achieve a higher throughput and preserve a low packet delay. By doing so, the stability region of the coded S-ALOHA has been enlarged, so that heavy loads can now be supported while the system is kept stable. Polydoros and Silvester [41] extended this work to develop a more generic model for the study of local throughput in slotted spread spectrum multiple-access (SSMA) networks where capture and retention mechanisms had been also elaborated. That is, they considered that the probability a receiver can capture the desired packet is not one anymore, as in [40], with the probability that the receiver will retain the captured packet with no remaining errors after correction. This was to render the model more realistic. By the evolution of modern mobile radio systems, high rate data services were achieved by evolutionary CDMA schemes whose management requires sets of protocols in order to make the systems feasible [42]. Because CDMA PHY layer provides services to the link layer may not be offered by other PHY layers [24] such as easily transmitting packets at variable data

rates [42], the S-ALOHA CDMA protocol was widely used in this context to carry out such task [32], [36], [43]-[45].

In addition, with the advancement of *all-optical* CDMA systems, OCDMA is viewed as a promising and challenging multiple-access techninque compared to the wavelength division multiple-access (WDMA) [2], [4], [19] for building high-speed optical fiber LANs accommodating the increasing demands on multimedia services (audio, video, image, file transfer, and so forth). Initially, most of the work done on this issue had focused on finding the best optimal codes which can minimize SIR and on designing encoder/decoder sets, as well, which can achieve the coding techniques [10]-[15], [22]. However, due to the dimension-growth of the optical network, more complexity has to be put on code design and on its corresponding hardware sets to reduce as much as possible the optical interference and noise while exchanging the data among the large number of users in the network. All these techniques are concerned with the PHY layer of the optical network. Nonetheless, powerful control mechanisms at higher layer to control the arrival of data bring additional improvement for the network performance even if non-optimal coding techniques are being employed at the PHY layer [28]. It had been shown in [28] that the throughput of OCDMA under heavy load can be improved by simple media access mechanisms that prevent interfering codewords form being sent simultaneously. S-ALOHA OCDMA has gained much attention to play the role of managing optical packet transmission among different users because of its simplicity and the ease of its implementation [23], [26], [28], [33], [37]. For example, Hsu and Li [26] analyzed the performance of S-ALOHA CDMA using code sequences with given orthogonality properties in both centralized and decentralized optical packet networks. Murali and Hughes [27] used S-ALOHA CDMA in broadcast (decentralized) optical network with forward error correction (FEC) in order to reduce the effect of large propagation delay on the network performance by immediate correction of erroneous packets at the receiver side. Lo *et al.* [33] compared S-ALOHA CDMA with channel sensing (CDMA/CS) and CDMA with both channel sensing and collision detection (CDMA-CS/CD) to a simple CSMA-CD. On the other hand, Stock and Surgent [18] performed a comparison between S-ALOHA CDMA and S-ALOHA WDMA and the results

indicated that the former one has superior performance. Moreover, Kamath *et al.* [28] and Shalaby [21] suggested alternative MAC protocols like ALOHA-CDMA with interference-avoidness/interference-detection and round-robin recever/transmitter protocols to deal with the packet access in optical networks. Finally, Xue *et al.* [23] have proposed a generalized approach for evaluating the performance of S-ALOHA CDMA in optical networks taking into account different nodal architectures.

Furthermore, the other perspective that yields improvement to CDMA networks is the resource allocation. This subject is widely exploited in CDMA networks especially in wireless networks [62], [64], [68]-[71]. Numerous proposals of optimization criteria were suggested for optimal recourse allocation either by maximizing the capacity in terms of the transmission rate, the number of users, or minimizing the sum of power, subject to minimum MAI and/or SNR as QoS requirements. Most of those proposals fall into a general framework of resource allocation and thus can be helpful tools in this context in OCDMA networks. For example, Yun and Messerschmitt [62] presented a power control algorithm which simultaneously minimizes interference and provides variable QoS contracts as functions of SNR for different traffic types in a CDMA system. If the QoS requirements of the sub-streams are too stringent, then the interference will be too great regardless of how much power is pumped. Also, by the absence of power control users dominate each others in terms of QoS demanded. Ramakrishna and Holtzman [64] proposed a mechanism for increasing the bit rate of nonreal-time (NRT) users while the priority is for real-time (RT) users. That was done by dynamically controlling the power and the spreading gain of NRT users. The throughput gain in terms of the transmission rate increase was then maximized, constrained to a given SIR and peak transmission power. The result was that the throughput gain was affected by the transmission scheme rather than the power. A similar approach can be found in Oh *et al.* [70] where they considered joint optimal transmission power and rate allocation strategy in multiservice CDMA networks. The objective was to maximize the spectral efficiency of the system by preserving the QoS of RT users while maximizing the best-effort aggregate throughput, in packets per second, of NRT users subject to constraints on peak transmission power and interference power. The rate was allocated by assigning an

optimal spreading gain that maximizes the signal-to-interference-plus-noise ratio (SINR). Then the optimal power was allocated so as the throughput was maximized and the peak power constraint was respected. However, this method was unfair among the users. Song and Wong [68] proposed to control the power and rate of multimedia traffic from an information-theoretic perspective. Moreover, Kwasinski and Farvardin [69] aimed at maximizing the number of real-time calls in CDMA networks by accepting a smooth increase of call distortion for a given frame loss rate target in mind to prevent channel-induced distortion. Finally, Zang *et al.* [71] investigated the optimal resource allocation for NRT traffic. The optimal allocation was based on the maximizing different forms of objective functions, based on Shannon capacity, subject to constraints on QoS, peak transmission power and received power. One objective function form was the total capacity. This form led to high resource allocation but it is unfair. Another form was the product of channel capacities. This form resulted in a proportionally fair allocation.

1.4 General Problem Description

We wish to explore the performance behavior of the optical OV-CDMA system which is proposed in [8] at the upper layers of the optical network and in particular at the link layer with regard to the PHY layer characteristics. The objective of that is to assess the feasibility of the proposed system when integrated in the optical packet access network, and to exploit its potential efficiency in improving such a network. First, we shall adopt S-ALOHA as a simple and easy-to-implement MAC protocol to control the arrival of bit-overlapping packet at the link layer. We have the following hypothesis.

We consider the optical OV-CDMA system as our case study. The optical system is represented at the PHY layer by its signal-to-interference ratio (SIR), derived in [8], [58] in terms of the transmission rate and the optical transmission power. In addition, the system can support multiple classes of users. Each class is characterized by its proper SIR as a required quality of service (QoS) to achieve correct transmissions. At the link layer, we consider the optical S-ALOHA/OV-CDMA as a simple solution to multiclass optical packet access

networks. This protocol is characterized by the overall network throughput and mean network delay.

Given a target QoS for each class of users, we are seeking the optimal number of bits that should be transmitted per packet of fixed time-slot in a slotted overlapped OCDMA packet network, and the optimal transmission intensity, which is directly controlled from the laser source, in order to optimize the packet network throughput under a certain delay constraint.

1) Find the relationship that governs the number of bits and the overlapping coefficient in the time-slotted system (i.e. find the new form of the transmission rate).
2) Find the average SIR experienced by a bit at a time-slot in terms of the overlapping transmission rate and the optical transmission power, as resources provisioned at the PHY layer.
3) Find the expression of the overall network throughput function at the link layer in terms of the PHY layer resources.
4) Find the expression of the average network delay encountered by the users at the link layer in terms of the PHY layer resources, as well.
5) Then, the following general optimization problem needs to be solved. Maximize the overall network throughput meeting a minimum average network delay constraint, QoS requirements, peak transmission powers constraint and bounded transmission rates of all classes.
6) The physical resource constraints should also satisfy certain criteria of optimality and fair distribution among the classes.

Thus, our proposed problem has to be solved following the general framework as illustrated in Fig. 1.5

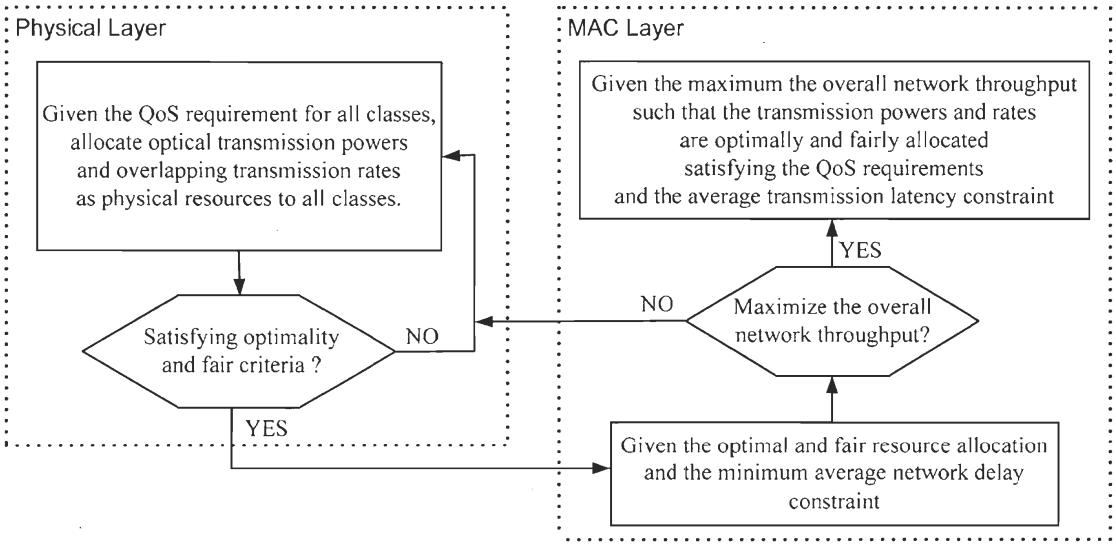

Fig. 1.5: General framework of the problem.

1.5 Thesis Organization

In addition to the introduction, the thesis comprises mainly three chapters and a conclusion. The chapters are devoted to the research work and its original results, while the conclusion briefly summarizes the basic achievements behind such work, and includes a prospective glance at several topics for future work. Besides the general introduction and the background presented herein, each chapter begins with an introductory part followed by a background knowledge part, which are pertinent to the particularity of the subject under discussion, and then the theory followed by the main results. This was done to preserve the coherence of the concept with its engendered results. Furthermore, the three chapters are presented in a sequential order involving several steps on the temporal line of research, so that each step is engendered on the light of the obtained results of the preceding one.

In Chapter 2, we propose a new multirate optical network based on a hybrid S-ALOHA/OV-CDMA system as an effective way of integrating multi-class traffic. The key issue in this proposal is to exploit the potential of the optical overlapped CDMA using fiber-Bragg grating when jointly used with the S-ALOHA protocol in a link layer. The newly

proposed system is modeled using a general Markov chain from which both the system throughput and the average packet delay are derived. The system stability passing through a general finite user model is also envisaged. The proposed system is then compared to the classical S-ALOHA/variable processing gain (VPG) CDMA system. Numerical results show that the former system outperforms the latter one especially at high transmission rates. In addition, stability measures demonstrate that the overlapped system tends to be more stable than the VPG system. Moreover, the system throughput and the average packet delay of optical S-ALOHA/FFH-CDMA are compared to that of optical round robin receiver transmitter [25] FFH-CDMA (R^3T/FFH-CDMA). It is shown that the S-ALOHA is better than the R^3T when the user's activity and offered load are high, while the R^3T is better for smaller values. At moderate offered load, both protocols can be competitive in terms of the system throughput with the advantage is for the R^3T protocol. However, R^3T suffers a higher delay mainly because of the presence of additional modes. Finally, the overlapped OCDMA system always outperforms the variable processing gain (VPG) OCDMA system regardless the MAC protocol used [46]-[49].

Chapter 3 addresses the problem of resource allocation in a multiservice optical network based on an OV-OCDMA system. A joint transmission power and overlapping coefficient (transmission rate) allocation strategy is provided via the solution of a constrained convex quadratic optimization problem. The solution of this problem maximizes the aggregate throughput subject to peak lasers transmission power constraints. The optimization problem is solved in a closed form, and the resource allocation strategy is simple to implement in an optical network. Simulation results confirm a total agreement between the derived analytical solution and the one obtained using a numerical search method. In addition, analytical and numerical results show that the proposed resource allocation strategy can offer substantial improvement in the system throughput [50], [51].

In Chapter 4 we develop a fair resource allocation scheme for a multi-class time-slotted optical overlapped code-division multiple-access (OV-CDMA) network. The resource management scheme is fair in the sense that the users have their power and rate allotted according to their quality of service (QoS) requirements. In addition, no class of users can

dominate over the other classes. A unified framework for the resource controlling scheme is proposed. It consists of simply finding a single control parameter based on which the optimal transmission rate and power are obtained for every class of users. Analytical results show that the maximum transmission rate for a given class of users is only achievable when the users in that class are transmitting with the highest possible laser transmission power. In addition, we have demonstrated that the optimal transmission rates can be obtained via the solution of the rate characteristic polynomial. It is shown that our proposed scheme provides a substantial improvement in the system capacity while preserving the required fairness criteria. Finally, the proposed scheme is employed to optimize the performance of MAC layer of the time-slotted OV-CDMA-based packet network while preserving the fairness and optimality of the resources allocated to the OV-CDMA users. Thus, a general delay-constraint optimization problem is formulated to maximize the network throughput subject to the average network delay, the fairness parameter and the optimal transmission rate constraints. Then, a numerical assessment is performed under S-ALOHA/OV-CDMA and R^3T/OV-CDMA protocols with binomial arrival distribution. The results indicate that delay-constraint optimization problem attains a feasible solution whereby the different MAC protocols have comparable performance [52], [53].

Chapter 5 summarizes the contributions and suggests further perspective and development to bring additional improvement and practicability to the optical overlapped CDMA system.

Chapter 2

Optical S-ALOHA/CDMA Systems for Multirate Applications: Architecture, Performance Evaluation, and System Stability

2.1 Introduction

Owing to the rapid progress in fiber-optic technology, optical CDMA utilizing FBG is gaining more interest in the creation of all-optical communication systems for integrating heterogeneous traffic sharing a single broadband optical channel with a multiplicity of quality of services (QoS) and traffic requirements [7], [9], [21]. In addition, the bursty characteristics of high speed data traffic in optical LANs should yield benefits for CDMA technologies that are capable of allocating a high number of simultaneous resources in a decentralized way while increasing the system throughput and decreasing the average packet delay. S-ALOHA techniques could fulfill these requirements when integrated with the newly proposed optical O-FFH-CDMA system [8].

Although there is a lot of research in the field of optical CDMA that has been done until now, most of it has focused on the PHY layer [5], [8], [9], [54]. This fact also applies to the works that have been conducted in the area of multirate OCDMA. A multirate optical FFH-CDMA system using variable PG has been proposed in [7]. The intention was to guarantee the one-to-one correspondence between the PG and the source transmission rate. The drawback of this system is the drastic decrease in the transmitted signal power especially for higher rate users for which the PG becomes very small. The solution to this problem is the use of power control. On the other hand, in [5], [6] multi-length frequency hopping codes are considered. Using these codes, rate and QoS are now dynamically matched to users' needs. The cutoff rate of the system is still limited by the physical constraints of the codes. Lately,

we have considered the overlapped CDMA (OV-CDMA) system [8] where we have shown that it is possible to increase a class bit rate beyond the nominal rate without decreasing the PG of the desired user or allowing any time delay between the data symbols.

Many researches have been conducted on S-ALOHA and random access CDMA [9], [39], [40]. Nevertheless, jointly used with OCDMA, random access packet-switching becomes a challenging issue [20], [21], [23], [55], to cope with the increasing packet-type demand with large population, shorter message-delay delivery and minimum packet-rejection probability. In [20], [55], protocols for high speed fiber optic local area network using passive star topology were proposed. New optical CDMA access protocols with and without pretransmission coordination were studied in [21]. On the other hand, Xue *et al.* [23] were concerned with two optical CDMA random access schemes that support tunable transmitter/fixed receiver and fixed transmitter/tunable receiver, respectively. In our research, we propose a new hybrid system that combines a variable-transmission-rate optical O-FFH-CDMA system [8] with the S-ALOHA protocol (S-ALOHA/O-FFH-CDMA) as a novel and simple scheme of achieving multi-user and multirate capability in a decentralized optical CDMA packet networks. In particular, variable transmission rate is achieved by increasing the bit rate beyond the nominal limits while keeping the processing gain (PG) and the time slot duration unchanged. This yields overlapping among bits in a single time slot. Thus varying the amount of overlapping bits can vary the transmission rate.

The remaining of this chapter is structured as follows. Section 2.2 introduces the system model, which employs the discrete time Markov chain describing the system states. SIR is derived in Section 2.3. Section 2.4 presents the performance evaluation of the system. Stability measures are discussed in Section 2.5. A performance comparison between S-ALOHA and R^3T protocols when deployed to control the optical FFH-CDMA systems is established in section 2.6. Numerical results provided by simulation are covered in Section 2.7. Finally, concluding remarks end this chapter in Section 2.8.

2.2 System Model

We consider an optical FFH-CDMA communication network that supports K terminals, which share the same optical medium in a star architecture [9]. The encoding and decoding are achieved passively using a sequence of fiber Bragg gratings. The gratings will spectrally and temporally slice an incoming broadband pulse into several components equally spaced at chip intervals T_c [9]. The chip duration, and the number of gratings will establish the nominal bit rate of the system, *i.e.* the round trip time of light, from a given transmitted bit, to be totally reflected from the encoder. This nominal bit duration in a structure of G gratings is given by T_n, where G is the PG. The corresponding nominal rate is $R_n = 1/T_n = 1/GT_c$.

Using the above mentioned passive network, we propose a hybrid S-ALOHA/FFH-CDMA optical packet network in which each user is assigned a unique code, which is characterized by zero auto-correlation property using a frequency shifted version (FSV) proposed in [9], and a cross-correlation between any two different codewords of at most one. Subsequently, up to K users can transmit simultaneously K packets in a given time slot.

The traffic model used in this work is the general Markov chain in which the traffic is distributed according to the user's activity as shown in Fig. 2.1. It is called a general arrival model.

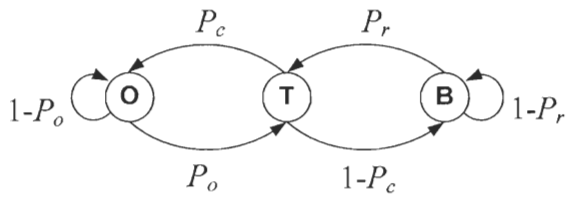

Fig. 2.1: Traffic model.

Each of the K terminals can be in one of the three operational modes at a time, origination mode, transmission mode, or backlog mode. The user in the origination mode generates and transmits a new packet at the beginning of the next time slot with a probability

P_o. The user enters the backlog mode when an attempt to transmit a new packet fails. This event occurs with probability $1-P_c$, where P_c is the correct packet probability of the corresponding system. The retransmissions of backlogged packet occur in any given time slot with probability P_r. In a backlogged mode, the blocked terminal cannot generate new packets until the backlogged packet is received correctly. According to the variations of P_o and P_r we obtain the following cases:

1) For $P_r = P_o = p$, the arrivals distribution can be approximated either by a binomial distribution if the number of users in the system, K, is finite or by a Poisson distribution if K is very high. For both distributions, the average offered load is approximated by $R = K \cdot P_o$.
2) For $P_r > P_o$, it is very difficult to obtain a closed form approximation for the arrivals distribution. Thus, we use the general Markov model to track the flow of packets in the system based on the user's activity without any approximation. In this case the offered load is at its maximum since it includes the fraction of the retransmitted packets. Note that 1) is considered as a particular case of 2).
3) For $P_r < P_o$, the interpretation is similar to case 2); however, the offered load is diminishing, and there is a high probability that the system queue will overflow and some backlogged packets will be lost. It is not a practical case especially in ultra high-speed optical systems.

For practical implementations, we assume that the priority of retransmitting the backlogged packets is always higher than that of generating new packets and the traffic distribution is based on the current users' activities, so it is general. Henceforth, case 2) is adopted in our analysis.

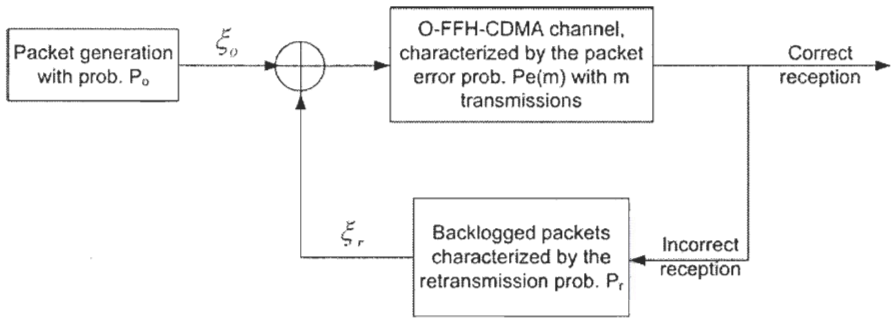

Fig. 2.2: Optical S-ALOHA/O-FFH-CDMA system model.

Fig. 2.2 represents the model of the proposed optical S-ALOHA/O-FFH-CDMA system. The streams of composite arrivals of this system consist of ξ_o newly generated packets plus ξ_r retransmitted packets.

The statistical behavior of the terminal can be described using a general discrete Markov chain [40]. The system state represents the number of backlogged terminals n.

Before continuing the analysis, let us impose some restrictions which help simplify the mathematical evaluations and improve the clarity of the problem under consideration. We assume 1) a synchronous system and discrete rate variation, 2) a single class system, and 3) unit transmission power for all the users.

In this chapter the transmission rate of the terminals R_s is allowed to be greater than R_n according to two different methods as explained below.

2.2.1 S-ALOHA/VPG-FFH-CDMA System

Assume a fixed packet-time duration of $T_p = LT_n = LGT_c$ where L is the nominal packet length. In this system, the variable transmission rate is accomplished by varying the processing gain G_V in such a way that increasing the transmission rate by a factor of $\alpha_V \geq 1$

allows the reduction of spreading factor by the same amount $G_V = G/\alpha_V$ [7]. The bit rate in this case is given by

$$R_s = \alpha_V R_n \ (bits/\sec) \tag{2.1}$$

In a packet network, $X_b^{(V)} = \lfloor \alpha_V L \rfloor$ bits are allocated in a time slot instead of L as shown in Fig. 2.3, where $\lfloor x \rfloor$ is the highest integer less than x. Then, the new transmission rate becomes

$$R_s = \frac{X_b^{(V)}}{L} R_n \ (bits/\sec) \tag{2.2}$$

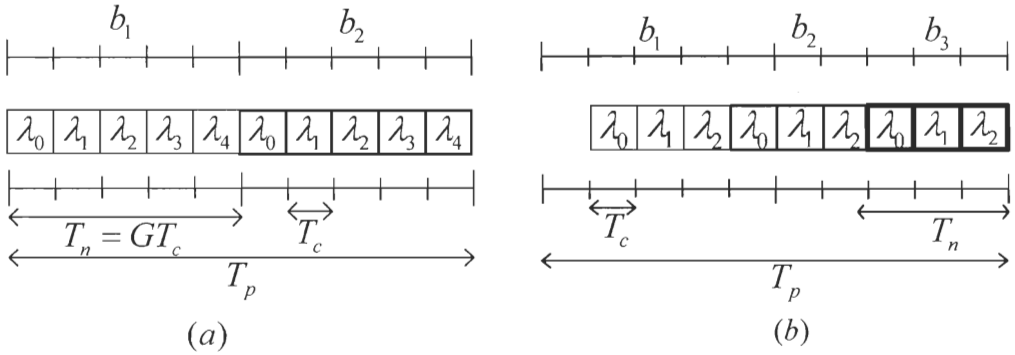

Fig. 2.3: Optical S-ALOHA/VPG-FFH-CDMA packet model of a single user in a given packet time slot. (a) $G_V = 5$. (b) $G_V = 3$.

In Fig. 2.3(a), we present a case study where $G_V = 5$ and $L = 2$, which means the nominal rate is two bits per packet. On the other hand, in Fig. 2.3(b), we have decreased the PG to $G_V = 3$ (which means $\alpha_V = 5/3$) in order to increase the transmission rate to three bits per packet.

2.2.2 S-ALOHA/O-FFH-CDMA System

In [8], we have shown that due to the linearity of the encoder-decoder set, multi-bits will be coded and transmitted when the data rate increases beyond R_n as shown in Fig. 2.4. At the receiver end, the decoder observes practically multicode, which are delayed according to the transmission rate of the source.

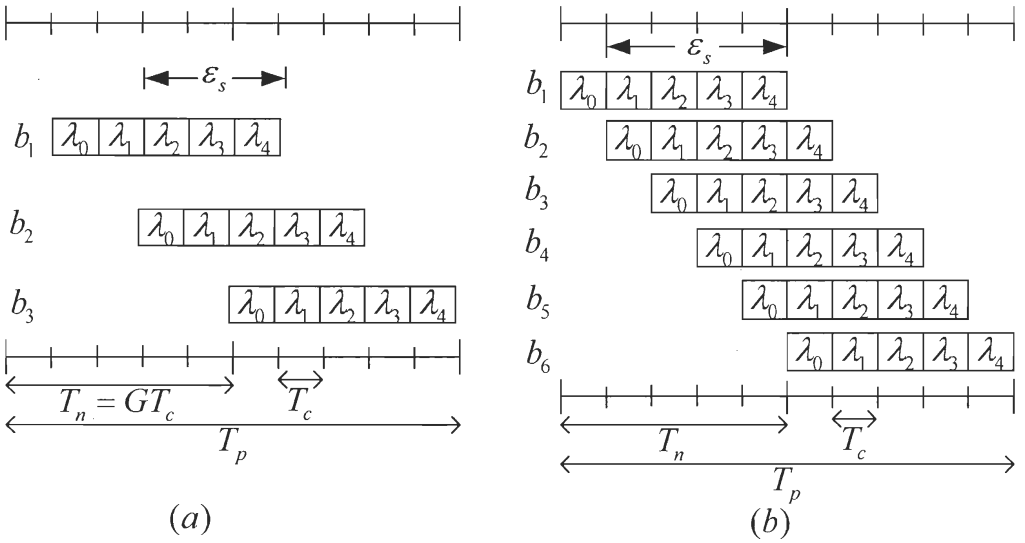

Fig. 2.4: Optical S-ALOHA/O-FFH-CDMA packet model of a single user in a given time slot. (a) $\varepsilon_s = 3$, (b) $\varepsilon_s = 4$.

Accordingly, in the S-ALOHA/O-FFH-CDMA, to increase the number of bits per packet of fixed length L, we increase the source transmission rate above the nominal rate without decreasing the PG as in the previous system. When a terminal transmits using a rate $R_s > R_n$, it introduces a bit overlap coefficient ε_s, which represents the number of overlapping chips between two consecutive bits [8]. Accordingly the new bit rate is related to R_n throughout the following equation

$$R_s = \frac{G}{G - \varepsilon_s} R_n \tag{2.3}$$

Let ε_s be the overlapping coefficient, and $X_b^{(O)}$ to be the total number of overlapped bits in a packet time slot.

Lemma 2.1: *Given a terminal k with* (G, ε_s) *transmitting data using the S-ALOHA/O-FFH-CDMA system with a nominal packet length L. The total number of transmitted bits per time slot is given by*

$$X_b^{(O)} = \left\lfloor \frac{LG - \varepsilon_s}{G - \varepsilon_s} \right\rfloor \tag{2.4}$$

Proof: For an overlapped packet to be complete for transmission, the following inequality must be satisfied:

$$\varepsilon_s + \underbrace{(G-\varepsilon_s)+\ldots+(G-\varepsilon_s)}_{X_b^{(O)}\,times} \le LG \tag{2.5}$$

$$X_b^{(O)} \le \frac{LG - \varepsilon_s}{G - \varepsilon_s} \tag{2.6}$$

Thus, (2.6) yields (2.4) which completes the poof. ■

Consequently the rate in a packet network will be

$$R_s = \frac{X_b^{(O)}}{L} R_n \left(bits/\sec\right) \tag{2.7}$$

Fig. 2.4 illustrates an example of the overlapping process in a packet time slot. In this example, the packet length is $L = 2$, and the PG is $G = 5$. If the transmission rate is the nominal rate, the packet format is as shown in Fig. 2.3(a), which means $\varepsilon_s = 0$ and the transmission rate is two bits per packet. When the overlapped coefficient is increased to $\varepsilon_s = 3$ as shown in Fig. 2.4(a), the transmission rate is increased to three bits per packet. On

the other hand, Fig. 2.4(b) shows the case where $\varepsilon_s = 4$. Accordingly, the transmission rate is six bits per packet.

The relation between the reduction factor α_V of the S-ALOHA/VPG-FFH-CDMA system and the overlapping coefficient ε_s of the S-ALOHA/O-FFH-CDMA system can be easily obtained by equating (2.2) and (2.7) to obtain

$$\alpha_V = \frac{G - \frac{\varepsilon_s}{L}}{G - \varepsilon_s} \tag{2.8}$$

2.3 Signal-to-Interference Ratio (SIR)

In this section, we derive the SIR for both systems. In general, we can write the SIR as follows

$$\mathrm{SIR}(K) = \frac{G^2}{\sum_{k=1}^{K-1} \sigma_{I_k}^2 + \sigma_n^2} \tag{2.9}$$

where $\sigma_{I_k}^2$ is the interference power from the k^{th} terminal and σ_n^2 is the additive white Gaussian noise (AWGN) power. The SIR for both systems differ in $\sigma_{I_k}^2$ and the PG.

2.3.1 S-ALOHA/VPG-FFH-CDMA System

Assume class-s users with transmission rate R_s and equivalent PG G_V. Also assuming equally probable data, we can write the interference power [7] as follows

$$\sigma_{I_k}^2 = \sum_{q=0}^{G_V-1} \left[H_k^2(0,q) + H_k^2(q, G_V) \right] \tag{2.10}$$

where

$$H_k(a,b)=\sum_{j=a}^{b-1} h\left(a_{j-q_v}^k, a_j^0\right) \tag{2.11}$$

is the discrete-time partial-period Hamming cross-correlation function of the k^{th} interferer [7]. In addition, $h(.)$[1] is the Hamming function [7]. The sequences $a_{j-q_v}^k$ and a_j^0 are numbers representing frequencies of the k^{th} interferer and the desired user, respectively. $\left(j-q_v^{(i)}\right)$ is evaluated modulo G. Notice that the interference power is equal for every bit in the packet time slot. Thus, we can write

$$\mathrm{SIR}^{(i)}(K)=\frac{G^2/\alpha_V^2}{\sum_{k=1}^{K-1}\sigma_{I_k}^2+\sigma_n^2} \quad \forall\, 1\le i\le X_b^{(V)} \tag{2.12}$$

where α_V is the reduction factor given in (2.1).

2.3.2 S-ALOHA/O-FFH-CDMA System

In the S-ALOHA/O-FFH-CDMA system, the problem is much more complex due to the fact that not every bit in the packet time slot will have the same SIR as shown in Fig. 2.5. Therefore, the SIR at the i^{th} bit position in the time slot is given by

$$\mathrm{SIR}^{(i)}(K)=\frac{G^2}{\sum_{k=1}^{K-1}\sigma_{I_k}^2(i)+\sigma_n^2} \quad \forall\, 1\le i\le X_b^{(O)} \tag{2.13}$$

where $X_b^{(O)}$ is given by (2.4) and $\sigma_{I_k}^2(i)$ can be computed as follows. Let

---

[1] $h(a,b)=\begin{cases}0, & a\neq b\\ 1, & a=b\end{cases}$

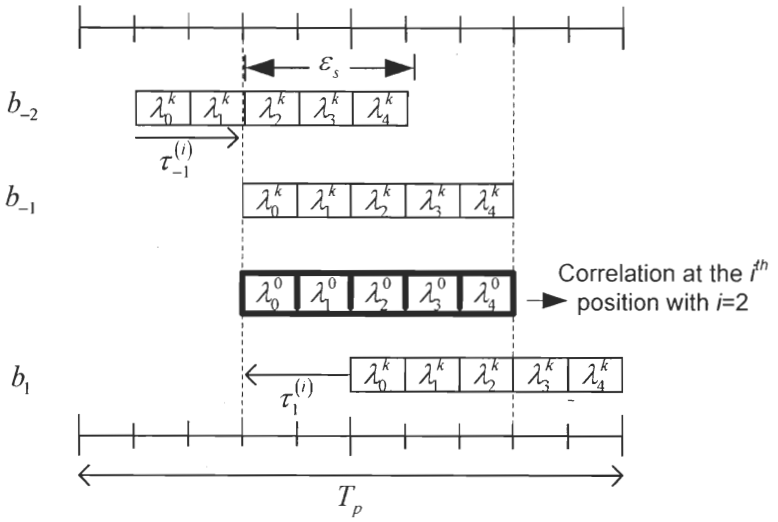

Fig. 2.5: Interference from user K on the desired user due to overlapping.

$$X_r = \lceil \varepsilon_s / (G - \varepsilon_s) \rceil \tag{2.14}$$

where $\lceil x \rceil$ is the smallest integer greater than x, we can notice that the problem can be divided into two parts:

1) $X_b^{(O)} - 2X_r \le 0$:

$$\sigma_{I_k}^2(i) = \begin{cases} \sum_{\nu=-i}^{-1} H_\nu^2\left(0, q_\nu^{(i)}\right) + \sum_{\nu=0}^{X_r} H_\nu^2\left(q_\nu^{(i)}, G\right), & 0 \le i \le X_b^{(O)} - X_r - 1 \\ \sum_{\nu=-i}^{-1} H_\nu^2\left(0, q_\nu^{(i)}\right) + \sum_{\nu=0}^{X_b^{(O)}-i-1} H_\nu^2\left(q_\nu^{(i)}, G\right), & X_b^{(O)} - X_r \le i \le X_r - 1 \\ \sum_{\nu=-X_r}^{-1} H_\nu^2\left(0, q_\nu^{(i)}\right) + \sum_{\nu=0}^{X_b^{(O)}-i-1} H_\nu^2\left(q_\nu^{(i)}, G\right), & X_r \le i \le X_b^{(O)} - 1 \end{cases} \tag{2.15}$$

where $q_\nu^{(i)} = \tau_\nu^{(i)} / T_c$ and $\tau_\nu^{(i)}$ is the time delay with respect to the i^{th} bit in the packet.

2) $X_b^{(O)} - 2X_r > 0$:

$$\sigma_{I_k}^2(i)=\begin{cases}\sum_{\nu=-i}^{-1} H_\nu^2\left(0,q_\nu^{(i)}\right)+\sum_{\nu=0}^{X_r} H_\nu^2\left(q_\nu^{(i)},G\right), & 0\le i\le X_r-1\\ \sum_{\nu=-X_r}^{-1} H_\nu^2\left(0,q_\nu^{(i)}\right)+\sum_{\nu=0}^{X_r} H_\nu^2\left(q_\nu^{(i)},G\right), & X_r\le i\le X_b^{(O)}-X_r-1\\ \sum_{\nu=-X_r}^{-1} H_\nu^2\left(0,q_\nu^{(i)}\right)+\sum_{\nu=0}^{X_b^{(o)}-i-1} H_\nu^2\left(q_\nu^{(i)},G\right), & X_b^{(O)}-X_r\le i\le X_b^{(O)}-1\end{cases} \tag{2.16}$$

2.4 Performance Evaluation

In this section, we derive the correct packet probability of systems, the network throughput and the average delay.

2.4.1 Correct Packet Probability

Usually the form of the bit error probability depends on the coding and the detection techniques. If a Gaussian hypothesis is used to model the interference, then the probability of bit error in a time slot when there are K simultaneous active terminals, using a simple On-Off Keying (OOK) modulation and direct detection, is related to the system's signal-to-interference ratio (SIR) using the following equation

$$P_b(i,K)=Q\left(\frac{1}{2}\sqrt{SIR^{(i)}(K)}\right) \tag{2.17}$$

where $SIR^{(i)}(K)$ is given in (2.12) or in (2.13).

2.4.1.1 S-ALOHA/VPG-FFH-CDMA System

Due to the fact that the bit error probability is equal for every bit in the packet, the probability of successfully receiving a packet is

$$P_c(K)=\left[1-P_b(i,K)\right]^{X_b^{(i)}} \tag{2.18}$$

where $P_b(i,K)$ is given in (2.17).

2.4.1.2 S-ALOHA/O-FFH-CDMA System

On the other hand, for the S-ALOHA/O-FFH-CDMA system, the bit error probability is not equal for every bit in the packet. It depends on the bit position *i* as revealed in (2.15) and (2.16). Thus we can write

$$P_c(K) = \prod_{i=0}^{X_b^{(O)}-1} \left[1 - P_b(i,K)\right] \tag{2.19}$$

2.4.2 System Throughput and Average Packet Delay

Let $P = [P_{nm}]$ be the transition matrix, where P_{nm} is the one step transition probability from state n to state m. Consider that P_{nm} is the probability that m backlogged users will be present in the next state given that n are present in the current state. It is given by

$$P_{nm} = \Pr\{x(t+1) = m \mid x(t) = n\} \tag{2.20}$$

For random access CDMA, transition can take place in a number of ways since there can be more than one successful transmission per time slot. The transition from state *n* to state *m* is determined by the difference between the number of unsuccessful new transmission $UNTX$ and successful retransmission $SRTX$, i.e. when $SRTX$ exceeds $UNTX$ by $(n-m)$ for $n \geq m$ or $UNTX$ exceeds $SRTX$ by $(m-n)$ for $m \geq n$. Let $NTX = \xi_o$ be the number of new transmissions and $RTX = \xi_r$ be the number of retransmissions. Let $b(\delta, \psi, p)$, denote the binomial distribution. It characterizes the total number of all possible ψ successes in any order given δ attempts and p is the probability of success. Then the joint probability distribution of $SRTX$ and $UNTX$ given n users in the backlogged mode can be written as

$$\Pr\{SRTX = k, UNTX = l \mid x(t) = n\}$$
$$= \sum_{\substack{\xi_o = l \\ 0 \le l \le K-n \\ 0 \le k \le n}}^{K-n} \sum_{\xi_r = k}^{n} \left\{ b\left[l, \xi_o, P_E\left(\xi_o + \xi_r\right)\right] \cdot b\left[\xi_o, K-n, P_o\right] \cdot b\left[k, \xi_r, P_C\left(\xi_o + \xi_r\right)\right] \cdot b\left[\xi_r, n, P_r\right] \right\} \tag{2.21}$$

where $b(\delta, \psi, p)$ is given by

$$b(\delta, \psi, p) \triangleq \binom{\psi}{\delta} p^{\delta} (1-p)^{\psi-\delta} \tag{2.22}$$

and $P_C(\cdot)$ is the correct packet probability and given by (2.18) and (2.19). In addition, $P_E(\cdot) = 1 - P_C(\cdot)$, which represents the packet error probability. Hence the steady-state transition probability is calculated as follows

$$P_{nm} = \begin{cases} \sum_{j=0}^{\min(n, K-m)} \Pr\left\{ \begin{matrix} SRTX = j, \\ UNTX = m - n + j \mid x(t) = n \end{matrix} \right\}, & m \ge n \\ \sum_{j=0}^{\min(m, K-n)} \Pr\left\{ \begin{matrix} SRTX = n - m + j, \\ UNTX = j \mid x(t) = n \end{matrix} \right\}, & m \le n \end{cases} \tag{2.23}$$

The long-term state occupancy probability $\mu(n)$ is given by the solution of:

$$\mu^T = \mu^T P, \ \mu^T = \left[\mu(0), ..., \mu(n)\right], \ \sum_{n=0}^{K} \mu(n) = 1 \tag{2.24}$$

The method to solve (2.24) is to find the eigenvalues of P^T and their corresponding eigenvectors. By sorting the $(K+1)$ eigenvalues in ascending order, the desired eigenvector is the one whose index is the index of the highest eigenvalue. Then, the long-term state probability vector will correspond to the desired eigenvector divided by the sum of their entries.

Thus, the probability of success can be seen as a binomial distribution by which S packets are received successfully given M attempted transmissions in a given time slot. This leads to the following:

$$\Pr\left(S = s \mid M = m\right) = b\left[s, m, P_c\left(m\right)\right] \tag{2.25}$$

The steady state composite arrival distribution given that there are n backlogged users in the system and m backlogged users in the next time slot is given by

$$\begin{aligned} f_M(m \mid x = n) &= \sum_{j=\max(m-n,0)}^{\min(m,K-n)} \Pr\left(NTX = j, RTX = m - j \mid x = n\right) \\ &= \sum_{j=\max(m-n,0)}^{\min(m,K-n)} b(j, K - n, P_o) \times b(m - j, n, P_r) \end{aligned} \tag{2.26}$$

The throughput in packet per time slot, θ, is defined as the expected number of successful transmission per time slot

$$\begin{aligned} \theta &= E\{S\} = E\{E\{S \mid M\}\} \\ &= E\left[\sum_{s=0}^{K} s \binom{M}{s} P_c^s \left(1 - P_c\right)^{M-s}\right] \\ &= \sum_{m=1}^{K} m P_C(m) \left[\sum_{n=0}^{K} f_M(m \mid n) \mu(n)\right] \end{aligned} \tag{2.27}$$

The offered traffic can be estimated by

$$R = \left(K - \overline{n}\right) P_o + \overline{n} P_r \tag{2.28}$$

where $\overline{n}$ is the expected backlog or the average system state, and is given by

$$\overline{n} = \sum_{n=0}^{K} n \mu\left(n\right) \tag{2.29}$$

The steady state delay according to Little's theorem can be written as

$$D = \overline{n} / \theta \tag{2.30}$$

2.5 Stability Measures

Stability analysis has considerable interest for assessing the performance of ALOHA systems [38]-[40], [43]. According to Kleinrock and Lam [39], a stable S-ALOHA system exists when the channel load line intersects non-tangentially the equilibrium throughput-delay contour by a single point called system operating point $(\theta_o, \overline{n}_o)$; otherwise, the system is unstable. Then, the authors introduce the stability measure as the average *first exit time* (FET) into the unsafe region where the average number of backlogged users $\overline{n}$ starts increasing exceeding a given threshold $\overline{n}_o$ and the system's throughput begins vanishing, assuming the system is initiated with no backlogged users. In [38], system stability is evaluated in terms of the expected drift in state n, which represents the expected deviation of the system state from its current state to any other state. Thus, the system remains in its current state, and when changing, it moves to lower states avoiding saturation. Therefore, the expected drift is the measure of the dynamics of the S-ALOHA system and it is defined as:

$$d(n) = \sum_{m=0}^{K} (m-n) P_{nm} \tag{2.31}$$

A stable system has a global stable equilibrium point at state $n = \overline{n}_o$ with zero drift and a monotonically decreasing slope. In this case, the system has an acceptable throughput rate and a tolerable time delay. The equilibrium points with zero drift and monotonically increasing slope make the system unstable. The system that has more than one equilibrium point is a bi-stable system [38].

It is shown by simulation (next section) that it is computationally very difficult to estimate the relative degree of stability between the overlapped and the VPG systems by using the expected drift analysis. FET stability measure offers a clear idea about the useful

operating time of both systems in the safe region before exiting to the unsafe region with much lower computational complexity.

Let the random variable T_i be the number of transitions the channel backlog $\overline{n}$ goes through before it surpasses $\overline{n}_0$ for the first time starting from state i. Therefore, FET is denoted by the expected value of $T_{i=0}$, $\overline{T}_0$, which is obtained by solving the set of linear equations

$$\overline{T}_i = 1 + \sum_{j=0}^{\overline{n}_o} P_{ij} \overline{T}_j \tag{2.32}$$

where P_{ij} is the transition probability from state i to state j. The solution of the linear system is derived as

$$\overline{\boldsymbol{T}} = \left(\boldsymbol{P} - \boldsymbol{I}\right)^{-1} \times \left(\mathbf{-1}\right) \tag{2.33}$$

where $\boldsymbol{P}$ is the transition matrix, $\boldsymbol{I}$ is the identity matrix and $\mathbf{1}$ is a column vector of ones. FET is then evaluated as

$$\overline{T}_0 = \sum_{j=0}^{\overline{n}_o} \overline{T}_j P_{0j} \tag{2.34}$$

$\overline{n}_o$ corresponds to the maximum throughput θ_o such that the system is stable when $\overline{n} < \overline{n}_o$ and unstable otherwise. The stability of both systems for a finite population model is studied numerically in section 2.7.

In multi-rate FFH-CDMA-based optical networks, different types of traffic loads can be observed. These different types of the traffics can be classified as functions of burstiness, QoS and/or delay requirements. Thus, different MAC protocol designs may provide different performances when handling those traffics [56]. To well judge the performance of the S-ALOHA protocol, we shall employ another MAC protocol that is originally designed for

OCDMA networks, namely the round-robin receiver/ transmitter (R^3T) protocol [25]. Then we compare the performances of both FFH-CDMA systems undergoing both reminiscent protocols in terms of the throughput and the delay as the offered traffic load varies. The R^3T/FFH-CDMA protocol is discussed in upcoming section.

2.6 R^3T/FFH-CDMA

Beside the S-ALOHA protocol, we attempt to control the packet access to the optical medium using the R^3T protocol [25].

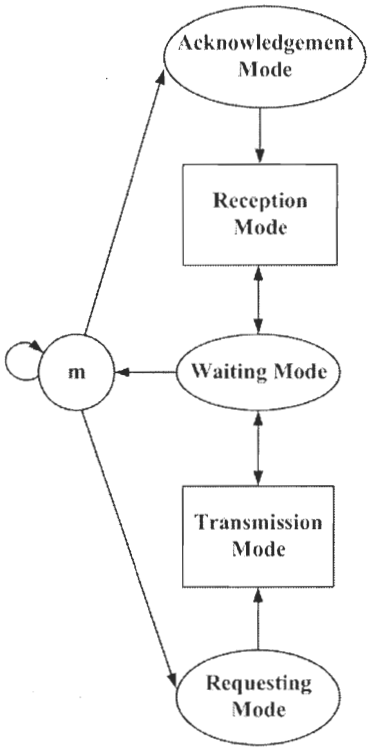

Fig. 2.6: Block diagram of R^3T protocol.

We assume that a packet corresponds to one bit and L bits form a message so that the message length is equal to the packet length in S-ALOHA. Each user transmits his message with a probability A, called user's activity. This message is stored in a single electronic buffer, freed once the message is sent correctly. Any message that arrives concurrently at a

non-empty buffer will be discarded. The terminal behavior is described by the block diagram shown in Fig. 2.6. The user wishing to transmit his packets sends a request to the destination station at first, and therefore he is in the requesting mode. The receiver of the destination station scans across all codes in a round-robin fashion, switches to the desired code signature at the next time slot and sends acknowledgements to the transmitting station to proceed on its transmission. At this time, the receiving station enters the reception mode.

Before expiring the timeout duration τ_o, if the transmitting station receives the acknowledgement, it enters the transmission mode and transmits the first t packets following the *go-back n* protocol [25], where $n = t$ is the two-way propagation time in slots between the transmitting and receiving stations. It can be $t \le L$ or $t \ge L$. It then enters the waiting mode, waiting for acknowledgements. If no acknowledgement is received after the time out duration, the station retransmits its last t packets in a round robin fashion as well. Once the message is received correctly and the station has nothing to transmit, it returns to its initial state m.

At the reception side, once a packet is received correctly, an acknowledgement is sent. Otherwise, the receiving station sends an ask-for-retransmission to the transmitting station and enters the waiting mode. If there is a message arrival and there is no request, then the receiving station asks the transmitting one for a connection request. If the latter does not respond, the receiving station returns to its initial state m.

The system throughput under the R^3T is computed in [25] as

$$\theta(K, A, t, \tau_o, L) = \frac{P_c(K) \cdot L \cdot r_o}{L + (1 - P_c(K))(\min\{t, L\} - 1)(L - \min\{t, L/2\})} \tag{2.35}$$

where $P_c(K)$ is given in (2.18) for the VPG-FFH-CDMA system and (2.19) for the O-FFH-CDMA system. r_o can be obtained such that the following condition is satisfied:

$$K\left[L+\left(1-P_c(K)\right)\left(\min\{t,L\}-1\right)\left(L-\min\{t,L/2\}\right)\right]=$$
$$r_o\left[\begin{array}{l}2tL\left(1-P_c(r_o)\right)+\left(2t+2L-1\right)P_c(r_o)+\dfrac{P_c(r_o)}{\rho}\\ +A(t-1)\dfrac{1-\rho}{\rho}P_c(r_o)+\left\{1-\left[1-\dfrac{\rho}{A(1-\rho)}\right]^{\frac{1}{\tau_o}}\right\}^{-1}P_c(r_o)\end{array}\right] \tag{2.36}$$

$$\rho=\rho(r_o)=0.5\left[\sqrt{u^2+4u}-u\right]$$

and $$u=\frac{AP_c(r_o)\cdot\tau_o\cdot r_o}{K\left[L+\left(1-P_c(r_o)\right)\left(\min\{t,L\}-1\right)\left(L-\min\{t,L/2\}\right)\right]}.$$

The delay is given by

$$D=\frac{K\cdot A}{\theta(K,A,t,\tau_o,L)} \tag{2.37}$$

where $K\cdot A$ is the average offered traffic.

2.7 Numerical Results

This part provides simulation results that evaluate the performance of O-FFH-CDMA and VPG-FFH-CDMA systems under S-ALOHA MAC protocol, respectively. The evaluation is in terms of the throughput, delay and stability. In addition, a comparison of performances between S-ALOHA and R^3T is conducted through simulation as well. It compares both the throughput and the delay as the offered load varies.

2.7.1 Performance Assessment of the S-ALOHA/FFH-CDMA Systems

Throughout this section, we present simulation results using the system model previously derived in sections 2.3, 2.4, and 2.5. Our target is to compare the network throughput, the

average packet delay, and the stability of the S-ALOHA/O-FFH-CDMA and the S-ALOHA/VPG-FFH-CDMA systems. Before presenting the simulation results, it is worthwhile to summarize the procedures adopted throughout this section.

1) Specify the total number of terminals, *K*.
2) Assign each terminal a code using the Extended Hyperbolic Congruential (EHC) family of codes characterized by a cross-correlation of at most one between two consecutive codewords [11].
3) Choose the transmission rate of each terminal, R_s, by specifying the processing gain G_V for the S-ALOHA/VPG-FFH-CDMA throughout equation (2.2) and by specifying the overlapping coefficient ε_s for the S-ALOHA/O-FFH-CDMA throughout (2.7).
4) Targeting a specific terminal, use a correlation receiver to compute the multiple access interference (MAI) power from each undesired terminal using the derived equations (2.10), (2.15), and (2.16).
5) The signal to interference power ratio (SIR) is therefore computed using (2.9), (2.12), and (2.13).
6) Then compute the probability of error and the correct packet probability using (2.17), (2.18), and (2.19).
7) The correct packet probabilities are used in the n-state Markov model in (2.21), (2.25), and (2.27) in order to obtain the state transition probabilities, the throughput and the average packet delay.
8) The computed transition probability matrix is used in (2.31) and (2.33) in order to obtain the stability analysis.
9) This process is done for both the S-ALOHA/VPG-FFH-CDMA and the S-ALOHA/O-FFH-CDMA system and a comparison is performed.

In the simulations, we have taken the number of active terminals $K = 6$, the packet length $L = 300$ bits per time slot, and $G = 29$. In addition, the transmission rate, R_s, is normalized in the sense that it represents the number of bits per time slot T_p. Note that, those values are

chosen in such a way to keep the runtime of the simulation within acceptable interval without affecting the general trend of the results.

In the upcoming simulations, we consider three different transmission bit rates, R_s = 668, 789, and 1239 bits/time slot, for both overlapped and VPG systems. For the S-ALOHA/O-FFH-CDMA, we will assume that the bits in a packet have an overlapping coefficients of ε_s = 16, 18, and 22 chips. This in turn yield increases in the bit rates to R_s = 668, 789, and 1239 bits/time slot, respectively. On the other hand, for the S-ALOHA/VPG-FFH-CDMA, the equivalent increases in the bit rates to R_s = 668, 789, and 1239 bits/time slot is achieved by reducing the processing gain (PG) to G_V = 13, 11, and 7, respectively.

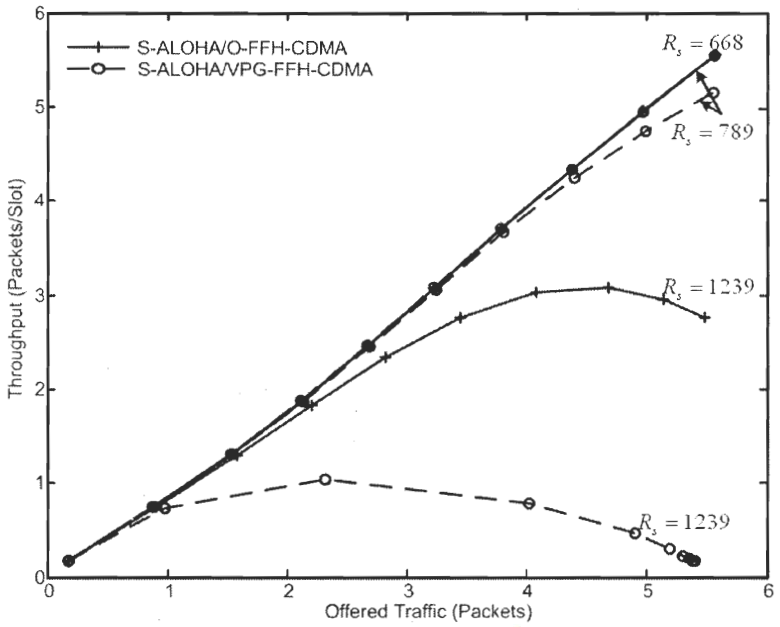

Fig. 2.7: Throughput vs offered traffic for P_r = 0.9.

First, assume that the probability of retransmission is taken to be $P_r = 0.9$. In Fig. 2.7 we plot the throughput versus the offered traffic for the three different values of R_s. Notice that at high bit rate, it is evident that when the offered load increases the throughputs of both systems degrade rapidly because they are governed by the SIR at the PHY layer as in (2.12)

and (2.13). In fact, as the SIR decreases, the packets are more vulnerable to distortion, which reduces the likelihood of their successful transmission and reception. Thus, the correct packet probabilities in (2.18) and (2.19) collapse and hence the throughput, while at low and moderate rates, is relatively higher. However, the overlapped system can tolerate more traffic than VPG.

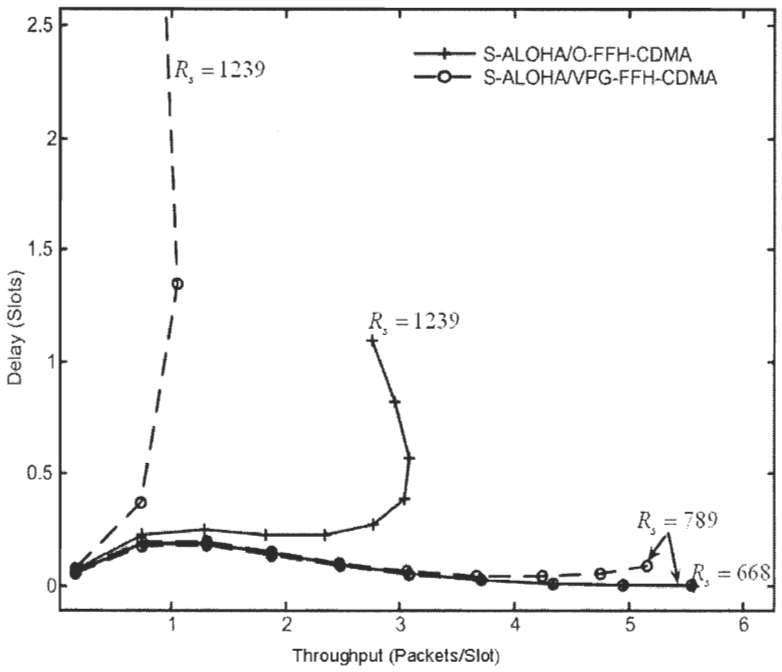

Fig. 2.8: Average delay vs throughput for $P_r = 0.9$.

On the other hand, Fig. 2.8 shows the average delay versus the throughput for the three different values of R_s. Since at low and moderate bit rates both systems can handle high loads, their throughputs are considerably higher. Therefore, rarely do backlogged packets occur and the systems' queuing delays are negligible. Nevertheless, as the bit rate increases to higher values, the overall interference degrades considerably the system throughput. In this case, a large portion of the offered load is corrupted and backlogged packets are delayed for retransmission. But since the systems operate at high rate, the retransmitted packets might face the same destiny, and then they will be further delayed.

It is clear that for both performance measures, the S-ALOHA/O-FFH-CDMA system always outperform the S-ALOHA/VPG-FFH-CDMA system and for different R_s. Notice that as the transmission rate increases, the S-ALOHA/O-FFH-CDMA becomes much better than the S-ALOHA/VPG-FFH-CDMA in the sense that its throughput becomes much higher and its delay becomes much smaller. This result is expected because when the transmission rate becomes very high, the PG becomes very small for the S-ALOHA/VPG-FFH-CDMA system. This in turn drastically decreases the SIR in (2.12) and therefore, the correct packet probability in (2.18). On the other hand, for the S-ALOHA/O-FFH-CDMA system the PG is fixed, which means that the signal power remains the same. In addition, the overlapping coefficient is increased, which in turns slightly increases MAI as revealed in (2.15) and (2.16). It seems that the slight increase in the MAI induced by the overlapping procedure in the S-ALOHA/O-FFH-CDMA system is much better than the huge decrease in the signal power in the S-ALOHA/VPG-FFH-CDMA system in terms of keeping the SIR high enough to achieve an acceptable correct packet probability.

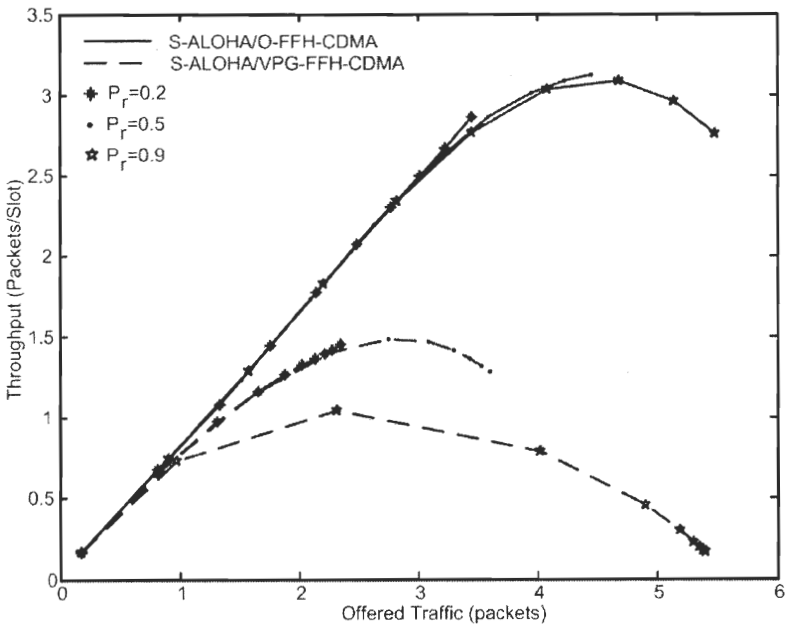

Fig. 2.9: Throughput vs offered traffic for R_s = 1239 bits/slot.

The effect of the retransmission probability P_r on the systems throughputs and the average packet delay is studied in Fig. 2.9 and Fig. 2.10, respectively, by varying P_r and fixing R_s to 1239 bits/slot. In Fig. 2.9 we plot the throughput versus the offered traffic and Fig. 2.10 shows the average delay versus the throughput. It is clear that as P_r decreases, the throughput decreases and the delay increases which is what we should expect. Note that in Fig. 2.9, increasing P_r from 0.2 to 0.9 yields faster degradation in throughputs of both systems due to the fact that higher priority is now given to the retransmissions, which overload the optical channel. However, in Fig. 2.10, the average packet delay is significantly reduced because the queuing time of backlogged packets is reduced as well. We can clearly notice that the S-ALOHA/O-FFH-CDMA system still outperforms the S-ALOHA/VPG-FFH-CDMA system.

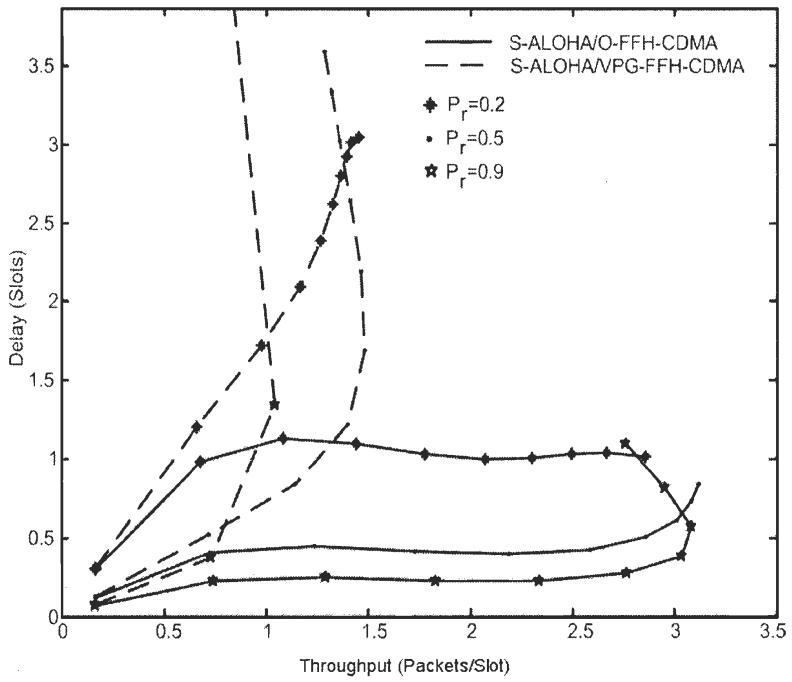

Fig. 2.10: Average delay vs throughput for R_s = 1239 bits/slot.

Fig. 2.11 depicts the state occupancy probability of both the overlapped and the VPG systems. For the latter, it is observed that higher order system states are occupying in a

monotonically increasing fashion of probability as the retransmission probability increases $(P_r = 0.9)$, which lead to more backlogged users in the system, whereas for the former, higher order system states are less probable to occur and the system converge to the initial state despite the variation of the retransmissions. This makes the overlapped system tolerate higher rates with acceptable delay.

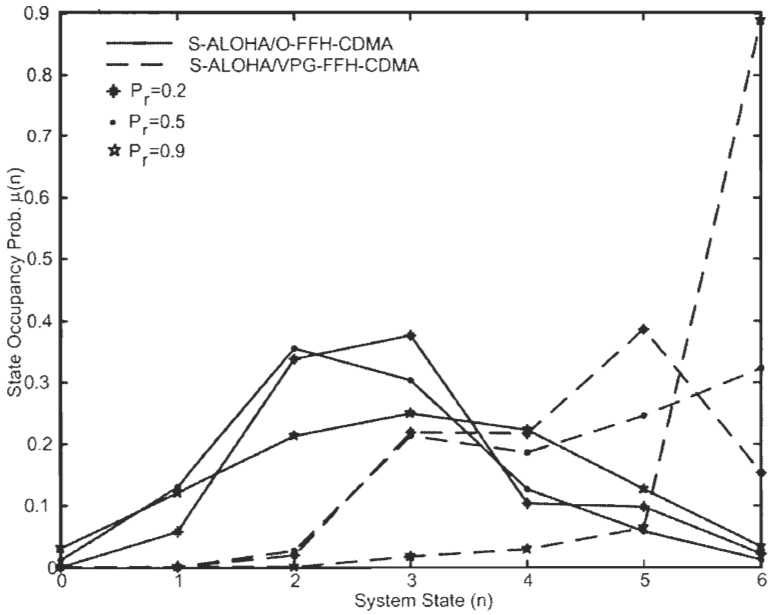

Fig. 2.11: State Occupancy Prob. vs System States for R_s = 1239 bits/slot.

Fig. 2.12 shows the expected drift stability assessment of both systems. It is shown that both systems have single global equilibrium points for small number of states. To achieve the second zero crossing point (which is the unstable point), the simulation should be conducted for much higher number of states, which is numerically very complex.

For this reason, to compare the stability of the overlapped and the VPG systems, the FET stability measure is used as depicted in Fig. 2.13. It is very clear that the FET for the overlapped system is always higher than that of the VPG system for different number of active terminals and transmission rates. This implies that the overlapped CDMA system is

more stable because it operates at longer time in the safe region before it exits to the unsafe region.

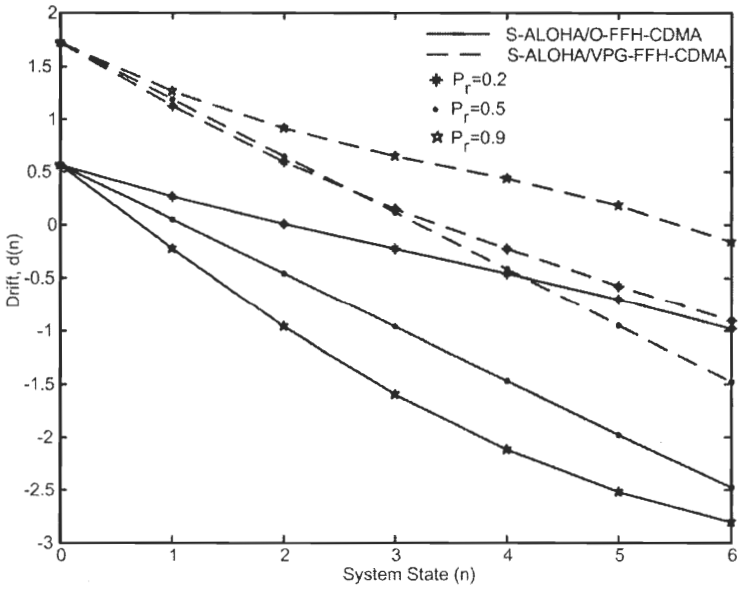

Fig. 2.12: The Expected Drift vs System States for R_s = 1239 bits/slot.

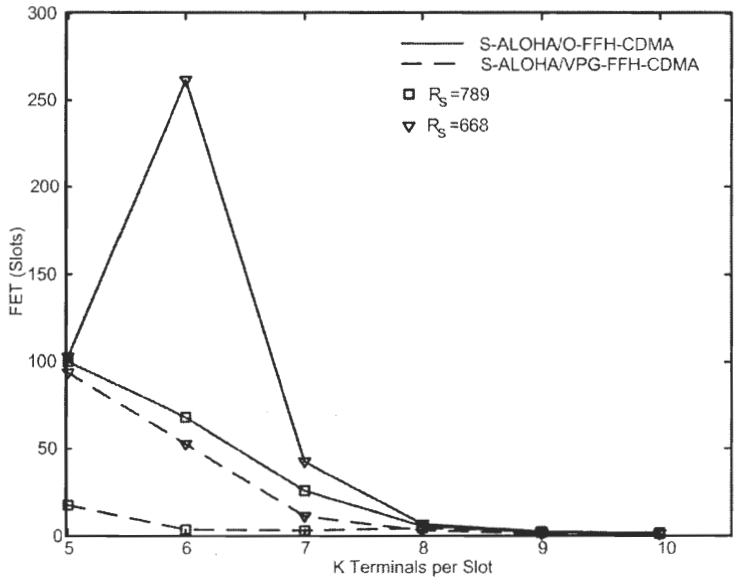

Fig. 2.13: FET at retransmission prob P_r = 0.9.

2.7.2 Performance Comparison Between S-ALOHA and R^3T Protocols

In this simulation we have assumed that the number of stations is $K = 23$, the processing gain $G = 31$, the packet length under S-ALOHA protocol is $L = 300$ bits/time slot and the message is one packet. While equivalently, under the R^3T protocol the packet length is one bit/time slot and L =300 designates the message length in packets. Note that there is a correspondence between A and P_r. In S-ALOHA, when a terminal enters the backlogged mode, it cannot generate new packets until all the accumulated ones in the system's buffer are retransmitted. Consequently, the offered traffic varies according to the retransmission probability, P_r. Meanwhile, in R^3T, the terminal in case of transmission failure retransmits the last unsuccessful t packets with the same transmission probability (user's activity) A which varies the offered traffic. For S-ALOHA, we assume $P_r = 0.9$, whereas for R^3T, we assume $A = 0.1$, 0.5, 0.6 and 1, the time out duration $\tau_o = 1$ time slot and the two-way propagation delay $t = 2$ and 8 time slots in fiber lengths of 200 m and 800 m, respectively. In addition, we consider that both multirate systems transmit at a normalized rate of $R_S = 714$ which corresponds to an increase of the overlapping coefficient ε_s from 0 to 18 for the overlapped system and a reduction of the PG to 13 for the VPG system.

The throughput of both systems is presented in Fig. 2.14 and Fig. 2.15 for two-way propagation delays of two and eight time slots ($t = 2$ and 8), respectively. Note that, the propagation delay has remarkable influence on the throughput of the OCDMA systems. This is due to the degradation of the signal power over the long distance in the fiber, which yields the available offered traffic to be susceptible to the MAI.

In addition, for low offered traffic, we notice that in both cases the R^3T protocol exhibits higher throughput than the S-ALOHA protocol when the user's activity $A < 0.6$, while, the throughputs of both protocols are matched when $A = 0.6$. It is clear that under the R^3T protocol the throughput curves of the overlapped system at moderate transmission rate reach around 10.5 packets per slot and decreases to 8.5 for $t = 2$ and 8 respectively; while those of the VPG system reach around 6 packets per slot, given that the maximum offered load is

relative to A. This means that the R^3T protocol always assures a successful transmission of its offered load when it is less than or equals to the maximum achievable throughput. In this case, this offered load is almost completely transmittable. As the offered load ($K.A$) increases, then at a certain level it exceeds the systems' capacities and becomes intolerable by such systems whose throughputs begin dropping off.

In fact, in our analysis, we have noticed that the throughput is always achieving a maximum value, which is referred to as "asymptotic throughput" as in [25], where the system's parameters reach their limiting values. That is, the number of transmitting users in a given slot approaches $N/2$ and the message length is sufficiently large. This yields the throughput to be invariant to A. However, for $A < 0.5$, this throughput exceeds the offered load for one reason, which is the average offered load of R^3T protocol does not involve the retransmitted packets whereas its throughput, computed by (2.35), does. Therefore, the actual number of packets in the network may exceed the number of the transmitting users because *go-back-n* has been adopted as a retransmission protocol. Since the load is already low, more packets that are available in the network can reach their destination successfully with low interference [25].

As A increases, the throughput of R^3T decreases compared to S-ALOHA. This is because more users are now transmitting and the offered traffic is increasing, which means that the MAI is intensifying. The packets facing such interference are susceptible to distortion, which, in turn, degrades the throughput.

For $A = 1$ all the users are transmitting at the same time, nevertheless the throughputs of both OCDMA systems undergoing R^3T are declining. This is because more users are now trying to transmit, while other users are still busy transmitting their long messages. Hence, the interference significantly increases and any unsuccessful transmission is replaced by the retransmission of the last t packets and the optical channel is highly utilized by the retransmitted packets. This problem can be resolved in the S-ALOHA protocol by randomly delaying the distorted packets, which are then retransmitted with a probability P_r. By increasing this probability, the protocol gives higher priority to the retransmissions over the

newly generated packets. In this way contention can be efficiently controlled and the throughput is optimized. On the other hand, for high offered traffic, the throughputs of R^3T decay faster than that of S-ALOHA, which means that R^3T has limited capacity. However, for large value of A (A = 1), the throughput of R^3T/VPG-FFH-CDMA is better than that of S-ALOHA. This means that VPG system undergoing R^3T can tolerate higher load than when undergoing S-ALOHA. Also, under both protocols, the throughput of the overlapped system outperforms that of VPG system.

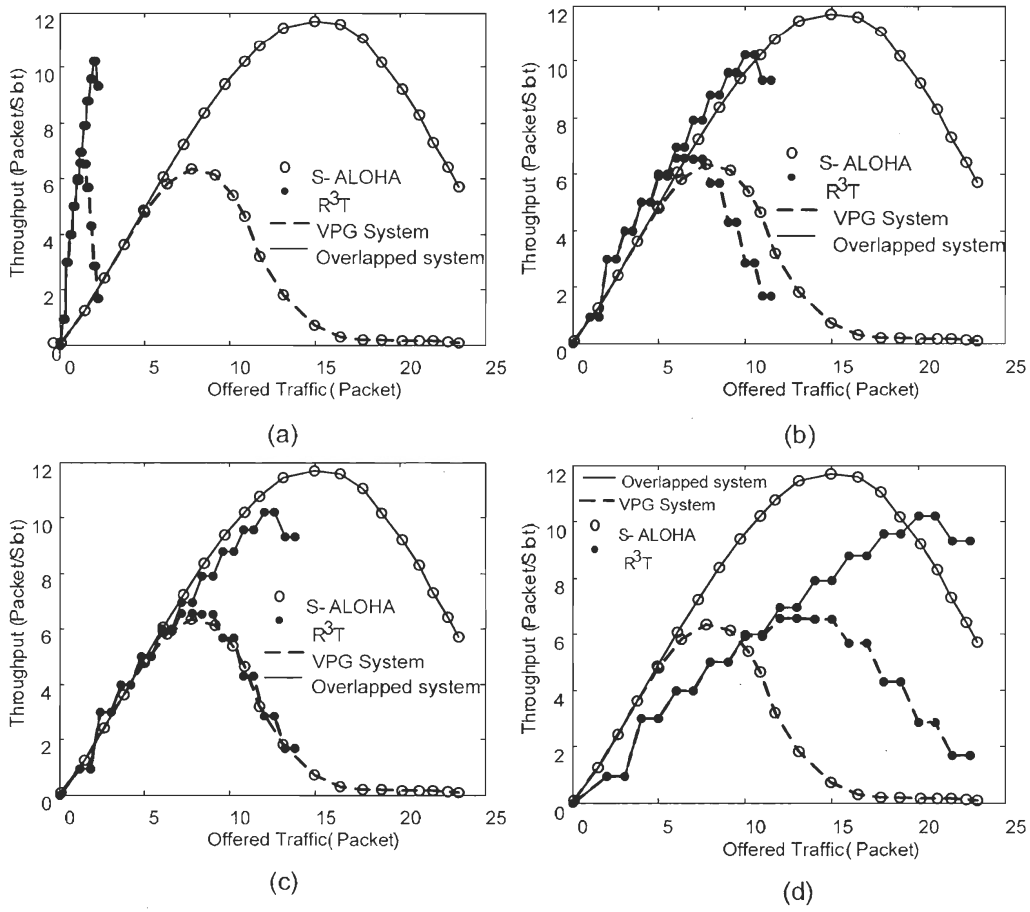

Fig. 2.14: The throughput versus the offered traffic of the multirate systems under the two MAC protocols: S-ALOHA and R^3T for a two-way propagation time of two time slots: (a) A= 0.1, (b) A= 0.5, (c) A= 0.6, (d) A= 1.

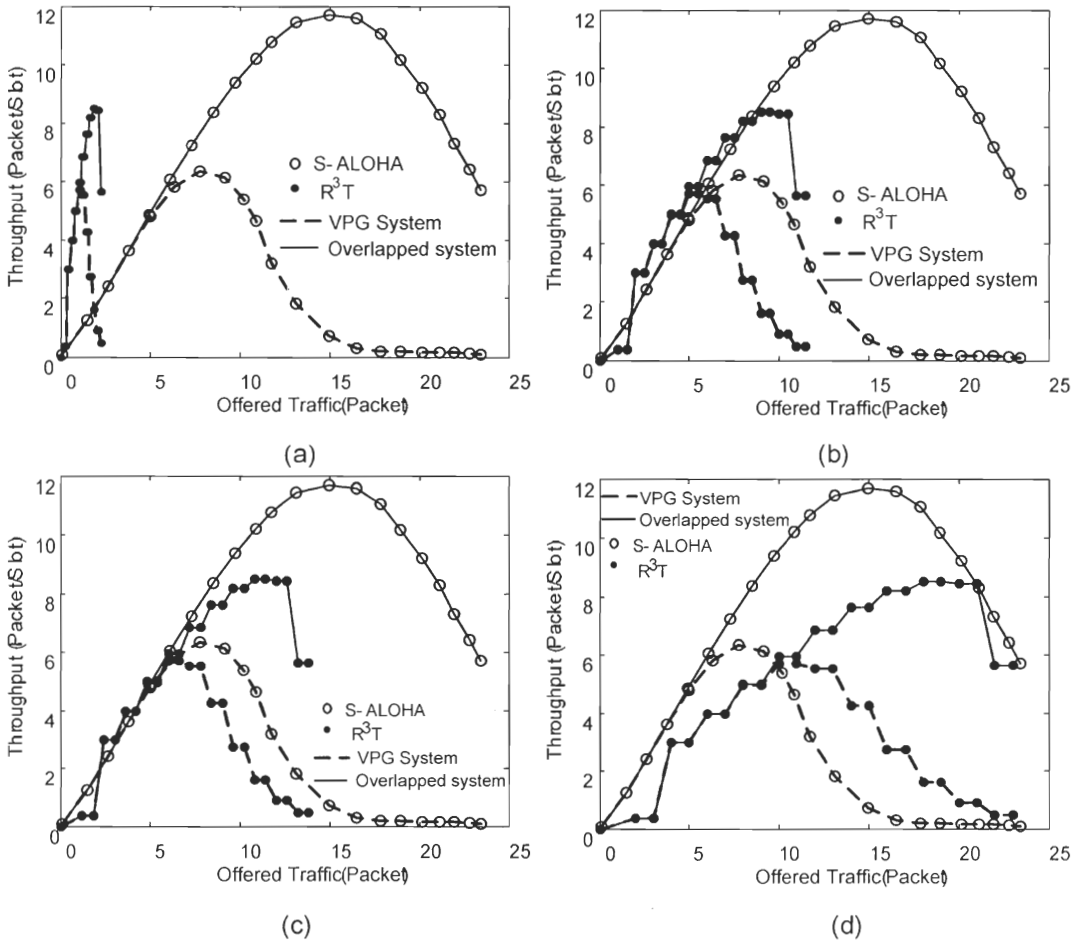

Fig. 2.15: The throughput versus the offered traffic of the multirate systems under the two MAC protocols: S-ALOHA and R^3T for a two-way propagation time of eight time slots: (a) A= 0.1, (b) A= 0.5, (c) A= 0.6, (d) A= 1.

In Fig. 2.16 and Fig. 2.17 we present the average packet delay versus the system throughput of both multirate OCDMA systems operating under the two mentioned protocols for $t = 2$ and 8, respectively. We remark that the R^3T protocol exhibits higher delay, especially at low throughput even if the user's activity and the two-way propagation time are reduced as revealed by both figures. This significant delay is caused by two factors: the adoption of *go-back-n* protocol for the retransmission of the distorted packets where $n = t$ and the signaling packets such as request, acknowledgement and ask-for-retransmission,

which in case of failure, place the system in the waiting mode for a certain period of time. Therefore, by minimizing the transmission activity of users (A = 0.1) and the propagation time to t = 2, the average system delay encountered by the R^3T when the throughput is low is still higher than that encountered by the S-ALOHA.

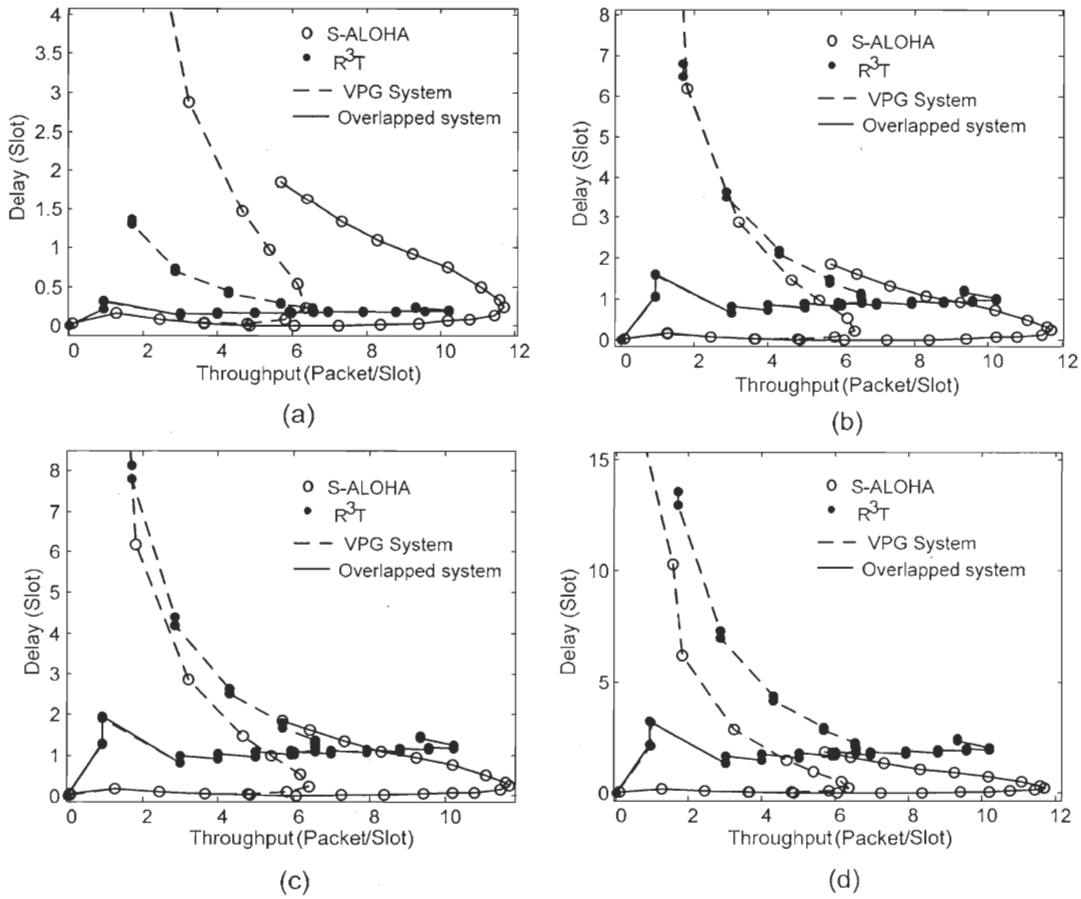

Fig. 2.16: The delay versus the throughput of the multirate systems under the two MAC protocols: S-ALOHA and R^3T for a two-way propagation time of two time slots: (a) A= 0.1, (b) A= 0.5, (c) A= 0.6, (d) A= 1.

In addition, for both t = 2 and 8, the average delay of the VPG system begins increasing as the throughput. This is due to the fact that as the load increases, the MAI level increases in the optical channel. Due to the reduction of the processing gain (PG) of the VPG system to G_V = 13, the optical signal intensity of users gets reduced and it is unable to persist to the

MAI. This in turn increases the likelihood of packet corruptions, and the erroneous packets will require longer time to be successfully transmitted. However, the delay of the overlapped system remains less affected as the traffic load increases since the PG is always preserved and hence the signal intensity. This yields the packets to be less susceptible to MAI and thus to failure. However, in the S-ALOHA/VPG-FFH-CDMA system the delay is significantly increased as the throughput increases because the excess load is not tolerable by the system; therefore, it is exposed to failure and equivalently to retransmission.

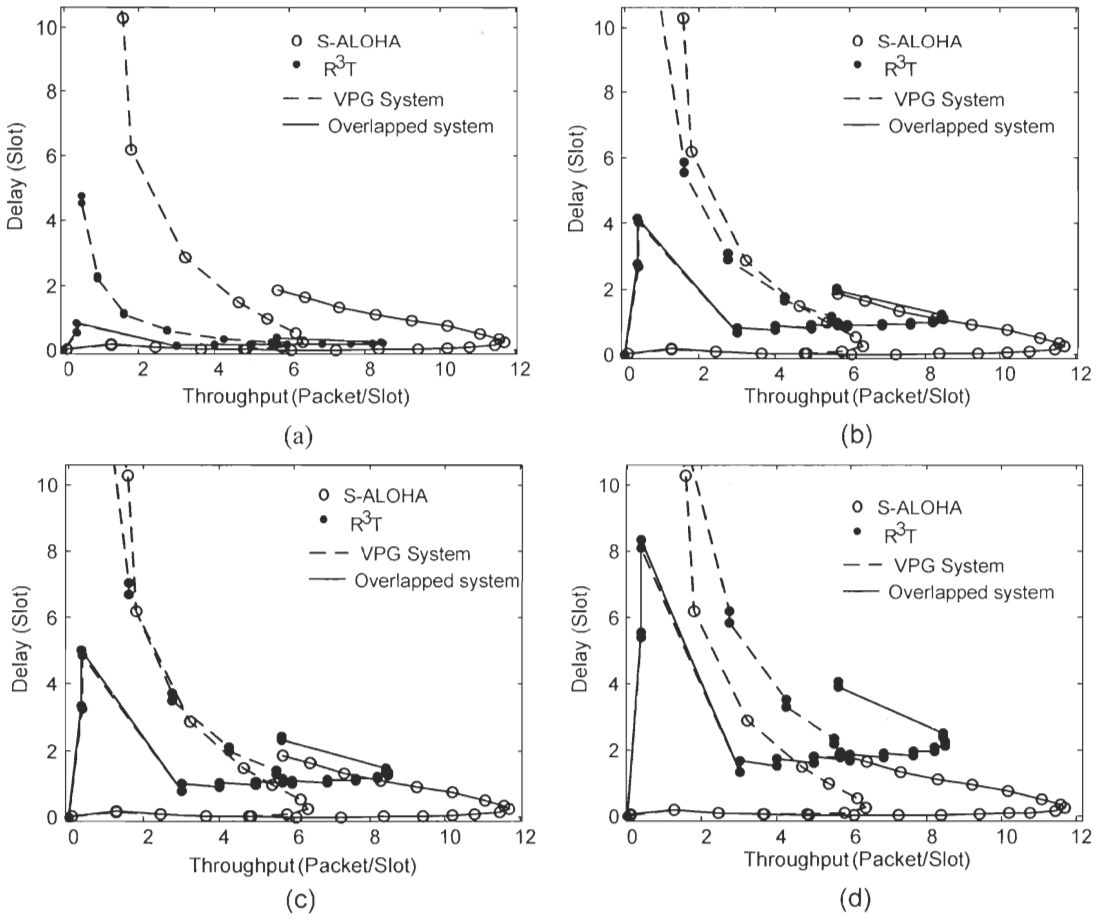

Fig. 2.17: The delay versus the throughput of the multirate systems under the two MAC protocols: S-ALOHA and R^3T for a two-way propagation time of eight time slots: (a) A= 0.1, (b) A= 0.5, (c) A= 0.6, (d) A= 1.

By comparing the performance of both systems under both protocols, we notice that for low and moderate offered load, the S-ALOHA is better than the R^3T when A is high; while the R^3T is better when A is small. In addition, the throughputs of both protocols are matched when A = 0.6. On the other hand, for high offered load, the S-ALOHA surpasses the R^3T. However, the VPG system under R^3T can provide improved performance over that under S-ALOHA when A is large and the offered load is relatively high. In addition, the S-ALOHA always outperforms the R^3T in terms of the average packet delay especially for large values of A.

2.8 Conclusion

In this chapter, a variable bit rate system based on hybrid S-ALOHA/O-FFH-CDMA system was proposed for optical CDMA time slotted packet networks. Two different systems were introduced and compared; the novel S-ALOHA/O-FFH-CDMA system and the classical S-ALOHA/VPG-FFH-CDMA system. The SIR for the new system was obtained. In addition, the time slotted system model has been derived using the general Markov chain from which the steady-state throughput and average packet delay have been evaluated. Simulation results showed that the newly proposed S-ALOHA/O-FFH-CDMA system outperforms the S-ALOHA/VPG-FFH-CDMA system, especially at higher transmission rates.

In addition, the stability of both systems has been studied in terms of expected drift and FET. Simulation results showed that the newly proposed S-ALOHA/O-FFH-CDMA system is relatively more stable than the S-ALOHA/VPG-FFH-CDMA system. Therefore, it has superior stability and is less susceptible to saturation.

Furthermore, a comparison of performances of the two multirate OCDMA systems under two different MAC protocols, the S-ALOHA and the R^3T, has been performed. It was shown that the S-ALOHA is better than the R^3T when the user's activity A and the offered traffic are high while the R^3T is better for moderate traffic and smaller values of A. In addition, both protocols can be competitive in terms of system throughput for moderate offered traffic by

fitting the corresponding parameters to an appropriate setting. However, the R^3T protocol suffers a higher delay mainly because the presence of additional modes (acknowledgement mode and requesting mode) which require a priori time setting for establishing a connection before data communication begins between the transmitting/receiving parties. Such modes are not available in S-ALOHA protocol. Finally, the overlapped OCDMA system always outperforms the VPG OCDMA system regardless of the protocol used.

Chapter 3

Optimal Resource Allocation Scheme in a Multirate Overlapped Optical CDMA System

3.1 Introduction

Optical code division multiple access (OCDMA) has received considerable attention as a multiple access scheme for optical local area networks (LAN) [15], [17]. In addition, heterogeneous services, entailing multirate transmission, are now feasible due to the rapid evolution of fiber optic technology [57] that offers ultra-wide optical bandwidth capable of handling these multirate transmissions and fulfilling good quality of service (QoS) requirements.

The first work toward this target was presented in [5], [6] where a novel coding technique that leads to the generation of a new family of Optical Orthogonal Codes (OOC) called *Strict* OOC. Although *Strict* OOC ensures both the auto- and the cross-correlation constraints to be less than or equal to one, the variability of transmission rate at constant power may not agree with the demanded QoS. Moreover, when the optical system attempts to transmit at a certain rate with very high power, a substantial increase in the interference occurs on the desired user at the receiver side [58]-[64]. This yields degradation in the system performance. One way to ameliorate the system efficiency is to adopt an efficient resource allocation strategy that regulates the amount of transmitted power with regard to the rate variation and the number of active users, so as to maximize the aggregate throughput of the multirate CDMA system [63].

Most of the analyses conducted on CDMA communication systems agree that optimal selection of the system's parameters such as the transmitted power and the bit rate would improve their performances [58]-[61]. This, in turn, gives rise to optimization problems

which are rarely discussed in the literature of OCDMA. For instance, a non linear programming power control algorithm has been proposed in [58] to maximize the capacity of multirate optical fast frequency hopping code division multiple access (OFFH-CDMA) system constrained by a predefined QoS based on the received signal-to-interference ratio (SIR) of each class of users. The rate of each class of users is chosen statically by choosing the corresponding processing gain (PG) in a way that higher rate users have smaller PG and lower rate users have larger PG. Then, the power of multirate users is optimally regulated with variable optical attenuator before transmission to limit the interference directly from the transmitter. In [59], a power control algorithm, based on optical power selector consisting of a set of optical hardlimiters and couplers, has been inspected for a multirate optical DS-CDMA system using one signature for each user with time hopping. In this work, the transmission rate and the bit error rate are controlled by the hopping rate and the optical power, respectively, to improve the system performance. Nevertheless, this algorithm employs ideal optical hardlimiters, which are practically very difficult to realize. In addition, an adaptive overlapped pulse-position modulator, employed to create multirate and multiquality transmission schemes, has been investigated in [60] for OCDMA networks where the power control mechanism is done by means of optical attenuators. It was proven that this system can tolerate four different services associated to four different classes of rates, which are easily differentiated by the intensity of the transmitted pulses and the number of transmitting slots, respectively. Moreover, the power control problem is also addressed in [61] for temporal prime coded OCDMA system taking into consideration the effect of the near-far problem caused by different fiber lengths connecting the users to the star network. It was shown that the fiber length after the star coupler is irrelevant to the optimal power evaluation. However, the consequences of having multirate users were not investigated in this analysis.

In this work, and for the first time, we propose a novel hybrid power/rate control algorithm for the OV-CDMA system [8], [9] in which multirate transmission is achieved by overlapping consecutive bits coded using fiber Bragg grating (FBG). It is shown in [8] that it is possible to increase the transmission of each class of users well beyond the nominal rate

without decreasing the PG. In addition, a service curve has been introduced, which relates the cutoff rates of the offered multimedia classes in a multi-class system. Our purpose in this work is to find the optimal overlapping coefficient through which we can achieve maximum transmission rate with minimum transmitted optical power directly from a laser source according to a predefined QoS required at the optical receivers for each class of users. In our analysis, we consider the average SIR as an adequate QoS requirement for each class of users. We derive an explicit solution of the optimal power as a function of the optimal data rate, from which the throughput function has been simplified to a quadratic function of the transmission rate vector. For each class of users, we provide a joint transmission power and overlapping coefficient allocation strategy, obtained via the solution of a constrained optimization problem, which maximizes the aggregate system throughput subject to a peak laser transmission power constraint. Under this strategy, the classes of users are allocated maximum transmission rate in decreasing order of the QoS requirements. It is also shown that there is at most one class of users that has an overlapping coefficient between zero and full overlap, and the remaining classes either transmit with full overlap or with no overlap.

Following the introduction, this chapter is structured as follows. Section 3.2 introduces the system model and the optimization problem formulation. The resource allocation problem is obtained in Section 3.3. Section 3.4 presents the solution for a two-class system. The three-class system evaluation is covered in Section 3.5. Finally, the conclusion is presented in Section 3.6 .

3.2 System Model and Problem Formulation

An OV-CDMA system that supports M users in S classes, sharing the same optical medium in a star architecture, has been proposed in [8]. We will consider that all users transmitting their data at the same QoS are clustered in the same class. All classes have the same processing gain G . The encoding-decoding is achieved passively using a sequence of fiber Bragg gratings (FBG). The gratings spectrally and temporary slice the incoming broadband pulse into several components, equally spaced at chip interval T_c. The chip

duration and the number of grating G determine the nominal bit duration to be $T_n = GT_c$. The corresponding nominal transmission rate is $R_n = 1/T_n$. Increasing the transmission rate beyond the nominal rate R_n without decreasing G introduces an overlapping of coefficient ε_j among the transmitted bits during the same period T_n, as revealed in Fig. 3.1.

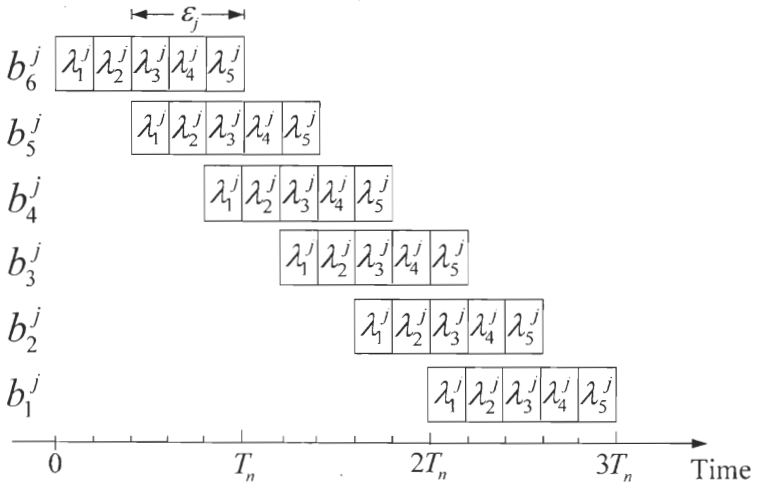

Fig. 3.1: The concept of overlapping among the bits of *class-j* users, showing the effect of the overlapping coefficient ε_j on their transmission rate.

In this case, the concept of overlapping is illustrated among six bits of $G = 5$ and the overlapping coefficient of class-j is $\varepsilon_j = 3$, which means that there are three chips in each OCDMA-coded bit that overlap with three chips of the other bits in the same class. This, in turn, augments the overall transmission rate of the users involved in this class from three bits after $3T_n$ to six bits. In general, the overlapping coefficient represents the number of overlapped chips among consecutive bits of class-j. Accordingly, the new transmission rate of class-j is given by

$$R_j = \frac{G}{G - \varepsilon_j} R_n \tag{3.1}$$

where $0 \le \varepsilon_j \le G-1$ for $j \in \{0,\ldots,S-1\}$. This implies that $R^{(\ell)} \le R_j \le R^{(u)}$ where $R^{(\ell)} = R_n$ and $R^{(u)} = GR_n$ are the lower and the upper data rate common to all classes, respectively. Also, we assume that the system is chip-synchronous and of discrete rate variation. Furthermore, all users of the same class transmit with the equal power and have the same overlapping coefficient. Hence, each class is characterized by its own QoS. Thus, let P_j and β_j be the transmitted power and QoS of *class-j*, respectively.

3.2.1 SIR as QoS measure

In many cases, it is reasonable to take the QoS requirements as meeting the SIR constraints [58], [63]. It was shown in [8] that the SIR for *class-j* using an OV-CDMA system is given by

$$SIR_j = \frac{P_j G^2}{\frac{(M-1)G^2}{2F}\sum_{i=0}^{S-1}\frac{p^{(i)}P_i}{G-\varepsilon_i} + \sigma_n^2}, \quad j \in \{0,\ldots,S-1\} \tag{3.2}$$

where F is the total number of available frequencies used in the code construction [11], and σ_n^2 is the variance of AWGN. On the other hand, $p^{(i)}$ is the multimedia probability density function and it represents the probability that a user selects class-*i*, where $\sum_{i=0}^{S-1} p^{(i)} = 1$. We can easily simplify (3.2) into the following

$$SIR_j = \frac{P_j}{\sum_{i=0}^{S-1} M_i P_i R_i + \frac{\sigma_n^2}{G^2}}, \quad j \in \{0,\ldots,S-1\} \tag{3.3}$$

where R_i is given in (3.1) and M_i represents the weight factor of *class-i* and it is given by

$$M_i = \frac{M-1}{2FGR_n} p^{(i)} \tag{3.4}$$

Note that by increasing $p^{(i)}$ of *class-i* as if we are increasing its weight for fixed system parameters $F, G, M,$ and R_n.

3.2.2 System Throughput

In this work, we aim at finding an appropriate resource allocation strategy that maximizes the transmission rates as well as minimizes the transmitted powers of the multirate users in an overlapped CDMA environment in order to maximize the system capacity. The criterion to achieve this optimality is to consider the aggregate throughput $\Omega^M : \mathbb{R}^S \times \mathbb{R}^S \to \mathbb{R}_+$ as the weighted sum of the ratios of the transmission rates over transmitted powers for the S classes and it is given by

$$\Omega^M(\mathbf{R},\mathbf{P}) = \sum_{j=0}^{S-1} M_j \frac{R_j}{P_j} \tag{3.5}$$

where $\mathbf{R} = (R_0, R_1, \ldots, R_{S-1})^T$ is the data rate vector, $\mathbf{P} = (P_0, P_1, \ldots, P_{S-1})^T$ is the power vector and M_j is the weight factor of *class-j*, as defined in (3.4) with $0 \le M_j \le 1$. This function of merit represents the system throughput, as the average number of bits per second per unit of power. Physically speacking, Ω^M meseaures the energy efficiency of the system, that is the average number of transmitted bits per unit of energy (bits/Joule).

Accordingly, we are interested in computing the jointly optimal power and rate allocation for users in each class that maximizes the aggregate throughput, subject to predetermined QoS constraints in terms of the SIR of each class. The optimal allocation policy is obtained by solving the following optimization problem

$$(\Pi_1) \qquad (\mathbf{R}^*, \mathbf{P}^*) = \arg \max_{(\mathbf{R}, \mathbf{P}) \in \Im} \{\Omega^M(\mathbf{R}, \mathbf{P})\} \tag{3.6}$$

where the feasible set is given by

$$\Im = \left\{ (\mathbf{R}, \mathbf{P}) : \ SIR_j = \beta_j, \ 0 < P_j \le P_{max}, \text{ and } R_n \le R_j \le GR_n \quad \forall \ j \in \{0,\ldots,S-1\} \right\} \tag{3.7}$$

where $P_{max} < \infty$ is the maximum permissible power of the laser source and β_j is the QoS of *class-j*.

The nonlinearity of the optimization problem is obvious from (3.5) and (3.7). Thus, to solve (Π_1), the problem is decoupled into two resource allocation scenarios: the power allocation scenario and the rate allocation scenario as will be shown in the next section. We first obtain the transmission power allocations, which are determined as a function of the QoS and the transmission rate of each class. We then maximize the aggregate throughput with respect to the transmission rate vector.

3.3 Jointly Optimal Power and Rate Allocations

In this scenario, we consider that the intensity of the transmitted optical signal is directly adjusted from the laser source with respect to the transmission data rate of users of the S classes. Thus, each class is allocated the minimum optical power capable of handling the traffic rate of its users while observing the transmission rate of all other classes and at the same time maintaining a low level of interference at the desired receiver. To do so, we fix the transmission rate of all the classes and we find out the optimal transmitted power corresponding to the desired class for a given QoS. Therefore, by taking $SIR_j = \beta_j$ and rearranging terms in (3.3), we get a set of linear equality constraints in terms of P_j. That is,

$$\sum_{i=0}^{S-1} P_i M_i R_i - \frac{P_j}{\beta_j} + \frac{1}{SNR_n} = 0, \qquad \forall j \in \{0,\ldots,S-1\} \tag{3.8}$$

where $SNR_n = G^2/\sigma_n^2$ is the nominal signal-to-noise ratio common to all classes. Then, by solving the linear system in (3.8) for P_j we get

$$P_j = \frac{1}{SNR_n} \times \frac{\beta_j}{1 - \sum_{i=0}^{S-1} \beta_i M_i R_i}, \qquad \forall j \in \{0, \ldots, S-1\} \tag{3.9}$$

The power is defined when the denominator is strictly greater than zero. That is,

$$\sum_{i=0}^{S-1} M_i \beta_i R_i < 1 \tag{3.10}$$

Consequently, the optimal *class-j* transmission power P_j^* is obtained by solving the rate allocation problem and finding the optimal rate R_j^*. Note that, the thermal noise, dark current and surface leakage current of the system are taken into consideration through the presence of the factor SNR_n in the power allocation strategy.

3.3.1 Optimal Rate Allocation

In this scenario, we will compute the optimal rate of the system classes that corresponds to the minimum power obtained in the previous section by substituting P_j in (3.9) into (3.5). We obtain

$$\Omega^M(\mathbf{R}) = SNR_n\left(-\mathbf{R}^{\mathrm{T}}\mathbf{Q}\mathbf{R} + \mathbf{C}^{\mathrm{T}}\mathbf{R}\right),\ \mathbf{Q} = \mathbf{Q}^{\mathrm{T}},\ \mathbf{Q} > 0,\ \mathbf{C} > 0 \tag{3.11}$$

where $\mathbf{Q}_{S\times S} = \left[\frac{1}{2} M_i M_j \left(\frac{\beta_i}{\beta_j} + \frac{\beta_j}{\beta_i}\right)\right]_{i,j=0,1\ldots,S-1}$ and $\mathbf{C} = \left[\frac{M_0}{\beta_0} \quad \frac{M_1}{\beta_1} \quad \cdots \quad \frac{M_{S-1}}{\beta_{S-1}}\right]^{\mathrm{T}}$. Notice that the throughput function is a quadratic function of the rate vector $\mathbf{R}$.

Thus, the optimization problem (Π_1) under the optimal power allocation becomes

$$(\Pi_2) \qquad \mathbf{R}^* = \arg\max_{\mathbf{R}\in\Im} \left\{\Omega^M(\mathbf{R})\right\} \tag{3.12}$$

where the feasible set $\Im$ is given by

$$\Im = \left\{ \mathbf{R}: \ \sum_{j=0}^{S-1} M_j \beta_j R_j \le 1 - \frac{\max\left(\beta_j\right)_{j=0,1,\ldots,S-1}}{P_{max} SNR_n}, \text{ and } R_n \le R_j \le G R_n \quad \forall \ j \in \{0,\ldots,S-1\} \right\} \tag{3.13}$$

Notice that the gradient of $\Omega^M(\mathbf{R})$ can be computed as

$$\nabla \Omega^M = SNR_n(-2\mathbf{QR} + \mathbf{C}) \tag{3.14}$$

and the Hessian matrix [65], [66] is

$$\mathbf{H} = \nabla^2 \Omega^M = -2SNR_n \mathbf{Q} \tag{3.15}$$

Because the Hessian matrix is negative, the throughput function is a concave function in $\mathbf{R}$, and therefore, the Kuhn-Tucker (KT) condition [66] is sufficient for an optimal point to be a maximum. To solve (Π_2), we use the method of Lagrange multiplier. Consequently, the Lagrangian function is defined as

$$L(\mathbf{R}, \mathbf{\Lambda}) = \Omega^M(\mathbf{R}) + \sum_{m=0}^{2S} \lambda_m g_m \tag{3.16}$$

where g_m is the m^{th} constraint and λ_m is the corresponding Lagrangian multiplier and $\mathbf{\Lambda}$ is the vector of Lagrangian multipliers. Applying the KT condition on (Π_2) we obtain

$$\frac{\partial L(\mathbf{R}, \mathbf{\Lambda})}{\partial R_j} = 0, \quad \forall j \in \{0,\ldots,S-1\} \tag{3.17}$$

$$\lambda_m g_m = 0, \quad \forall m \in \{0,\ldots,2S\} \tag{3.18}$$

$$g_m \ge 0 \tag{3.19}$$

$$\lambda_m \ge 0 \tag{3.20}$$

The nature of the stationary points is governed by the second order derivative of the Lagrangian function [65]. Notice that the second order derivative is strictly negative and independent of R_j i.e.

$$\frac{\partial^2 L(\mathbf{R},\boldsymbol{\Lambda})}{\partial R_j^2} = -2SNR_n M_j^2 \tag{3.21}$$

and

$$\frac{\partial^2 L(\mathbf{R},\boldsymbol{\Lambda})}{\partial R_i \partial R_j} = -SNR_n M_i M_j \left(\frac{\beta_i}{\beta_j} + \frac{\beta_j}{\beta_i}\right), \; i \neq j \tag{3.22}$$

This implies that (3.21) and (3.22) are sufficient conditions for the stationary points to be maxima [66]. The following two propositions show that the global maximum of $\Omega^M(\mathbf{R})$ is not the solution of (Π_2).

Proposition 3.1: *Given an $S \times S$ positive symmetric matrix $\mathbf{Q}$ of the form*

$$\mathbf{Q}_{S\times S} = \left[\frac{1}{2} M_i M_j \left(\frac{\beta_i}{\beta_j} + \frac{\beta_j}{\beta_i}\right)\right]_{\forall i,j \in \{0,1,\ldots,S-1\}}$$

where all $\beta_i \neq \beta_j$, $\mathbf{Q}$ is non-singular for $S = 2$, and it is singular for $S \geq 3$.

Proof: Let $\mathbf{A}_{2\times 2}$ be any 2×2 matrix of the form

$$\mathbf{A}_{2\times 2} = \begin{bmatrix} \frac{1}{2} M_i M_k \left(\frac{\beta_i}{\beta_k} + \frac{\beta_k}{\beta_i}\right) & \frac{1}{2} M_i M_\ell \left(\frac{\beta_i}{\beta_\ell} + \frac{\beta_\ell}{\beta_i}\right) \\ \frac{1}{2} M_{i+1} M_k \left(\frac{\beta_{i+1}}{\beta_k} + \frac{\beta_k}{\beta_{i+1}}\right) & \frac{1}{2} M_{i+1} M_\ell \left(\frac{\beta_{i+1}}{\beta_\ell} + \frac{\beta_\ell}{\beta_{i+1}}\right) \end{bmatrix}$$

where $i = S-2$, $S \geq 2$ and $k \neq \ell, k, \ell \in \{0,1,\ldots,S-1\}$.

Then, the determinant of $\mathbf{A}_{2\times 2}$ is equal to

$$\det\left(\mathbf{A}_{2\times 2}\right) = -\frac{1}{4} M_i M_{i+1} M_k M_\ell \left(\frac{\beta_i}{\beta_{i+1}} - \frac{\beta_{i+1}}{\beta_i}\right)\left(\frac{\beta_k}{\beta_\ell} - \frac{\beta_\ell}{\beta_k}\right) \neq 0,$$

given that all βs' are distinct. This implies that the matrix is non-singular. For $S = 2$, $\mathbf{Q}_{2\times 2}$ is a special case of $\mathbf{A}_{2\times 2}$ where $i = 0$, $k = 0$, and $\ell = 1$. Hence, $\mathbf{Q}_{2\times 2}$ is symmetric and non-singular.

Now, let $\mathbf{A}_{3\times 3}$ be any 3×3 matrix of the form

$$\mathbf{A}_{3\times 3} = \begin{bmatrix} \frac{1}{2} M_i M_k \left(\frac{\beta_i}{\beta_k} + \frac{\beta_k}{\beta_i}\right) & \frac{1}{2} M_i M_\ell \left(\frac{\beta_i}{\beta_\ell} + \frac{\beta_\ell}{\beta_i}\right) & \frac{1}{2} M_i M_r \left(\frac{\beta_i}{\beta_r} + \frac{\beta_r}{\beta_i}\right) \\ \frac{1}{2} M_{i+1} M_k \left(\frac{\beta_{i+1}}{\beta_k} + \frac{\beta_k}{\beta_{i+1}}\right) & \frac{1}{2} M_{i+1} M_\ell \left(\frac{\beta_{i+1}}{\beta_\ell} + \frac{\beta_\ell}{\beta_{i+1}}\right) & \frac{1}{2} M_{i+1} M_r \left(\frac{\beta_{i+1}}{\beta_r} + \frac{\beta_r}{\beta_{i+1}}\right) \\ \frac{1}{2} M_{i+2} M_k \left(\frac{\beta_{i+2}}{\beta_k} + \frac{\beta_k}{\beta_{i+2}}\right) & \frac{1}{2} M_{i+2} M_\ell \left(\frac{\beta_{i+2}}{\beta_\ell} + \frac{\beta_\ell}{\beta_{i+2}}\right) & \frac{1}{2} M_{i+2} M_r \left(\frac{\beta_{i+2}}{\beta_r} + \frac{\beta_r}{\beta_{i+2}}\right) \end{bmatrix}$$

where $i = S-3$, $S \geq 3$ and $k \neq \ell \neq r, k, \ell, r \in \{0,1,\ldots,S-1\}$.

Then, $\det\left(\mathbf{A}_{3\times 3}\right) = 0$. This implies that this matrix is singular. Consequently, all the 3×3 minors in the determinant of $\mathbf{Q}_{S\times S}$ are zeros; hence $\det\left(\mathbf{Q}_{S\times S}\right) = 0$ and $\mathbf{Q}_{S\times S}$ is singular for $S \geq 3$. ■

Proposition3. 2: *The global maximum of the optimization problem* (Π_2) *is not feasible.*

Proof: The throughput function has a global maximum only when the gradient is null, $\nabla\Omega^M = 0$. This implies

$$\mathbf{R}^* = \tfrac{1}{2}\mathbf{Q}^{-1}\mathbf{C} \tag{3.23}$$

The global maximum in (3.23) exists if and only if the matrix $\mathbf{Q}$ is invertible. In addition, $\mathbf{R}^*$ is feasible if it is in the feasible set $\Im$ of (Π_2). By proposition 1, $\mathbf{Q}$ is non singular for $S=2$. Thus, for any two-class system, say *class-i* and *class-j*, the global maximum is found when the gradient is null. That is $\nabla\Omega^M = 0$, which yields

$$R_i^* = \frac{\beta_i}{M_i\left(\beta_i^2 - \beta_j^2\right)}$$

$$R_j^* = \frac{\beta_j}{M_j\left(\beta_j^2 - \beta_i^2\right)}$$

By assumption, $\beta_i \neq \beta_j$, so both rates are finite. Also, notice that, $\beta_i M_i R_i + \beta_j M_j R_j = 1$, which violates the condition in (3.10). This means that this solution is not feasible and hence the global maximum. For $S \geq 3, \mathbf{Q}$ is singular by proposition 1 and therefore the global maximum does not exist. ■

3.3.2 Problem Solution

The solution of (Π_2) is obtained via the following lemmas, the first of which shows that the feasible set $\Im$ can be reduced to its boundaries. It also shows that there is at most one class of users that has an overlapping coefficient between zero and full overlap, and the remaining classes either transmit with full overlap or with no overlap.

Lemma 3.1: *Assume that* $\mathbf{R}^* = \left(R_0^*, R_1^*, ..., R_{S-1}^*\right)^T$ *solves the optimization problem* (Π_2). *If* $P_{Max} < \infty$, *there exists at most one* R_j^* *such that* $R^{(\ell)} \leq R_j^* \leq R^{(u)}$, *and* $R_i^* = R^{(u)}$ *or* $R_i^* = R^{(\ell)} \quad \forall i \neq j = 0,1,...,S-1$.

Proof: The throughput function is concave in R^* and thus, the optimal rate allocation lies on the boundary of the feasible set$(\Im)$. Consider the KT conditions on (Π_2) $\forall j \in \{0,1,\ldots,k,\ldots,S-1\}$ as follows:

$$\frac{\partial \Omega^M}{\partial R_j} + \lambda_j - \lambda_{S+j} - \lambda_{2S} M_j \beta_j = 0 \tag{3.24}$$

$$\lambda_j \left(R_j - R^{(\ell)} \right) = 0 \tag{3.25}$$

$$\lambda_{S+j} \left(R^{(u)} - R_j \right) = 0 \tag{3.26}$$

$$\lambda_{2S} \left(1 - \frac{\max\left(\beta_j\right)_{\forall j \in \{0,1,\ldots,S-1\}}}{P_{Max} SNR_n} - \sum_{i=0}^{S-1} M_i \beta_i R_i \right) = 0 \tag{3.27}$$

There are four cases to consider.

a) If $\lambda_j \neq 0$, then $\lambda_{S+j} = 0$. This implies that $R_j^* = R^{(\ell)}, \forall j \in \{0,1,\ldots,k,\ldots,S-1\}$.

b) If $\lambda_{S+j} \neq 0$, then $\lambda_j = 0$ This implies that $R_j^* = R^{(u)}, \forall j \in \{0,1,\ldots,k,\ldots,S-1\}$.

In both cases, there are $(S+1)$ equations of $(S+1)$ unknowns in λ_j and/or λ_{S+j} plus λ_{2S}. If $\lambda_{2S} \neq 0$, or $\lambda_{2S} = 0$ then

$$\sum_{i=0}^{S-1} M_i \beta_i R_i^* \leq \left(1 - \frac{\max\left(\beta_j\right)_{\forall j \in \{0,1,\ldots,S-1\}}}{P_{Max} SNR_n} \right)$$

which satisfies condition (3.10). Therefore, R_j^* are indeed feasible solutions for (Π_2).

c) Consider the class-k of users for which $\lambda_k = 0$ and $\lambda_{S+k} = 0$. This implies that the feasible solution is $R_k^* \neq \left\{R^{(\ell)}, R^{(u)}\right\}$. In addition to this condition if cases a) and/or b) are occurring for all $j \neq k$, there are also $(S+1)$ equations of $(S+1)$ unknowns in $\lambda_{j\neq k}$ and/or $\lambda_{S+j\neq k}$ plus λ_{2S} and R_k. If $\lambda_{2S} \neq 0$, R_k^* is computed from the constraint (3.27) and it is given by

$$R_k^* = \frac{1}{M_k \beta_k}\left\{\left(1 - \frac{\max\left(\beta_j\right)_{\forall j\in\{0,1,\ldots,S-1\}}}{P_{Max} SNR_n}\right) - \sum_{\substack{i=0 \\ \neq k}}^{S-1} M_i \beta_i R_i^*\right\} \text{ where } R_i^* \in \left\{R^{(l)}, R^{(u)}\right\}$$

In addition, λ_{2S} is computed from (3.24). On the other hand if $\lambda_{2S} = 0$, then

$$\sum_{i=0}^{S-1} M_i \beta_i R_i^* \leq \left(1 - \frac{\max\left(\beta_j\right)_{\forall j\in\{0,1,\ldots,S-1\}}}{P_{Max} SNR_n}\right)$$

because R_i^* are feasible by assumption. In this case, R_k^* is computed from $\frac{\partial \Omega^M}{\partial R_k} = 0$. Since by assumption R_k^* is feasible, $R^{(\ell)} \leq R_k^* \leq R^{(u)}$, where all $R_j^* = R^{(\ell)}$ or $R^{(u)}$ $\forall j \neq k$.

d) If $\lambda_j = 0$ and $\lambda_{S+j} = 0$ for more than one class at same time, then the system has no feasible solution by proposition 1. ■

This means that there exists at most one class of users that transmits with rate between R_n and GR_n, and the remaining classes either transmit with the maximum rate GR_n or with the minimum rate R_n.

Lemma 3.2: *Consider that* $\beta_i > \beta_j \; \forall i < j$. *If* $\mathbf{R}^* = \left(R_0^*, R_1^*, \ldots, R_{S-1}^*\right)^T$ *solves the optimization problem* (Π_2), *then* $R_i^* \leq R_j^*$ *if and only if* $0 \leq i < j \leq S-1$.

Proof: Appendix A.

3.4 Two Class System

In this section, we analyze the feasible region of the two-class system by providing a graphical representation of system's solution. Thereafter, we proceed on by a numerical analysis to assess the validity of the optimal results.

3.4.1 Feasible Region Analysis

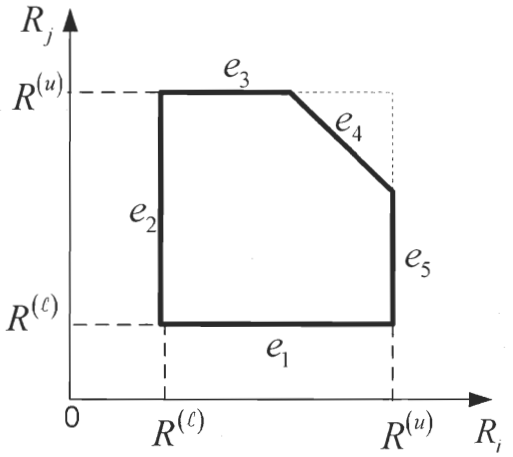

Fig. 3.2: The feasible region for a 2-class system.

Due to the complexity of the problem under consideration, and without loss of generality, we present the case of a two-class system. Consider a two-class system, the *class-i* and the *class-j* with $\mathbf{R} = \left(R_i, R_j\right)^T$. The boundaries of the feasible region are illustrated in Fig. 3.2. To solve $\left(\Pi_2\right)$, we should obtain the optimal solution which is defined in predetermined intervals of β_i and β_j. Let the set of edges of the feasible region be $\mathbf{E} = \left\{e_1, e_2, e_3, e_4, e_5\right\}$ to be the locus of our optimal solution. By Lemma 3.1, we know that at most one class of users transmits with transmission rate between $R^{(\ell)}$ and $R^{(u)}$, and the remaining classes either

transmit with $R^{(u)}$ or with $R^{(\ell)}$. Thus, the search space of the optimal solution is $\mathbf{E}' = \{e_1, e_2, e_3, e_5\}$. In addition, without loss of generality, consider that $\beta_i > \beta_j$. By Lemma 3.2, we know that if $\beta_i > \beta_j$ then $R_i \leq R_j$. This means that the locus of the optimal solution has been reduced to $\mathbf{E}'' = \{e_2, e_3\}$.

3.4.2 Numerical Results

In this part, we evaluate the effectiveness of the proposed power/rate control algorithm for two-class. First of all, we consider the two-class system for which we assume that $M = 61$ users are active, the processing gain of the user's signature is $G = 61$, the total number of available wavelengths is $F = 62$, the nominal signal-to-noise ratio is $SNR_n = 35.7$ dB, the upper bound on the laser power is $P_{\max} = 5$ dBm, the QoS of *class-0* is fixed to $\beta_0 = 8$ dB, and the nominal transmission rate is $R_n = 1$ Mbps. Again, the choice of these values is done is such a way to point out the original aspects of the obtained results in a clear manner without affecting the general trend. Besides, in order to assess the validity of our results, we make use of a numerical method consisting of a sequential quadratic method, based on the quasi-Newton method, in which a quadratic programming sub-problem is solved at each iteration, and an estimate of the Hessian of the Lagrangian function is updated using the BFGS method (suggested by Broyden, Fletcher, Goldfarb, and Shannon in 1970) [66]. The simulation shows that the explicit analytic solution matches completely the numeric one. This means that the derived solution is indeed the exact optimal solution. In addition, the performance of the proposed resource allocation strategy is compared with that of a classical power control algorithm with fixed transmission rates. We assume that *class-0* users transmit at rate $R_0 \cong 2R_1$ when $\beta_0 < \beta_1$, and *class-1* users transmit at rate $R_1 \cong 2R_0$ when $\beta_1 < \beta_0$, then the classical power control strategy allocates the best transmission laser power to each user in either classes in order to guarantee the QoS requirements.

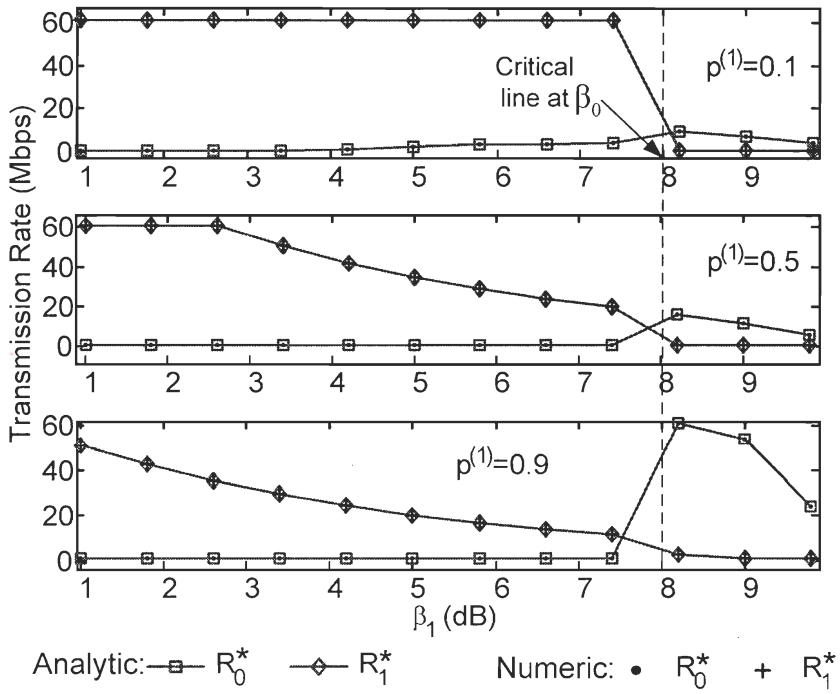

Fig. 3.3: The transmission rates versus QoS of *class-1* users for different multimedia distribution.

In Fig. 3.3, the transmission rates are evaluated as a function of β_1, and they are plotted for different multimedia distributions. For $p^{(1)} = 0.1$, the multimedia traffic is denser in *class-0* than in *class-1*. Since a small number of users are choosing *class-1*, the minority *class-1* users transmit at rate $R_1^* = R^{(u)}$ for $\beta_1 < 8\,\text{dB}$. On the other hand, the majority *class-0* users transmit at rate $R_0^* = R^{(\ell)}$ for $\beta_1 < 4\,\text{dB}$, and $R^{(\ell)} < R_0^* < R^{(u)}$ for $4\,\text{dB} < \beta_1 < 8\,\text{dB}$. In addition, for $\beta_1 > 8\,\text{dB}$, *class-1* users now transmit at rate $R_1^* = R^{(\ell)}$, while *class-0* users transmit at rate $R^{(\ell)} < R_0^* < R^{(u)}$. For $p^{(1)} = 0.9$, *class-1* users are allowed to transmit only at $R^{(\ell)} < R_1^* < R^{(u)}$ for $\beta_1 < 8\,\text{dB}$, while *class-0* users transmit at $R^{(\ell)}$. Also, notice that for $8\,\text{dB} < \beta_1 < 9\,\text{dB}$, $R^{(\ell)} < R_1^* < R^{(u)}$ and $R_0^* = R^{(u)}$. This, in turn, shows a total agreement with the hypotheses proposed in the two lemmas, proven in previous sections. Furthermore, as the number of users in a certain class increases and hence the multimedia traffic, the allocated

transmission rate decreases in order to keep the MAI at an acceptable level for satisfying the required QoS.

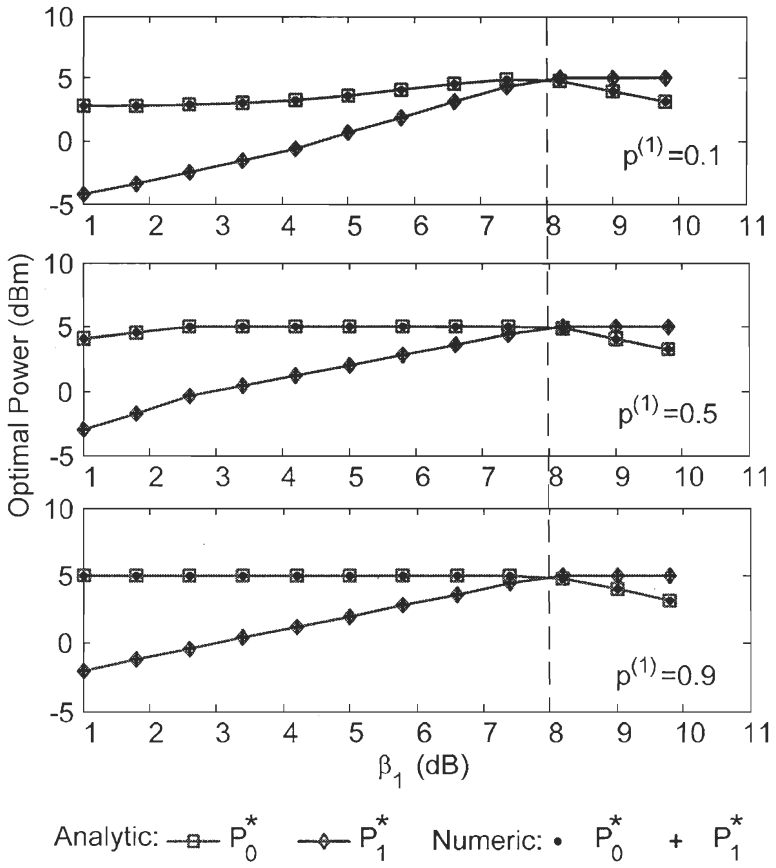

Fig. 3.4: The power consumption of *class-0* and *class-1* for different multimedia distributions.

The optimal transmission power for the corresponding multimedia distributions is illustrated in Fig. 3.4. Note that, as the number of *class-0* users decreases, their allowable transmission power increases. Therefore, when $p^{(1)}$ increases from 0.1 to 0.9, the MAI effect of *class-0* on *class-1* decreases, and the system allows *class-0* to transmit at the upper-bound laser power to improve the service requirement. In addition, *class-1* power is proportional to QoS. Therefore, it is monotonically increasing as β_1 until it reaches a constant level at the maximum attainable laser power for $\beta_1 > \beta_0$. The constant power in this

interval of β_1 is necessary to assure the data transmission at such QoS. Further, we remark that an additional augmentation of β_1 above 10 dB is no more supportable because the laser power of the source becomes inadequate.

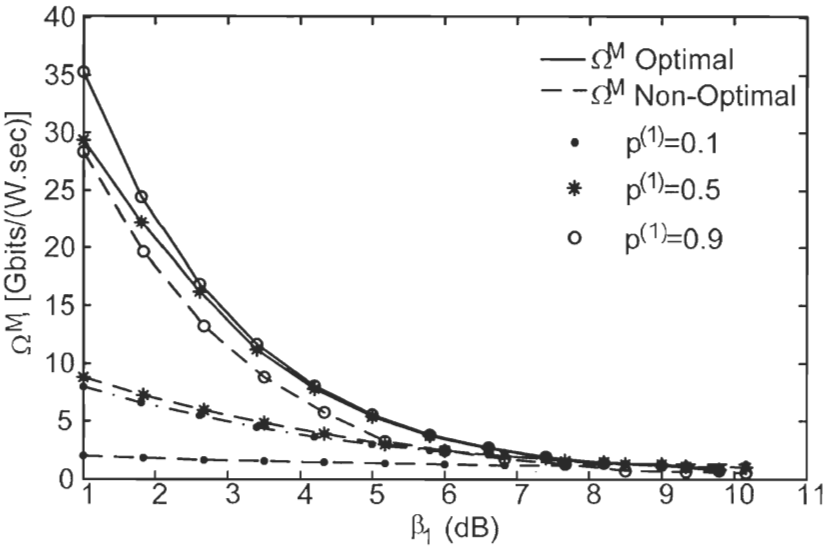

Fig. 3.5: The throughput versus QoS of *class-1* for different multimedia distributions.

The optimal throughput is plotted in Fig. 3.5 and compared to the non-optimal one achieved by the classical power control strategy. The optimal throughput decays as β_1 increases because at high QoS the allocated resources are used to preserve the QoS requirement rather than to increase the system capacity. In addition, we observe that an appropriate traffic distribution gradually enhances the system throughput according to allocated resources. For $p^{(1)} = 0.1$, both R_0^* and R_1^* are high and hence the interference. Alongside, the allowable transmission power is relatively low. This yields the lowest optimal throughput due to the fact that the allocated power is insufficient to satisfy the QoS requirement and to combat the MAI increase. As $p^{(1)}$ increases, the MAI relaxes and the average system throughput increases. Also, we can clearly observe that the system throughput of the proposed resource allocation strategy is superior to that of the non-optimal one for the different multimedia distributions.

Next, we study the effectiveness of the proposed resource allocation strategy with respect to the number of stations accessing the system for different multimedia distributions. We keep the same parameter settings as in the previous part but in this case we fix QoS of *class-1* to $\beta_1 = 5\,\text{dB}$, which is 3 dB less than β_0. By this setting, the classical power control criteria with constant transmission rate turns out to be the equal energy criteria (EEC). We show that the EEC results are feasible but non optimal.

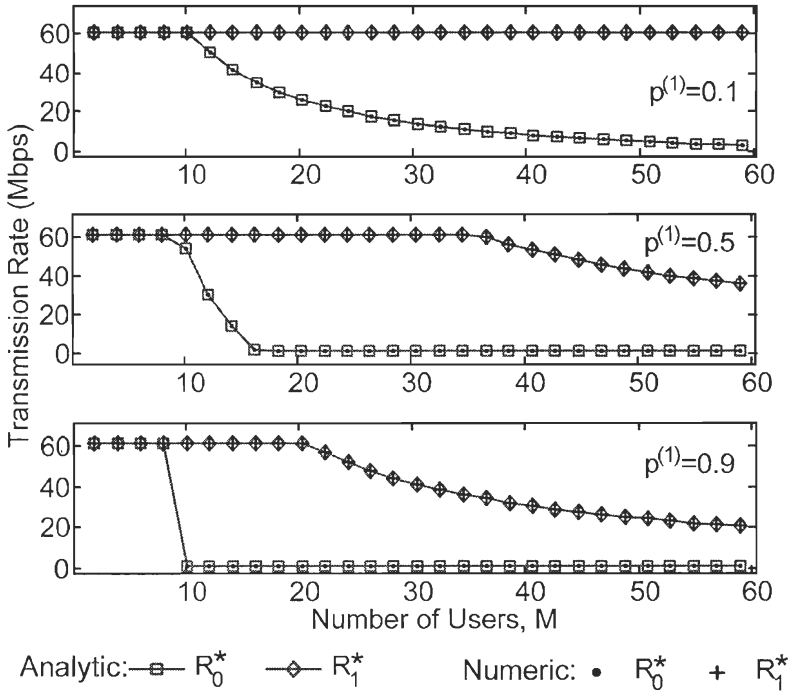

Fig. 3.6: The optimal transmission rates versus the number of users for a two-class system.

The optimal transmission rates in terms of M are examined in Fig. 3.6. Consequently, for small M, the system allows both classes to transmit at maximum rate $R^{(u)}$ because the MAI is sufficiently small. However, when $M \geq 10$ as the user population in a given class increases, its transmission rate decreases to keep the MAI at regular level and to accommodate to the QoS requirement. Note that, when $R^{(\ell)} \leq R_0^* < R^{(u)}$, $R_1^* = R^{(u)}$, and

when $R_0^* = R^{(\ell)}$, $R^{(\ell)} < R_1^* \le R^{(u)}$ which is consistent with Lemma 3.1. Furthermore, because $\beta_0 > \beta_1$, it is clear that we always have $R_0^* \le R_1^*$, which validates Lemma 3.2.

Recall that our objective is to determine the optimal overlapping coefficient ε_j^*, which is a point on the service curve proposed in [8]. By obtaining the optimal rates R_0^* and R_1^* for both classes, the optimal overlapping coefficients ε_0^* and ε_1^* satisfying the system requirements are now computed using (3.1).

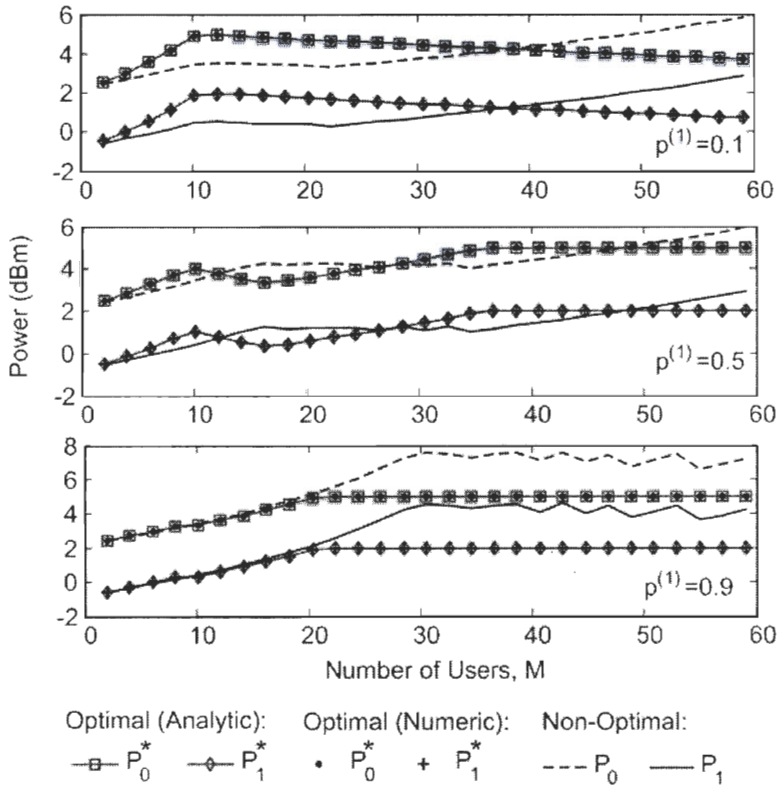

Fig. 3.7: The transmission power versus the number of users for a two-class system.

In Fig. 3.7, the optimal power is compared to the non optimal one as M varies. Notice that when $p^{(1)}$ is small, the EEC allocates less power for small M and more power for large M compared to our newly proposed algorithm. This criterion makes the users always

susceptible to MAI. In contrast, our proposed strategy provides more power for small M to improve the optical signal, and less power for large M to reduce the MAI intensity. On the other hand, when $p^{(1)} = 0.5$, the EEC follows the optimal one. Finally, when $p^{(1)} = 0.9$, the EEC power matches the optimal one for small M. However, it exceeds the upper bound laser power for large M. On the other hand, our proposed strategy controls this excess of power by clamping it to the maximum allowable laser power.

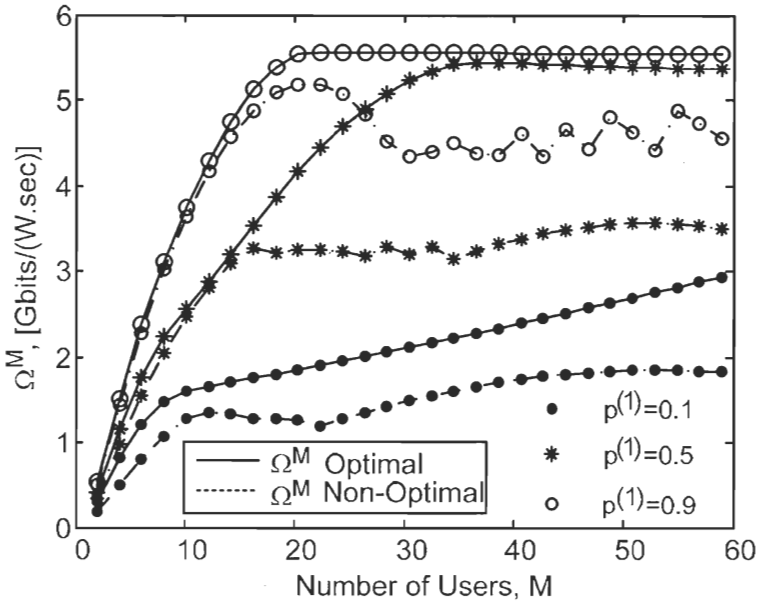

Fig. 3.8: The optimal throughput versus the total number of users for a two-class system.

The impact of the total number of users on the system throughput is shown in Fig. 3.8. For small M, the performance of the EEC approaches the optimal one especially when the probability of selecting *class-1* is high. As M increases, the system throughput of our proposed strategy outperforms that of the EEC. Note that as M becomes higher, the system throughput mounts for increasing values of $p^{(1)}$. This happens because when $p^{(1)}$ is small, both classes transmit at rates higher than the nominal one as revealed in Fig. 3.3. This in turn requires high overlapping coefficients. It follows that the interference level in the optical channel increases. In addition, the transmission power level dedicated for such rate is also

low as shown in Fig. 3.4. This creates degradation in the system throughput. When $p^{(1)}$ increases, the transmission rates decrease, whereas the power increases relatively. Consequently, the throughput is significantly improved.

3.5 Three-Class System Numerical Evaluation

Since our algorithm is derived for any number of multimedia classes, let us consider the case of a three-class system. Consider the three classes – *class-0*, *class-1* and *class-2* among which the users are equally distributed i.e. $p^{(0)} = p^{(1)} = p^{(2)} = 1/3$. Each class is characterized by its own QoS such that $\beta_0 = 11\,\text{dB}$, $\beta_1 = 8\,\text{dB}$, $\beta_2 = 5\,\text{dB}$, respectively. Without loss of generality, the classes are rearranged by descending order of QoS, such that the additional class comes first. Let $P_{Max} = 8\,\text{dBm}$ to be the maximum laser power. In order to respect the EEC power settings, notice that there are 3 dB differences between each two consecutive QoS's, and the transmission rates of the three classes are set to be $R_2 \cong 2R_1$ and $R_1 \cong 2R_0$.

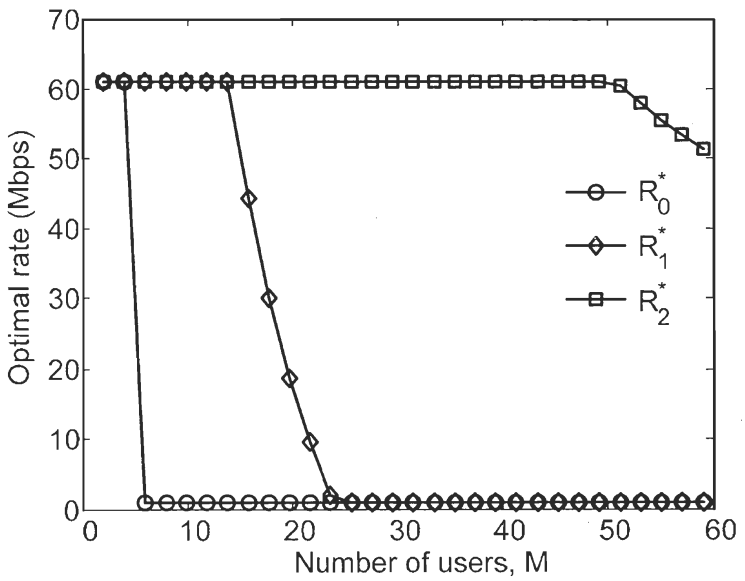

Fig. 3.9: The optimal transmission rates versus the number of users for a three-class system.

The three-class optimal transmission rates versus M are illustrated in Fig. 3.9. It is clear that only one class can transmit at rate between $R^{(\ell)}$ and $R^{(u)}$, and the other classes either at $R^{(\ell)}$ or $R^{(u)}$. This completely agrees with Lemma 3.1. Also, note that $R_0^* \le R_1^* \le R_2^*$ as $\beta_0 > \beta_1 > \beta_2$, which confirms the validity of Lemma 3.2 for the three-class system as well.

The effect of adding a third class, with high QoS, to the multirate system on the optimal transmission power is illustrated in Fig. 3.10. As M increases, the power increases to stabilize to 8 dBm. In addition, the upper bound powers of *class-1* and *class-2* have not changed since the two-class system even though their overall allocated powers have been slightly diminished with 3 dBm differences between each two consecutive classes. This is caused by the reduction in the user's population in each of the three classes and the augmentation of the total optical power in the fiber link. Furthermore, the power provided by EEC is not properly allocated. So that, less power is allocated for small number of users ($M < 20$), while more power is allocated for large number of users ($M > 20$).

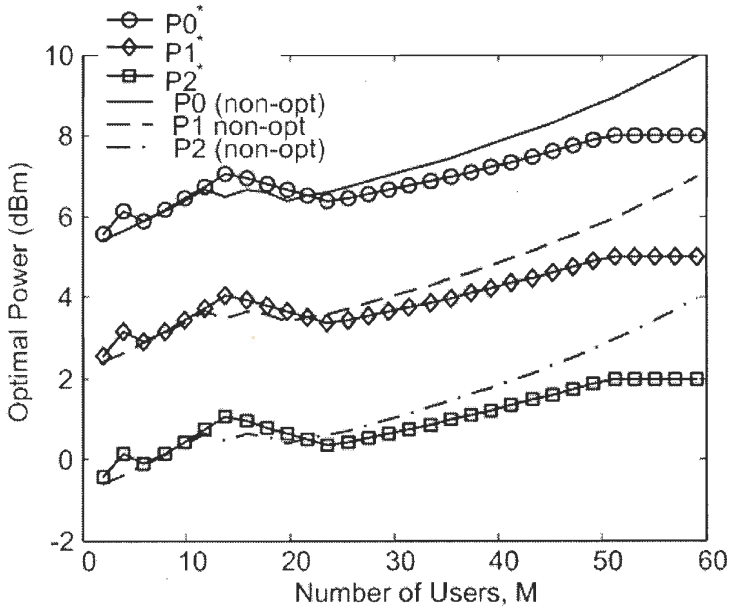

Fig. 3.10: The transmission power versus the number of users for a three-class system.

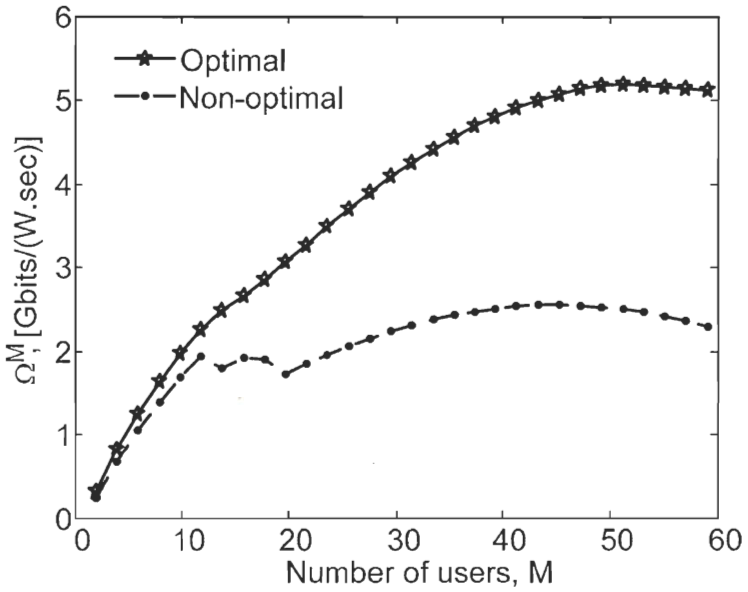

Fig. 3.11: The optimal throughput versus the total number of users for a three-class system.

The throughputs of both strategies are shown in Fig. 3.11. Notice that the performance of our proposed strategy is always superior to that of EEC.

3.6 Conclusion

A new resource allocation strategy was proposed for OV-CDMA system. With this strategy, the system throughput is the average successfully transmitted bits per second per unit of power. However, due to the non linearity of the throughput and the constraint functions and hence the optimization problem, two recourse allocation scenarios were derived for both power and rate to simplify the analysis. Then, the KT theorem had been applied on the rate allocation scenario to find out the optimal transmission rates upon which the optical intensity of each class was optimally regulated directly from the laser source. It was proven that this system, in general, has no global maximum but a local maximum for a given set of QoS's. This local maximum has as coordinates the transmission rates of the S classes satisfying Lemmas 3.1 and 3.2. Afterward, two- and three-class systems have been simulated as particular case-studies. The simulations assessed that multirate transmission

alternates among classes depending on which QoS region, users are adhering to, whether low or high, as well as on the total number of users exploiting the system and their distribution among those classes.

Chapter 4

A Fair QoS-Based Resource Allocation Scheme for a Time-Slotted Optical OV-CDMA Network: a Unified Approach

4.1 Introduction

Optical communications have become very mature, especially in the recent years. Many optical networks have been deployed with the aim of accommodating novel information-services generated by modern communication terminals like high-speed personal computers, FTTX networks and many others [67]. Those services require a huge amount of bandwidth, multirate transmission capabilities and consume more power due to the amount of data that can be handled. In this regard, we believe that this work can contribute to this research trend.

The optical overlapped CDMA (OV-CDMA) system has been proposed in [8] to increase the transmission rate of an optical communication system by overlapping consecutive bits while transmitted along the fiber. The question that arises here is: to what extent of bit overlapping and hence of transmission rate can the system admit such that the signal can be successfully received? In fact, all depends on the interference level and on the signal power that is injected into the fiber, or in other words on the signal-to-interference ratio (SIR). For this reason, we consider the SIR as the quality of service (QoS) metric in our analysis. Resource allocation schemes are necessary to enhance the performance of the optical network in order to guarantee successful data transmission and to satisfy the users' requirements. Many algorithms are found in the literature to cope with this problem. However, most of them have been proposed to deal with wireless systems [68]-[71], while few have been investigated to deal with optical-channel-based networks [58]-[61].

In Chapter 3, we have proposed a novel hybrid power/rate control algorithm for the optical OV-CDMA system. Our objective was to find the optimal overlapping coefficient through which we can achieve maximum transmission rate with minimum transmitted optical power directly from a laser source. The problem of this strategy is that it is not fair in the sense that there is at most one class of users that has an overlapping coefficient between zero and full overlap, and the remaining classes either transmit with full overlap or with no overlap. In addition, the model used in Chapter 3 did not support a time-slotted packetized network configuration as the one proposed in Chapter 2.

Further, the resource allocation at the PHY of the OV-CDMA-based packet network layer can have an impact on the contention for channel access at the MAC layer. The optimal resource allocation determines the best OV-CDMA transmission rate with the appropriate transmission power, tolerating a certain level of MAI by responding to the QoS requirement. Consequently, shaping the packets to the user population of various QoS conditions, the resource allocation reduces the risk of packet distortion. This influences the collision in the optical link especially when the offered load of the subscribers increases. Also, the resource allocation scheme enables the MAC protocol to bear multiple classes of QoS through supporting active users with dense OV-CDMA packets of fixed time-slot.

The first contribution of this work is to propose a unified framework for allocating and controlling the transmission rate and power for an OV-CDMA-based packet network, using matrix analysis. This approach is general in the sense that it can be applied for any expression of the system capacity. In addition, it is generalized to a time-slotted packetized system. The second contribution is the reduction of the optimization search space into one dimensional space. This target guarantees the simplicity of the algorithm, which is an important requirement in optical networks. Our third contribution is to solve the problem of unfairness in the resource allocation strategy presented in Chapter 3. In this way, we have extended the degree of freedom for allocating and controlling the resources of every class of users. Finally, the fourth contribution is the employment of the fair resource allocation scheme to optimize the performance of the OV-CDMA-based packet network at the MAC layer. In this way, the fairness and the optimality criteria of the allocated resource at the

PHY layer are preserved. The network throughput, subject to a minimum delay requirement, is then maximized through a delay-constraint fair resource allocation optimization approach.

The rest of the chapter is organized as follows. In Section 4.2, we present the system model where we introduce the main system parameters and the network under study. The performance of the network at the PHY layer has been discussed in Section 4.3. In Section 4.4, we investigate the proposed resource allocating and controlling scheme of the OV-CDMA-based packet network. In Section 4.5, we define and we analyze the network capacity upon which we determine the optimal control parameter that optimizes the allocated resources among classes. In Section 4.6, the delay-constraint fair resource allocation optimization approach is described. The simulation results and discussion are provided in Section 4.7. Finally, we close our work with a conclusion in Section 4.8.

4.2 System Model

Consider a multiclass time-slotted OV-CDMA system in an optical packet network in which K users are connected in a star topology as the one proposed in Chapter 2. The users are assigned different optical code signatures of equal PG G and are distributed over S classes. Each class-j, $\forall\ j \in \{0,1,...,S-1\}$, is characterized by its own and unique QoS, so that it has its proper transmission power P_j and its proper overlapping coefficient ε_j or equivalently a transmission rate R_j. We assume that this system operates at the link layer of the optical network. The users in this case transmit their coded bits at a given time slot in the form of packets of nominal length of L bits. However, due to the overlapping process, the maximum number of bits which a user can transmit per packet exceeds L as presented in Chapter 2 and shown in Fig. 2.4. Let $0 \le \varepsilon_j \le G-1$, $\forall\ j \in \{0,1,...,S-1\}$, be the overlapping coefficient and $X_{b,j}$ to be the total number of overlapped bits in a packet time slot. The expression of $X_{b,j}$ can be found in (2.4) and it is given by

$$X_{b,j} = \left\lfloor \frac{LG - \varepsilon_j}{G - \varepsilon_j} \right\rfloor \tag{4.1}$$

Consequently, the achievable transmission rate of class-*j* users is given by

$$R_j = \frac{X_{b,j}}{L} R_n \tag{4.2}$$

The main objective of this work is to determine the optimal number of bits to be transmitted per packet using the time-slotted OV-OCDMA system. In this system, the fundamental signal intensity that guarantees the transmission of such packet is directly controlled from the laser source. As a result, an improvement in the network capacity is attained with good performance, answering the required QoS. Accordingly, we investigate a resource controlling scheme which is strictly based on QoS and includes optimal allocations of the transmission rate and power to different classes.

4.3 System Performance

We are interested in evaluating the average SIR per bit in a given time slot for every class-*j*, which has its own power and overlapping coefficient and supporting K_j users. Then, the average SIR, as derived in [8], [58], is given by

$$\mathrm{SIR}_j(\boldsymbol{\varepsilon}, \mathbf{P}) = \frac{P_j G^2}{(K_j - 1) P_j \bar{\sigma}^2_{I_{kj}}(\varepsilon_j) + \sum_{\substack{s=0 \\ s \neq j}}^{S-1} \sum_{k=1}^{K_s} P_s \bar{\sigma}^2_{I_{ks}}(\varepsilon_s) + \sigma_n^2} \tag{4.3}$$

where $\boldsymbol{\varepsilon}$ and $\mathbf{P}$ are vectors of the overlapping coefficients and the transmission power of all classes, respectively. Using (2.15) and (2.16), $\bar{\sigma}^2_{I_{kj}}$ is the average multiple access interference (MAI) power imposed by a class-*j* user on the desired bit in a given time slot, and it is computed as

$$\bar{\sigma}^2_{I_{k_j}} = 2\sum_{i=0}^{X_{b,j}-X_{r,j}-1}\left[\sum_{\nu=-i}^{-1} H_\nu^2\left(0,q_\nu^{(i)}\right)+\sum_{\nu=0}^{X_{r,j}} H_\nu^2\left(q_\nu^{(i)},G\right)\right]\frac{\left(X_{b,j}-X_{r,j}\right)}{X_{b,j}}$$
$$+\sum_{i=X_{b,j}-X_{r,j}}^{X_{r,j}-1}\left[\sum_{\nu=-i}^{-1} H_\nu^2\left(0,q_\nu^{(i)}\right)+\sum_{\nu=0}^{X_{b,j}-i-1} H_\nu^2\left(q_\nu^{(i)},G\right)\right]\frac{\left(2X_{r,j}-X_{b,j}\right)}{X_{b,j}}$$
$$, \quad X_{b,j}-2X_{r,j}\le 0 \qquad (4.4)$$

and

$$\bar{\sigma}^2_{I_{k_j}} = 2\sum_{i=0}^{X_{r,j}-1}\left[\sum_{\nu=-i}^{-1} H_\nu^2\left(0,q_\nu^{(i)}\right)+\sum_{\nu=0}^{X_{r,j}} H_\nu^2\left(q_\nu^{(i)},G\right)\right]\frac{X_{r,j}}{X_{b,j}}$$
$$+\sum_{i=X_{r,j}}^{X_{b,j}-X_{r,j}-1}\left[\sum_{\nu=-X_{r,j}}^{-1} H_\nu^2\left(0,q_\nu^{(i)}\right)+\sum_{\nu=0}^{X_{r,j}} H_\nu^2\left(q_\nu^{(i)},G\right)\right]\frac{\left(X_{b,j}-2X_{r,j}\right)}{X_{b,j}}$$
$$, \quad X_{b,j}-2X_{r,j}>0 \qquad (4.5)$$

where $X_{r,j}=\left\lceil \varepsilon_j/\left(G-\varepsilon_j\right)\right\rceil$ as computed in [8]. In addition, $H_\nu^2\left(0,q_\nu^{(i)}\right)$ and $H_\nu^2\left(q_\nu^{(i)},G\right)$ are the partial period Hamming correlation functions. σ_n^2 represents the power of the other sources of noise modeled as Gaussian noise. It involves thermal noise, shot noise, dark current, and surface leakage current [72]-[75].

Assuming one-coincidence sequences, the average value of the partial period Hamming correlation functions can be easily computed and they are given by

$$\bar{H}_\nu^2\left(0,q_\nu^{(i)}\right)=\left(G+\nu(G-\varepsilon_j)\right)/F \qquad (4.6)$$

$$\bar{H}_\nu^2\left(q_\nu^{(i)},G\right)=\left(G-\nu(G-\varepsilon_j)\right)/F \qquad (4.7)$$

where F is total number of available wavelengths from which the code is constructed and ν is the bit index in packet. Using (4.6) and (4.7) in (4.4) and (4.5), we get $\bar{\sigma}^2_{I_{k_j}}$ in terms of the number of bits per packet as follows:

$$\bar{\sigma}^2_{I_{k_j}} = \begin{cases} \dfrac{-\frac{1}{3}\left(A_4 X_{b,j}^4 + A_3 X_{b,j}^3 + A_2 X_{b,j}^2 + A_1 X_{b,j} + A_0\right)}{F\left(L-1\right)^3 \left(X_{b,j}-1\right) X_{b,j}}, & L \le \dfrac{3X_{b,j}}{X_{b,j}+2}, \\ \dfrac{\left(B_3 X_{b,j}^3 + B_2 X_{b,j}^2 + B_1 X_{b,j} + B_0\right)}{F\left(L-1\right)^3 X_{b,j}}, & L > \dfrac{3X_{b,j}}{X_{b,j}+2}, \end{cases} \tag{4.8}$$

where A_i for $0 \le i \le 4$ and B_j for $0 \le j \le 3$ are constant coefficients, functions of the OV-CDMA system parameters G, F, and L. Their values are shown in appendix B.

We consider that the users are dispersed among classes according to a given distribution with a probability mass function (PMF) $p^{(j)}$ such that $\sum_{j=0}^{S-1} p^{(j)} = 1$. Therefore, the total number of users in class-j is given by $K_j = K\, p^{(j)}$ for $0 \le j \le S-1$.

4.4 Resource Allocation Strategy

Our strategy is very simple. It is based of the assumption that the QoS of class-j in the presence of other classes, given in (4.3), should meet the requirement

$$SIR_j \ge \beta_j \tag{4.9}$$

We define the solitary class-j SIR as the desired signal power over the power of a class-j interferer. It is given by

$$\gamma_j = \frac{G^2}{\bar{\sigma}^2_{I_{kj}}} \tag{4.10}$$

In addition, we define the nominal signal-to-noise ratio (SNR) that is common to all classes as

$$\gamma_n = \frac{G^2}{\sigma_n^2} \tag{4.11}$$

Using the definitions of the solitary class SIR in (4.10) and the nominal SNR in (4.11), the minimum requirements in (4.9) (which means with equality) gives S linear equations in the laser transmission power of each class as follows

$$\sum_{s=0}^{S-1}\frac{K_s}{\gamma_s}P_s-\left(\frac{1}{\gamma_j}+\frac{1}{\beta_j}\right)P_j+\frac{1}{\gamma_n}=0,\ \forall\ 0\le j\le S-1 \tag{4.12}$$

The solution of (4.12) represents the power allocation for all classes, and it can be obtained using a matrix analysis approach. It is clear that the power allocation is controlled by the solitary class SIR assuming the total number of users is constant and users transmit with given QoS's. Let $\Gamma=\mathrm{diag}\left(\frac{1}{\gamma_0},\cdots,\frac{1}{\gamma_{S-1}}\right)$, $\mathcal{B}=\mathrm{diag}\left(\frac{1}{\beta_0},\cdots,\frac{1}{\beta_{S-1}}\right)$, and $\mathcal{K}=\mathrm{diag}\left(K_0,\ldots,K_{S-1}\right)$ be $S\times S$ diagonal matrices. $\mathbf{P}=\left(P_0,\ldots,P_{S-1}\right)^T$ is the vector of the unknown transmission powers of the S classes, and $\mathbf{e}_{S\times 1}$ is a unity vector. Also, let $\mathbf{N}_D=\Gamma+\mathcal{B}$, $\mathbf{M}_D=\left(\mathbf{N}_D-\mathcal{B}\right)\mathcal{K}=\Gamma\mathcal{K}$. Then, the linear system in (4.12) can be reduced to $\left(-\mathcal{M}\right)\mathbf{P}=\frac{1}{\gamma_n}\mathbf{e}$, where $\mathcal{M}^{\mathrm{T}}=\mathbf{M}_D\mathbf{e}\mathbf{e}^T-\mathbf{N}_D$ is the system-performance matrix. Thereby, the power vector is given by

$$\mathbf{P}=\frac{1}{\gamma_n}\left(-\mathcal{M}^{-1}\right)\mathbf{e} \tag{4.13}$$

The objective here is to determine the optical power that maintains the demanded QoS while forcing the chip overlapping to occur to a certain extent that will be determined later in order to increase the transmission rate of the users. From linear algebra, we have $\left(-\mathcal{M}^{-1}\right)^T=\left(-\mathcal{M}^T\right)^{-1}$. Applying the Sherman-Morrison matrix inversion formula [76], which states that for any nonsingular matrix $A\in\mathbb{R}^{n\times n}$, $b,c\in\mathbb{R}^n$ and $1+c^TA^{-1}b\neq 0$,

$$\left(A+bc^T\right)^{-1}=A^{-1}-\frac{A^{-1}bc^TA^{-1}}{1+c^TA^{-1}b}, \tag{4.14}$$

we obtain

$$\left(\mathbf{N}_D - \mathbf{M}_D \mathbf{e}\mathbf{e}^T\right)^{-1} = \mathbf{N}_D^{-1} + \frac{\mathbf{N}_D^{-1}\mathbf{M}_D \mathbf{e}\mathbf{e}^T \mathbf{N}_D^{-1}}{1 - \mathbf{e}^T \mathbf{N}_D^{-1}\mathbf{M}_D \mathbf{e}}$$
$$= \left(\mathbf{I} + \frac{1}{\zeta}\mathbf{N}_D^{-1}\mathbf{M}_D \mathbf{e}\mathbf{e}^T\right)\mathbf{N}_D^{-1} \tag{4.15}$$

where $\mathbf{I}$ is an $S \times S$ identity matrix. This implies that

$$\left(-\mathcal{M}^{-1}\right) = \frac{1}{\zeta}\begin{bmatrix} \left(\frac{\beta_0}{1+\frac{\beta_0}{\gamma_0}}\right)\left(\zeta + \frac{K_0\frac{\beta_0}{\gamma_0}}{1+\frac{\beta_0}{\gamma_0}}\right) & \cdots & \left(\frac{\beta_0}{1+\frac{\beta_0}{\gamma_0}}\right)\left(\frac{K_{S-1}\frac{\beta_{S-1}}{\gamma_{S-1}}}{1+\frac{\beta_{S-1}}{\gamma_{S-1}}}\right) \\ \left(\frac{\beta_1}{1+\frac{\beta_1}{\gamma_1}}\right)\left(\frac{K_0\frac{\beta_0}{\gamma_0}}{1+\frac{\beta_0}{\gamma_0}}\right) & \cdots & \left(\frac{\beta_1}{1+\frac{\beta_1}{\gamma_1}}\right)\left(\frac{K_{S-1}}{1+\frac{\beta_{S-1}}{\gamma_{S-1}}}\right) \\ \vdots & \ddots & \vdots \\ \left(\frac{\beta_{S-1}}{1+\frac{\beta_{S-1}}{\gamma_{S-1}}}\right)\left(\frac{K_0\frac{\beta_0}{\gamma_0}}{1+\frac{\beta_0}{\gamma_0}}\right) & \cdots & \left(\frac{\beta_{S-1}}{1+\frac{\beta_{S-1}}{\gamma_{S-1}}}\right)\left(\zeta + \frac{K_{S-1}\frac{\beta_{S-1}}{\gamma_{S-1}}}{1+\frac{\beta_{S-1}}{\gamma_{S-1}}}\right) \end{bmatrix} \tag{4.16}$$

where

$$\zeta \equiv 1 - \mathbf{e}^T \mathbf{N}_D^{-1}\mathbf{M}_D \mathbf{e} = \sum_{s=0}^{S-1}\left[\frac{K_s}{1+\beta_s/\gamma_s}\right] - (K-1), \quad \zeta > 0 \tag{4.17}$$

Notice that the matrix depends on the QoS requirement and the solitary SIR of each class of users namely β_j and γ_j, respectively. Consequently, substituting (4.15) in (4.13) we get

$$\mathbf{P} = \frac{1}{\gamma_n}\left(\mathbf{e}^T\left(\mathbf{I} + \frac{1}{\zeta}\mathbf{N}_D^{-1}\mathbf{M}_D \mathbf{e}\mathbf{e}^T\right)\mathbf{N}_D^{-1}\right)^T = \frac{\mathbf{N}_D^{-1}\mathbf{e}}{\zeta\gamma_n}$$
$$= \frac{1}{\zeta\gamma_n}\left(\frac{\beta_0}{1+\beta_0/\gamma_0}, \cdots, \frac{\beta_{S-1}}{1+\beta_{S-1}/\gamma_{S-1}}\right)^T \tag{4.18}$$

When $\zeta = 0$, the optical intensity is extremely high, which leads to nonlinear effects and causes severe degradation of the signal [75]. To avoid this situation, we impose constraints on the power of each class of users. Therefore, we consider that the optical power is upper bounded by $\Pi = (\pi_0, ..., \pi_{S-1})^T$ such that

$$P_j \le \pi_j, \quad \forall \quad 0 \le j \le S-1 \tag{4.19}$$

Lemma 4.1*: The linear system in (4.12) constrained by (4.19) has a solution if and only if the solitary class-j SIR, γ_j, is lower bounded by*

$$\gamma_j^* = \frac{(K-1)\pi_j}{\sum_{s=0}^{S-1} \frac{K_s \pi_s}{\beta_s} - (K-1)\frac{\pi_j}{\beta_j} - \frac{1}{\gamma_n}} \tag{4.20}$$

Proof:

$\mathbf{P} \le \Pi$ and $\Pi = (\pi_0, ..., \pi_{S-1})^T$ is the upper bound power level vector. The power allocation vector can thus be written as

$$\begin{aligned} \mathbf{P} &= \frac{\mathbf{N}_D^{-1}\mathbf{e}}{\gamma_n\left(1 - \mathbf{e}^T \mathbf{N}_D^{-1}\mathbf{M}_D\mathbf{e}\right)} \\ &= \frac{\mathbf{N}_D^{-1}\mathbf{e}}{\gamma_n\left((\mathcal{K}\mathbf{e})^T \mathcal{B}\mathbf{N}_D^{-1}\mathbf{e} - \mathbf{e}^T\mathcal{K}^T\mathbf{e} + 1\right)} \le \Pi \end{aligned} \tag{4.21}$$

From (4.21) we are able to derive a minimal bound for γ_j due to the linearity of the system. Thereby, by arranging the terms we obtain

$$\mathbf{N}_D^{-1}\mathbf{e} \ge \gamma_n(K-1)\left(-\left(\mathbf{I} - \gamma_n \Pi(\mathcal{K}\mathbf{e})^T \mathcal{B}\right)^{-1}\right)\Pi$$

Using Sherman-Morrison formula [76] to compute the inverse, we get

$$\left(\mathbf{I}-\gamma_n\Pi\left(\mathcal{K}\mathbf{e}\right)^T\mathcal{B}\right)^{-1}=\left[\left(\mathbf{I}-\gamma_n\mathcal{B}^T\left(\mathcal{K}\mathbf{e}\right)\Pi^T\right)^{-1}\right]^T$$
$$=\mathbf{I}+\frac{\gamma_n\Pi\left(\mathcal{K}\mathbf{e}\right)^T\mathcal{B}}{1-\gamma_n\Pi^T\mathcal{B}^T\left(\mathcal{K}\mathbf{e}\right)}$$

This yields

$$\mathbf{N}_D^{-1}\mathbf{e}\geq\frac{\gamma_n\left(K-1\right)}{\gamma_n\left(\mathcal{K}\mathbf{e}\right)^T\mathcal{B}\Pi-1}\Pi \tag{4.22}$$

Then, from (4.22) we evaluate the upper bound of γ_j for each class. This gives

$$\left(\frac{\beta_0}{1+\beta_0/\gamma_0},\cdots,\frac{\beta_{S-1}}{1+\beta_{S-1}/\gamma_{S-1}}\right)^T\geq\frac{\gamma_n\left(K-1\right)}{\gamma_n\left(\mathcal{K}\mathbf{e}\right)^T\mathcal{B}\Pi-1}\Pi$$

Therefore, we can write

$$\frac{1}{\gamma_j}\leq\frac{\sum_{s=0}^{S-1}\frac{K_s\pi_s}{\beta_s}-\frac{1}{\gamma_n}}{\left(K-1\right)\pi_j}-\frac{1}{\beta_j}$$

which implies that the SIR of solitary class-*j* should satisfy

$$\gamma_j\geq\gamma_j^*\equiv\frac{\left(K-1\right)\pi_j}{\sum_{s=0}^{S-1}\frac{K_s\pi_s}{\beta_s}-\left(K-1\right)\frac{\pi_j}{\beta_j}-\frac{1}{\gamma_n}} \tag{4.23}$$

and γ_j^* is the minimal bound of the signal-to-interference ratio of solitary class-*j* that should be respected to guarantee the system's requirements. ■

Lemma 4.2: *For a given value of* π_j *and* β_j, γ_j^* *in (4.20) always exists* $\forall\, 0 \le j \le S-1$.

Proof:

We know that $\gamma_j^* > 0$ which implies that

$$\sum_{s=0}^{S-1} \frac{K_s \pi_s}{\beta_s} - (K-1)\frac{\pi_j}{\beta_j} - \frac{1}{\gamma_n} > 0, \forall\, 0 \le j \le S-1. \tag{4.24}$$

By averaging (4.24) over all classes, we obtain

$$E_s\left\{\frac{\pi_s}{\beta_s}\right\} > \frac{1}{\gamma_n} \tag{4.25}$$

On the other hand, from (4.24) we have

$$\frac{\pi_j}{\beta_j} < \frac{KE_j\left\{\pi_j/\beta_j\right\} - \dfrac{1}{\gamma_n}}{K-1}, \quad \forall\, j \in \{0,1,...,S-1\}. \tag{4.26}$$

In addition, (4.24) can be written in a matrix form as

$$\left(\mathcal{K}\mathbf{e}\mathbf{e}^T - (K-1)\mathbf{I}\right)^T \mathcal{B}\Pi > \frac{1}{\gamma_n}\mathbf{e} \tag{4.27}$$

Then, by solving the linear system (4.27) for $\frac{\pi_j}{\beta_j}$, we get

$$\mathcal{B}\Pi > \frac{1}{\gamma_n}\left(-\left((K-1)\mathbf{I} - \mathcal{K}\mathbf{e}\mathbf{e}^T\right)^{-1}\right)^T \mathbf{e} \tag{4.28}$$

$$\Rightarrow \frac{\pi_j}{\beta_j} > \frac{1}{\gamma_n}, \forall j \tag{4.29}$$

Thus, we can write

$$\frac{1}{\gamma_n} < \frac{\pi_j}{\beta_j} < \frac{KE_j\left\{\frac{\pi_j}{\beta_j}\right\} - \frac{1}{\gamma_n}}{K-1}, \quad \forall\, 0 \le j \le S-1 \tag{4.30}$$

Using (4.30), it is clear that γ_j^* is bounded as follows

$$0 < \gamma_j^* < \infty \quad \forall\, 0 \le j \le S-1 \tag{4.31}$$

This means that γ_j^* is finite, therefore it always exits. ■

Notice that (4.30) yields the admissible interval of the power convergence. Also, we remark that if a high QoS is required, then either high power or a high SNR is needed in order to recuperate the information signal merged in the induced noise.

In this chapter, the power allocation is assumed to be fair among all classes, which means that no class can dominate the others due to a high power allocation. Hence, let the ratio π_j/β_j be arbitrarily identical for all classes. Thus, let α be a control parameter whose role is to manage the power level that is necessary to satisfy the required QoS and to achieve a rate augmentation whenever possible while maintaining the fairness criterion. It is given by

$$\frac{\pi_j}{\beta_j} = \frac{\alpha}{\gamma_n}, \forall\ 0 \le j \le S-1 \tag{4.32}$$

The domain of α can be obtained from Lemma 4.2. The optimal value of α should be the one that maximizes the network capacity. On the other hand, substituting (4.32) in (4.23) yields

$$\gamma_j^* = \frac{\alpha}{\alpha - 1}(K-1)\beta_j \tag{4.33}$$

4.4.1 Rate Allocation and Control Scheme

Note that, as γ_j increases, $\bar{\sigma}^2_{I_{k_j}}$ decreases. This, in turn, results in a reduction of the number of overlapping bits per packet, and hence a reduction of the transmission rate. From (4.10) and (4.23), we define the rate characteristic polynomial as the difference between the average interference variance per bit period and the target interference variance as

$$\rho\left(R_j\right) \equiv \bar{\sigma}^2_{I_{k_j}} - \frac{G^2}{\gamma^*_j} \tag{4.34}$$

It is clear that because $\gamma_j \geq \gamma^*_j$, $\rho\left(R_j\right)$ should be less or equal to zero. Setting $\rho\left(R_j\right)$ to zero, we compel the system to hit the target MAI. Since $\bar{\sigma}^2_{I_{k_j}}$ is a function of $X_{b,j}$, and hence of R_j, the rate-characteristic polynomial permit us to determine the feasible transmission rate region as well as to extract the transmission rate that meets the QoS requirement as it will be proved next in lemma 4.3. Therefore, the admissible region of the transmission rate is given by

$$\mathcal{R} = \left\{ R_j : R_n \leq R_j \leq \frac{(L-1)G+1}{L} R_n, s.t.\ \rho\left(R_j\right) \leq 0, \forall\ j \in \{0,1,...,S-1\} \right\} \tag{4.35}$$

Lemma 4.3*: Let $\beta^{(\ell)}$ and $\beta^{(u)}$ be the lower and the upper-bound QoS, respectively. They are given by*

$$\beta^{(\ell)} = \frac{G^2\left(1-1/\alpha\right)}{(K-1)\max\left\{\bar{\sigma}^2_{I_{k_j}}\right\}},\quad \beta^{(u)} = \frac{G^2\left(1-1/\alpha\right)}{(K-1)\min\left\{\bar{\sigma}^2_{I_{k_j}}\right\}}$$

The maximum admissible transmission rate of class-j users is given by the highest admissible root of the rate-characteristic polynomial when $\beta^{(\ell)} \leq \beta_j \leq \beta^{(u)}$, and it is the

maximum possible rate $R^{(u)}$ *of the optical OV-CDMA system when* $\beta_j < \beta^{(\ell)}$. *The system has no feasible solution when* $\beta_j > \beta^{(u)}$.

Proof:

Let $R^{(\ell)} = R_n$ and $R^{(u)} = \frac{(L-1)G+1}{L} R_n$ be the lower and the upper possible transmission rates of the system, respectively. Also, let $R_j \in \mathcal{R}$ be the rate for class-*j* users. In addition, we define $r_j^{(\kappa)}$ as the κ^{th} root of the rate-characteristic polynomial $\rho\left(R_j\right) = 0$ of class-*j*. From (4.8) and (4.34), we note that $\rho\left(R_j\right) = 0$ can be either third or forth order polynomial. Thus, $\kappa \in \mathbf{I}_r \equiv \{1,2,3,4\}$. On the other hand, $\rho\left(R_j\right) = 0$ can have either one, two or three extremes. Thus, we define $R_j\left(\rho_{\min}\right)$ and $R_j\left(\rho_{\max}\right)$ to be the transmission rates for class-*j* users that correspond to any minimum or any maximum of ρ, respectively.

First, we need to show that the polynomial roots cannot go beyond $R^{(u)}$, i.e. $\forall\kappa$, $r_j^{(\kappa)} \le R^{(u)}$. Given a class-*j* whose users transmit at $R^{(u)}$, then the induced MAI is the maximum possible one. Hence, let $\bar{\sigma}^2_{I_{k_j}}\left(R^{(u)}\right) \equiv \bar{\sigma}^2_{\max}$. This yields $\bar{\sigma}^2_{I_{k_j}}\left(R_j \le R^{(u)}\right) \le \bar{\sigma}^2_{\max}$, so $\gamma_j \ge \gamma^{(\ell)} \equiv G^2/\bar{\sigma}^2_{\max}$. On the other hand, $\forall\kappa$, $r_j^{(\kappa)}$ corresponds to the case where $\rho\left(R_j = r_j^{(\kappa)}\right) = 0$, i.e. $\gamma_j = \gamma_j^*$. By hypothesis, this implies that $r_j^{(\kappa)}$ satisfy the QoS requirement (i.e. $SIR_j \ge \beta_j$); hence $\gamma^{(\ell)} \le \gamma_j^*$. Using (4.33), the lowest possible QoS allowed for all classes is given as

$$\beta^{(\ell)} = \frac{G^2\left(1-1/\alpha\right)}{\left(K-1\right)\bar{\sigma}^2_{\max}} \tag{4.36}$$

This means that the minimal solitary class-*j* SIR cannot go beneath the one that is determined by the system as long as $\beta_j \ge \beta^{(\ell)}$. Thus, the polynomial roots are always

smaller than the upper bound transmission rate. (In view of the above, if $r_j^{(\kappa)} > R^{(u)}$, then the required QoS is less than β_j, which contradicts the hypothesis.)

Second, we prove that there exists $r_j^{(\kappa)}$ such that $R^{(\ell)} \le r_j^{(\kappa)} \le R^{(u)}$. So, assume that $\exists \kappa \in \mathbf{I}_r$, $r_j^{(\kappa)} \ge R^{(\ell)}$. This implies $\bar{\sigma}^2_{I_{k_j}}\left(r_j^{(\kappa)}\right) > \bar{\sigma}^2_{I_{k_j}}\left(R^{(\ell)}\right) \equiv \bar{\sigma}^2_{\min}$, which in turn yields

$$\gamma_j^* \le \frac{G^2}{\bar{\sigma}^2_{\min}} \equiv \gamma^{(u)} \tag{4.37}$$

Notice that the last inequality is inherently valid because as the transmission rate R_j moves toward $R^{(\ell)}$, γ_j goes far beyond γ_j^* and lemma 1 is satisfied. Combining (4.33) with (4.37), we obtain the maximum QoS for all classes below which $r_j^{(\kappa)} \ge R^{(\ell)}$ as

$$\beta^{(u)} = \frac{G^2\left(1-1/\alpha\right)}{\left(K-1\right)\bar{\sigma}^2_{\min}} \tag{4.38}$$

Since $\bar{\sigma}^2_{\min}$ is the minimum interference when no overlapping occurs, the maximum number of bits transmitted per time slot is $X_{b,j} = L$ which satisfies the second term in (4.8). Then, $\bar{\sigma}^2_{\min} = \frac{LG}{F}$ and the upper bound QoS becomes

$$\beta^{(u)} = \frac{GF\left(1-1/\alpha\right)}{\left(K-1\right)L} \tag{4.39}$$

In order for the rate-characteristic polynomial to have at least one solution $r_j^{(\kappa)}$ such that $R^{(\ell)} \le r_j^{(\kappa)} \le R^{(u)}$, the condition $\beta^{(\ell)} \le \beta_j \le \beta^{(u)}$ must be fulfilled.

Accordingly, we will determine the admissible region of the transmission rate of all classes by considering the following cases:

(i) If $R^{(\ell)} \le r_j^{(\kappa)} < R_j < R_j(\rho_{\min}) \le R^{(u)}$, $\rho(R_j) < 0$ and $\frac{d\rho}{dR_j} < 0$. This means that $\rho(R_j)$ is a monotonically decreasing function of R_j. In other words, the induced interference diminishes as the transmission rate increases, which is a contradiction. It implies that this region is not feasible in $\mathcal{R}$.

(ii) If $R^{(\ell)} \le R_j(\rho_{\min}) \le R_j < r_j^{(\kappa)} \le R^{(u)}$, $\rho(R_j) < 0$ and $\frac{d\rho}{dR_j} > 0$. This means that $\rho(R_j)$ is a monotonically increasing function of R_j. This implies that $\rho(R_j)$ increases toward zero as R_j increases toward $r_j^{(\kappa)}$, a deduction which agrees with our assumption. Hence, this region is feasible in $\mathcal{R}$.

(iii) If $R^{(\ell)} \le R_j = r_j^{(\kappa)} \le R^{(u)}$, it is the region of R_j that corresponds to the set of roots $r_j^{(\kappa)}, \kappa \in \mathbf{I}_r$, of $\rho(R_j) = 0$. It represents the case where the induced interference is the highest. Thus, this region is also feasible in $\mathcal{R}$.

As a result, the admissible region of the transmission rate R_j of class-*j* can be written as $(\mathcal{E}1 \cup \mathcal{E}2)$ where

$$\mathcal{E}1 = \left\{ R_j : R_j \in \mathcal{R}, \exists \kappa \in \mathbf{I}_r, \max\left(R^{(\ell)}, R_j(\rho_{\min})\right) \le R_j \le r_j^{(\kappa)} \le \min\left(R_j(\rho_{\max}), R^{(u)}\right) \right\}$$
$$\mathcal{E}2 = \left\{ R_j : R_j \in \mathcal{R}, \exists \kappa \in \mathbf{I}_r, \max\left(R^{(\ell)}, R_j(\rho_{\max})\right) \le R_j = r_j^{(\kappa)} \le \min\left(R_j(\rho_{\min}), R^{(u)}\right) \right\} \tag{4.40}$$

Now, let the transmission rate $R_j^* \in \mathcal{E}1 \cup \mathcal{E}2$ represent the highest transmission rate that a user in a given class-*j* can reach. If $\exists r_j$, $r_j = \max_{r_j^{(\kappa)} \in \mathcal{R} \cap (\mathcal{E}1 \cup \mathcal{E}2)} \left(r_j^{(\kappa)}\right)$, then

$$R_j^* = \sup_{R_j \in \mathcal{E}1 \cup \mathcal{E}2} (R_j) = r_j . \tag{4.41}$$

In the case where $\beta_j < \beta^{(\ell)}$ or $\beta_j > \beta^{(u)}$, the roots of the rate-characteristic equation fall outside the feasible range and we have two situations. First, if $\forall \kappa$, $r_j^{(\kappa)} < R^{(\ell)}$, $\beta_j > \beta^{(u)}$. The system has no feasible solution. In other words, the system cannot tolerate any optical bit-overlapping process with such QoS. Second, if $\forall \kappa$, $r_j^{(\kappa)} \notin \mathcal{R}$, there exists at least one root $r_j^{(\kappa')} > R^{(u)}$ ($\beta_j < \beta^{(\ell)}$) and $r_j^{(\kappa)} < R^{(\ell)} < R^{(u)} < R_j(\rho_{\min}) < r_j^{(\kappa')}$ (similar to statement (i)); the system does not have a feasible solution, as well. Otherwise, we define the admissible region

$$\mathcal{E}3 = \left\{ R_j : R_j \in \mathcal{R}, \forall \kappa \in \mathbf{I}_r, r_j^{(\kappa)} \notin \mathcal{R}, \max\left(R^{(\ell)}, R_j(\rho_{\min})\right) \le R_j \le R^{(u)} \right\}. \qquad (4.42)$$

This implies that if $R_j^* \in \mathcal{E}3$, $R_j^* = R^{(u)}$. ■

As an example, consider a three-class system. Assume that the users are distributed among the classes as follows: 40% in class-0 and 30% in each class-1 and class-2. The *PG* is G = 61. Finally, we select $\gamma_n = 15\,\text{dB}$ common to all classes. The QoS requirements are assumed to be β_0 = 4 dB, β_1 = 8 dB, and β_2 = 12 dB for class-0, class-1 and class-2, respectively. Fig. 4.1 depicts the third-order rate-characteristic polynomial by which the transmission-rate feasible regions for the three classes are determined, given that the nominal packet time-slot is $L = 1024$ bit-period and assuming $\alpha = 1.5$. It is obvious that as K and β_j increase, $\rho(R_j/R_n)$ moves up above the zero-axis. For instance, for $K = 10$ users, the admissible regions $\mathcal{E}1 \cup \mathcal{E}2$ (in boldface line) of class-0, class-1 and class-2 are $\{4.25 \le R_0/R_n \le 7.41\} \cup \varnothing$, $\{2.71 \le R_1/R_n \le 4.67\} \cup \varnothing$, and $\{1.72 \le R_2/R_n \le 2.95\} \cup \varnothing$, respectively. Clearly, when K and β_j exceed certain values, there will be no feasible solution. Thus, the numerical results in Fig. 4.1 absolutely comply with the theoretical results obtained in Lemma 4.2 and Lemma 4.3.

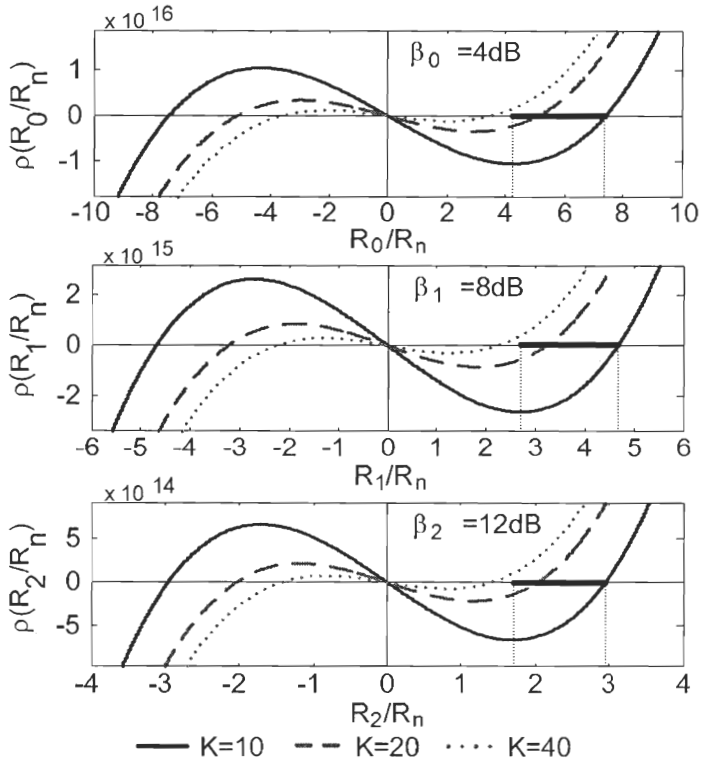

Fig. 4.1: The rate characteristic polynomials of three classes for $L = 1024$, $\alpha = 1.5$ and $\gamma_n = 15$ dB.

4.4.2 Power Allocation and Control Scheme

The optimal transmission power for every class of users is obtained throughout the following lemma.

Lemma 4.4: *The optimal transmission power of users in any class-j, transmitting at the maximum admissible rate* R_j^*, *is given by*

$$P_j^* = \begin{cases} \pi_j = \alpha \dfrac{\beta_j}{\gamma_n}, & \text{for } \beta^{(\ell)} \le \beta_j \le \beta^{(u)} \\ \dfrac{\dfrac{\beta_j}{1+\beta_j/\gamma^{(\ell)}}}{\gamma_n\left(\displaystyle\sum_{s=0}^{S-1}\frac{K_s}{1+\beta_s/\gamma^{(\ell)}} - (K-1)\right)} < \pi_j, & \text{for } \beta_j < \beta^{(\ell)} \end{cases} \tag{4.43}$$

and P_j^* *is not feasible for* $\beta_j > \beta^{(u)}$.

Proof:

From Lemma 4.1 and Lemma 4.3, we have that for $\beta^{(\ell)} \le \beta_j \le \beta^{(u)}$ the maximum admissible transmission rate of any class-*j* is achieved when $\gamma_j = \gamma_j^*$. Substituting this in (4.18), we get $P_j^* = \pi_j$, $\forall j$. On the other hand, for $\beta_j < \beta^{(\ell)}$, we have from Lemma 4.3 $R_j^* = R^{(u)}$. This means that lowering the QoS below $\beta^{(\ell)}$ does not yield a rate increment above the upper-bound cutoff-rate $R^{(u)}$. This yields $\bar{\sigma}_{I_{k_j}}^2\left(R_j^*\right) = \bar{\sigma}_{\max}^2$ and hence $\gamma_j = \gamma^{(\ell)}$. Substituting the last term in (4.18) we get $P_j^* < \pi_j$. Also, for $\beta_j > \beta^{(u)}$ there is no feasible transmission rate and thus, no feasible power. ■

Lemma 4.4 states that optimal transmission power that guarantees a user in specific class to achieve a maximum transmission rate is the upper bound intensity level $\left(P_j^* = \pi_j\right)$ in the case where $\beta^{(\ell)} \le \beta_j \le \beta^{(u)}$. π_j has to be determined according to the system requirements since it depends on the control parameter, whereas, in the case $\beta_j < \beta^{(\ell)}$, the optimal transmission power is less than the upper bound power $\left(P_j^* < \pi_j\right)$, and it is known since it depends on the system's design parameters.

Observation: *When $\beta_j < \beta^{(\ell)}$, the resource allocation is uncontrollable. It results directly from Lemma 4.3 and Lemma 4.4 that both R_j^* and P_j^* are independent of the control parameter α. Therefore, both resources are uncontrollable.* ■

In light of the above observation, we adopt $\beta^{(\ell)} \le \beta_j \le \beta^{(u)}$ as the QoS operating interval for the remaining analysis. Thus, Lemma 4.3 and Lemma 4.4 indicate that any class-*j* user in the OV-CDMA packet-network can realize its highest transmission rate at the minimum required QoS (i.e. $SIR_j = \beta_j$) in the QoS operating interval when the optical transmission power is at the maximum level (i.e. π_j).

4.5 Capacity Analysis

One of the challenges that exist usually in resource allocation problems is the model of the network throughput or the actual network capacity that reflects real situations [71]. In most network applications, researchers attempt to raise the amount of the transmitted bits while preserving the existing channel characteristics. This task necessitates a complex control mechanism while keeping network power consumption as low as possible. Therefore, it is logical to model the capacity in our network as the ratio of the total transmission rate to the total transmission power which is given by

$$C = \frac{\sum_j p^{(j)} R_j^*(\alpha)}{\sum_j p^{(j)} P_j^*(\alpha)} = \frac{\sum_j K_j R_j^*(\alpha)}{\sum_j K_j P_j^*(\alpha)} \tag{4.44}$$

where $R_j^*(\alpha)$ is the transmission rate for class-*j* users given in (4.41) and obtained by Lemma 4.3. On the other hand, $P_j^*(\alpha)$ is the laser transmission power for class-*j* users given in (4.43) and obtained by Lemma 4.4. If we consider R_j^* normalized by R_n, then C can be seen as the per-user network capacity normalized by R_n per unit of power. Our proposed criterion consists of finding the optimal control parameter α^* that maximizes $C(\alpha)$ such as

$$\alpha^* = \arg\max_{\alpha>1}\{C(\alpha)\} \tag{4.45}$$

As a result, $P_j^*(\alpha^*)$ and $R_j^*(\alpha^*)$ are optimally controlled via α^*.

Furthermore, we define the nominal capacity when all users transmit at nominal rate R_n as

$$C_n = \frac{R_n}{\sum_j p^{(j)} P_j^*} = \frac{R_n}{\alpha \sum_j p^{(j)} \beta_j} \gamma_n \tag{4.46}$$

The control parameter is obtained as $\alpha_n^* = \arg\max_{\alpha>1}\{C_n(\alpha)\}$. This implies $\alpha_n^* = \min(\alpha > 1)$.

Having obtained the optimal control parameter that fairly and optimally allocates the physical resources, the maximum average physical capacity per user in each class is guaranteed. Fig. 4.2 summarizes the fair resource allocation algorithm based on the QoS demand in the OV-CDMA-based packet access network. The flowchart illustrates the simplicity of the proposed scheme which makes it easy to apply in the optical network.

Note that, in Chapter 2, we investigated the performance of OV-CDMA-based packet access network without any optimality consideration of the system's parameters at both the PHY layer and the MAC layer. However, the numerical results showed that the OV-CDMA system still offers a good throughput with a low delay at low and medium transmission rate levels and an acceptable performance at high rate. In addition, the performance was assessed at unity transmission power. Thus, in order to achieve an optimal MAC performance while preserving the optimality consideration of the PHY layer, the fair resource allocation scheme is considered in the MAC optimization. In other words, the optimal control parameter that optimizes the maximum transmission rate and power, obtained by the proposed scheme at the PHY layer, should be now the one that maximizes the MAC throughput. At the same time, a maximum average packet delay should be satisfied as a requirement. Hence, a delay-

constraint fair resource allocation approach is proposed to optimize the throughput of the OV-CDMA-based packet access network at the MAC layer while preserving the fairness and the optimality criteria at the PHY layer. Note that, due to its simplicity, the proposed resource allocation can be easily integrated in the MAC optimization as described in the next section.

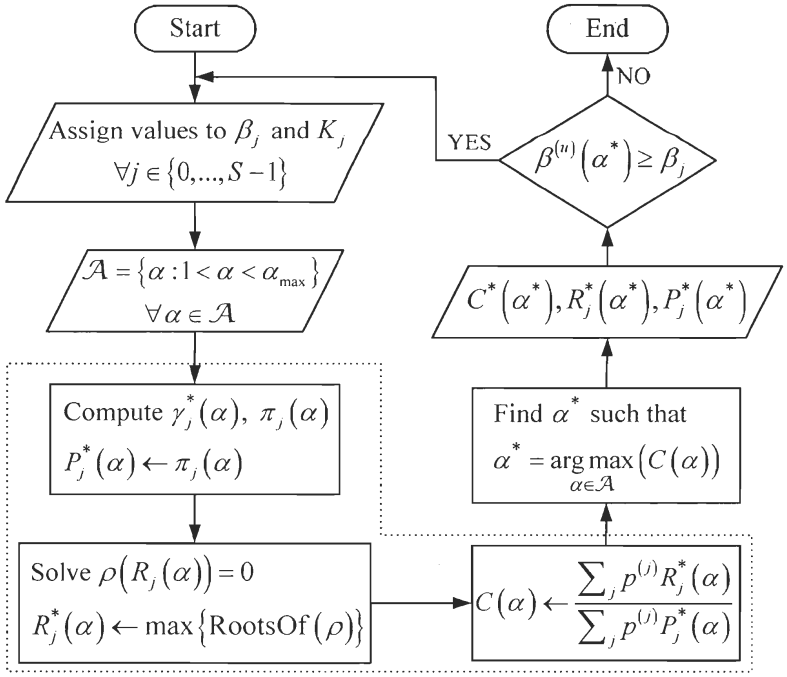

Fig. 4.2: Fair QoS-based resource allocation flowchart.

4.6 Delay-Constraint Fair Resource Allocatoin

At the MAC layer, a general control protocol is used to manage the packet transmission of OV-CDMA users of each class j in a general framework. Each user is equipped with a buffer to store one newly originated packet at a time. This packet is transmitted in the next available time slot. If K_j users are supported by class-j, then K_j forms the offered load of this class, so that up to K_j packets can be delivered in any time slot. Consequently, the offered load constitutes the link parameter between the MAC layer and the PHY layer where

the value of K_j strictly depends on the allocated resources. However, due to MAI of undesired users and that of the overlapping process, some packets are unsuccessfully received at the destination. The packet collision is introduced as the case where a certain number of users simultaneously attempt transmitting their packets in a noisy channel, those packets are collided with the MAI-induced noise (i.e. the transmitting users exceed the MAI channel capacity). Therefore, MAI reduces the number of successfully delivered packets, and hence reduces the network throughput. The erroneous packets then need to be retransmitted after a random delay. Thus, the queueing sojourn time of the backlogged packet, which is the period of time a packet stay backlogged in the buffer until it is successfully delivered increases, and hence the network delay. In order to avoid large network delay, a delay bound is imposed to form a requirement at the MAC layer as a service that should be respected by the PHY layer. That is, the resources should be optimally allocated to the users at the PHY layer in a way that to maximize the MAC layer throughput while considering its delay requirement.

4.6.1 Perfomance Evaluation

Assuming that the QoS of class-*j* in the presence of other classes meet the minimal requirement i.e. $SIR_j = \beta_j$, the average bit error probability faced by each class-*j* user with target QoS β_j, is constant and is expressed as

$$\overline{P}_{b,j}\left(\beta_j\right) = Q\left(\frac{1}{2}\sqrt{\beta_j}\right) \tag{4.47}$$

It was shown in Chapter 2 that in the joint BER, $P_{b,j}\left(K_j, i\right)$, the error bit depends on the bit position i in the packet since SIR varies according to the number of overlapping bits at every bit position. Thus, by taking the average of SIR over all bits of the packet, targeted to a certain values β_j, the average BER becomes constant i.e. independent of the number of users which is included implicitly, and also independent of *i*, which is uniformly distributed

over the interval $\left[1, X_{b,j}\right]$. The joint probability of the average erroneous bit at any bit position can be written as

$$\overline{P}_{b,j}\left(\beta_j, i\right) = \frac{P_{b,j}\left(K_j, i\right)}{X_{b,j}} = \frac{1}{X_{b,j}} Q\left(\frac{1}{2}\sqrt{\beta_j}\right) \tag{4.48}$$

where the average BER turns out to be of the form

$$\overline{P}_{b,j}\left(\beta_j\right) = \sum_i \overline{P}_{b,j}\left(\beta_j, i\right) \tag{4.49}$$

The correct packet probability is then written as

$$P_{c,j}\left(X_{b,j}\right) = \prod_{i=0}^{X_{b,j}-1}\left(1-\overline{P}_{b,j}\left(\beta_j, i\right)\right) = \left(1-\frac{1}{X_{b,j}} Q\left(\frac{1}{2}\sqrt{\beta_j}\right)\right)^{X_{b,j}} \tag{4.50}$$

The throughput of class-*j* in packets per slot is given as

$$\theta_j = P_{c,j}\left(X_{b,j}\right)\sum_{m=0}^{K_j} m f_M\left(m\right) \tag{4.51}$$

where $f_M\left(m\right)$ is the composite arrival distribution. Simplifying the model in (2.26), the binomial arrival model is considered with a transmission probability P_{tr}, and it is given by

$$f_M\left(m\right) = \binom{K_j}{m}\left(P_{tr}\right)^m\left(1-P_{tr}\right)^{K_j-m} \tag{4.52}$$

Then, the throughput in (4.51) gets simplified to

$$\theta_j = K_j P_{tr} P_{c,j}\left(X_{b,j}\right). \tag{4.53}$$

Note that, $P_{tr}=1$ represents the ideal situation when all users successfully transmit their packets, simultaneously. For S-ALOHA/OV-CDMA $P_{tr}<1$ (see appendix C). In addition, the average delay encountered by class-j in slots is defined by Little's theorem as the ratio D_j of the average number of backlogged packets over the throughput,

$$D_j=\frac{\overline{n}_j}{\theta_j} \tag{4.54}$$

where $\overline{n}_j$ is the average number of unsuccessful transmissions. For a general MAC protocol, $\overline{n}_j=K_j-\theta_j$, for S-ALOHA, $\overline{n}_j=1+d_j$ and for R^3T, $\overline{n}_j=K_j\cdot A$. To shed light on the characteristic of the OV-CDMA system for increasing the transmission rate above the nominal limit, the overall network throughput is measured in bits per second as

$$\theta=\sum_j \theta_j R_j \tag{4.55}$$

Further, the average network delay in time slots is computed as

$$D=\frac{\sum_j n_j R_j}{\theta} \tag{4.56}$$

4.6.2 Delay-Constraint Optimization Problem

In this section, we set the delay-constraint fair resource allocation strategy to jointly optimize the allocation of the multimedia transmission rate and the power consumption at the transmission as well as the network throughput, abiding certain delay requirements, d slots, and QoS demands. The optimization is done on the basis of the predetermined OOK modulation scheme at the PHY layer, and the selected S-ALOHA and R^3T protocols at the MAC layer.

The optimization problem ($\mathcal{O}p1$):

$$\left(\mathbf{X}_{\mathbf{b}}^{*}, \mathbf{P}^{*}\right) = \arg\max \theta\left(\mathbf{X}_{\mathbf{b}}, \mathbf{P}\right) \tag{4.57}$$

Constrained to:

$$D \le d \tag{4.58}$$

$$L \le X_{b,j} \le \left(L-1\right)G+1, \forall j \tag{4.59}$$

$$0 < P_j \le \pi_j, \forall j \tag{4.60}$$

where $\mathbf{X}_{\mathbf{b}}$ and $\mathbf{P}$ are the transmission rate vector and the transmission power vector for all classes, respectively. (4.58) is the average network delay requirement constraint that should be respected by the PHY layer. (4.59) is the domain of the transmission rate of each class-*j* of users. (4.60) is the transmission power constraint of each class-*j* of users, too.

The common parameter which coordinates between the two layers is the tolerable number of users that plays the role of the offered load at the MAC layer. This parameter is derived from $SIR_j = \beta_j$ for each class *j* as

$$K_j = \frac{p^{(j)}\left(\left(\frac{1}{\gamma_j}+\frac{1}{\beta_j}\right)P_j - \frac{1}{\gamma_n}\right)}{\sum_s p^{(s)}\frac{P_s}{\gamma_s}} \tag{4.61}$$

By applying the fair QoS-based resource allocation scheme for the time-slotted optical OV-CDMA network, the transmission rate of class-*j* users is maximized when the users achieve their transmission at the upper bound optical transmission power. Then, the maximum transmission rate and the corresponding maximum transmission power are optimally controlled via a control parameter α, which is also the fairness parameter. Recall that, this term comes from the fact that α controls the allocated resources based on the

required QoS by each class of users as an aspect which is considered satisfactory among the users. Therefore, the implication of the proposed scheme is realized by solving (4.12) for P_j when satisfying the minimal QoS, and then by using (4.60) to get $\gamma_j \geq \gamma_j^*$ (Lemma 4.1). Thereafter, the maximum transmission rate is obtained when $\gamma_j = \gamma_j^* = \frac{\alpha}{\alpha - 1}\left(K_j - 1\right)\beta_j$ (Lemma 4.3) with a corresponding transmission power $P_j^* = \pi_j = \alpha\,\beta_j / \gamma_n$ where $\alpha > 1$ (Lemma 4.4). Consequently, (4.61) is reduced to $K_j\left(X_{b,j}, \alpha\right) = \left\lceil p^{(j)}\left(1 + \frac{\gamma_j}{\beta_j}\left(1 - \frac{1}{\alpha}\right)\right) - \frac{1}{2}\right\rceil$ such that $K_j\left(X_{b,j}, \alpha\right) \in \mathbb{N}^*, 1 \leq K_j \leq p^{(j)}G,\ \forall j$, and $\sum_j K_j = K$. The function $\lceil x - 1/2 \rceil$ rounds off x to the nearest integer.

It follows that the search dimension of $(\mathcal{O}\boldsymbol{p}1)$ has been reduced, and $(\mathcal{O}\boldsymbol{p}1)$ can be simplified to $(\mathcal{O}\boldsymbol{p}2)$:

$$\left(\mathbf{X}_\mathbf{b}^*, \alpha^*\right) = \arg\max\left(\sum_j \theta_j R_j\right) \tag{4.62}$$

Constrained to:

$$\sum_j \left(n_j - d\theta_j\right) R_j \leq 0 \tag{4.63}$$

$$L \leq X_{b,j} \leq \left(L - 1\right)G + 1,\ \forall j \tag{4.64}$$

$$\alpha = \left(1 - \left(\sum_j K_j - 1\right)\frac{\beta_j}{\gamma_j}\right)^{-1},\ \forall j \tag{4.65}$$

$$\max_j\left(1, \left(1 - \left(\frac{1}{p^{(j)}} - 1\right)\frac{\beta_j}{\gamma_j}\right)^{-1}\right) \leq \alpha \leq \min_j\left(\left(1 - \left(G - 1\right)\frac{\beta_j}{\gamma_j}\right)^{-1}\right) \tag{4.66}$$

$$\frac{\gamma_j}{\beta_j} \geq \left(\max\left(1/p^{(j)}, G\right) - 1\right),\ \forall j \tag{4.67}$$

The constraint (4.63) represents the delay bound. (4.65) is to preserve the distribution of the classes in the allocation process. (4.66) is to guarantee a finite transmission power and the assumption of unique EHC-code assignment. The characteristic of EHC [11], which is a family of one-coincidence two-dimensional codes, is that the cardinality of the codebook equals the PG. Hence, up to G users can be coded simultaneously. (4.67) is to guarantee valid bounds of the control parameter. Since it is a non-linear and non-convex optimization problem, the proposed design is evaluated numerically.

Among the different MAC protocols, our focal interest will be on the S-ALOHA/OV-CDMA protocol. This is due to its ease of implementation and its achievable performance as the numerical results illustrate in the next section.

Finally, for practical implementations, our proposed control protocol design can be implemented on an FPGA platform or a fix transistor chip to operate electronically at the MAC layer of the network. The mechanism of operation can work as follows. Once the optimal rate has been determined, the total number of bits that should be transmitted per packet time slot is known, and the bits are stored in the electronic buffer before optically modulated. Owing to the absence of the one-to-one correspondence between the electrical transmission rate and the bit duration $\left(T_b = GT_c\right)$ in the OV-CDMA system, increasing the rate will not affect the bit duration of the optical system and hence the optical packet time-slot. So, having determined the optical time-slot, the electrical data is optically modulated and sequentially transmitted over the FBG through which the overlapping process occurs. The optical modulation is performed at intensity levels which are optimally allocated in advance by evaluating the resource allocation algorithm about the system's parameters settings. When all bits are transmitted, the electronic buffer is freed once the optical packet is successfully transmitted and correctly received. Thus, S-ALOHA/OV-CDMA tends to electronically control the intensity and the arrival of data, hence the optical collision, through managing the multiple access interference in the optical fiber from the link layer.

4.7 Numerical Results and Discussion

In this part we assess numerically the feasibility of resource allocation proposal and its performance at the link layer with different MAC protocols.

4.7.1 The Fair Resource Allocation Scheme Assessement

In this section, we provide a numerical analysis of our analytical results in order to gain more insight into the problem. In addition, the analytical results are then compared to numerical ones obtained using a numerical search method. This method is based on the quasi-Newton method, in which a quadratic programming sub-problem is solved at each iteration, and an estimate of the Hessian of the Lagrangian function is updated using the BFGS method (suggested by Broyden, Fletcher, Goldfarb, and Shannon in 1970) [65], [66]. It finds numerically the optimal transmission rate and the optimal transmission power of class-j users that maximize $C(\alpha)=\sum_j p^{(j)}R_j(\alpha)/\sum_j p^{(j)}P_j(\alpha)$ as functions of α such that $\alpha>1$. The optimization problem is subject to the constraints $SIR_j=\beta_j$, $R^{(\ell)}\le R_j\le R^{(u)}$ and $0<P_j\le\pi_j$. Note that, from (4.32) π_j varies in term of α, which has to be determined. Thus, we set a search space of α as $\mathcal{A}=\{\alpha:1<\alpha\le 10\}$. Then, for each value of $\alpha\in\mathcal{A}$, incremented by a small step size in each iteration, we make use of the aforementioned numerical search method to solve the optimization problem as described in Fig. 4.2. Consequently, $C^*(\alpha)$, $R_j^*(\alpha)$ and $P_j^*(\alpha)$ are obtained. The optimal control parameter satisfies $\alpha^*=\arg\max_{\alpha\in\mathcal{A}} C^*(\alpha)$. The numerical results show a total agreement with the analytical ones and validate our analysis.

We consider a three-class system, S = 3, where each class is characterized by its own QoS. The total number of users in the network changes from K = 10 to 40 users. The users are distributed among the classes as follows: 40% in class-0, 30% in class-1, and 30% in class-2. All the users are assigned codes of fixed PG G = 61 through which they can generate packets of length L = 1024 bits per time slot. Finally, we select γ_n = 15 dB

common to all classes. Assume that QoS requirements are β_0 = 4 dB, β_1 = 8 dB, and β_2 = 12 dB for class-0, class-1 and class-2, respectively.

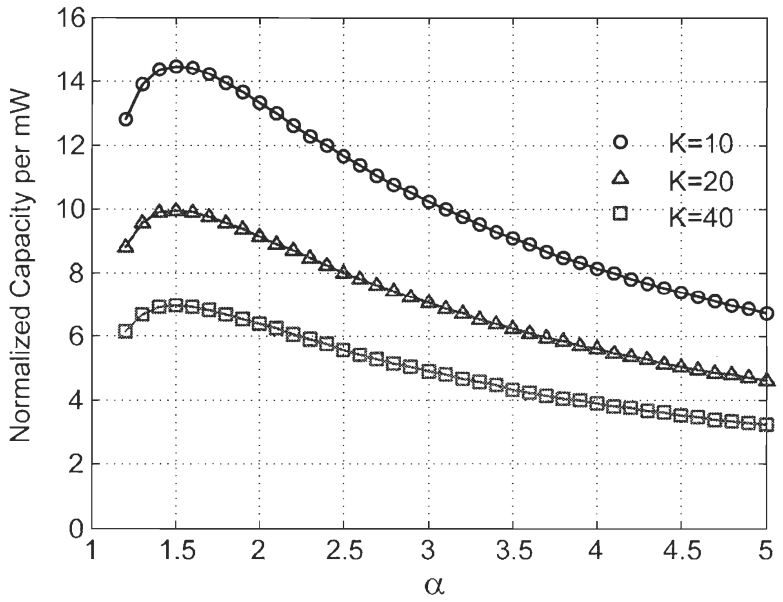

Fig. 4.3: The network capacity shape versus the control parameter α.

The normalized network capacity is examined in Fig. 4.3 as a function of the control parameter α. Notice that the normalized capacity per user has a global maximum, which means that there exists a value of α that maximizes the normalized capacity. Obviously, in this case it is 1.5. As α goes to infinity, the user's capacity degrades. Consequently, the high optical intensity-level turns out to be destructive, a case which fits to our target revealed in the model of the capacity function depicted in (4.44). Also, we notice a steadiness for the control parameter when K varies. This can be interpreted as follows. From (4.32) the maximum transmission power is proportional to α. Since increasing the total number of users necessitates a reduction of optical power, the control parameter should be small. On the other hand, (4.33) and lemma 4.3 reveal a one-to-one correspondence between the control parameter and the maximum transmission rate such that increasing α is followed by an augmentation of the maximum transmission rate. Thus, two paradoxical objectives are abided by the network capacity which is the main objective function to be maximized. The

proposed control algorithm solves the problem by steadying α. Indeed, the results of Fig. 4.3 assert that the constant control parameter is the one that maximizes the network capacity whose level varies according to K.

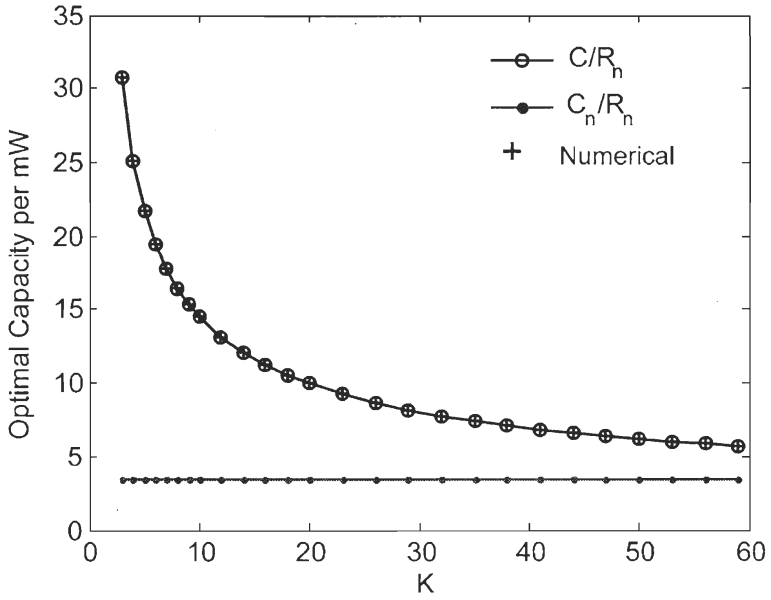

Fig. 4.4: The improved and the nominal capacities, normalized to R_n.

Fig. 4.4 illustrates the optimal capacity C versus the nominal capacity C_n per active user when the number of users increases. The figure shows clearly the improvement of the optimized capacity per user with respect to the nominal one which can be seen as a lower bound. A large capacity is provided in the region of small number of users because more bits can be tolerated per time slot due to overlapping. As K increases, this capacity gets reduced until it eventually reaches the nominal one.

The optimal transmission power of each class of users as a function of K is shown in Fig. 4.5. We observe that the allocated transmission power per user is fairly chosen for each class according to its QoS requirement. Class-2 users transmit with the highest power because they require the highest QoS. In addition, users always transmit with the highest power π_J, a result which validates Lemma 4.4.

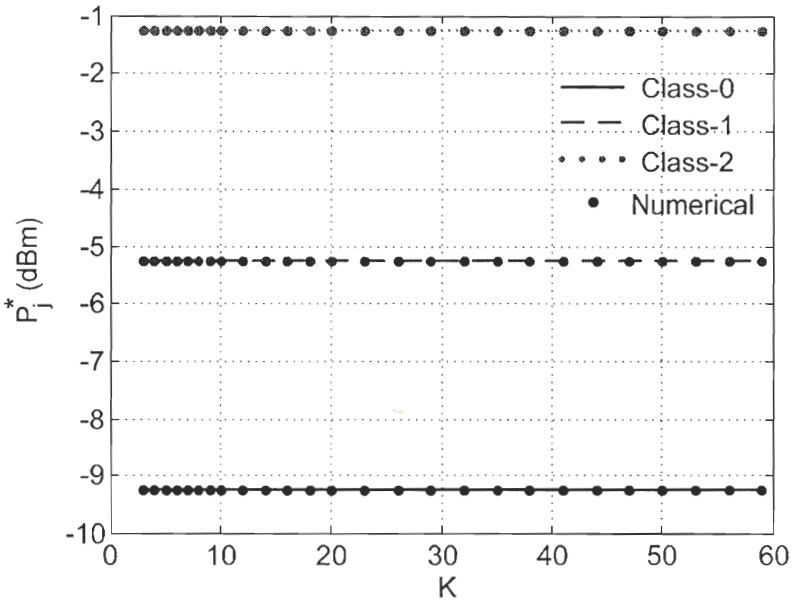

Fig. 4.5: The optimal transmission power versus the total number of users.

The optimal transmission rates for each class of users are depicted in Fig. 4.6. Using our proposed algorithm, it is clear that there is an increase in the transmission rate of each class of users. All classes can simultaneously transmit at rates varying between the lower and the upper bound cutoff rates of the OV-CDMA system. Note that in Chapter 3, only one class at a time can transmit at rate between the cutoff bounds while the other classes transmit either at the lower or at the upper cutoff bound, a fact which can be considered as unfair. As K increases, each user is required to diminish the transmission bit rate to reduce the MAI effect in the optical channel.

In the remaining part, we evaluate the effect of the QoS on the proposed resource allocation and control algorithm. In this direction, we keep the same QoS's of class-0 and class-2 as in the previous part and we vary that of class-1. The other design parameters remain unchanged.

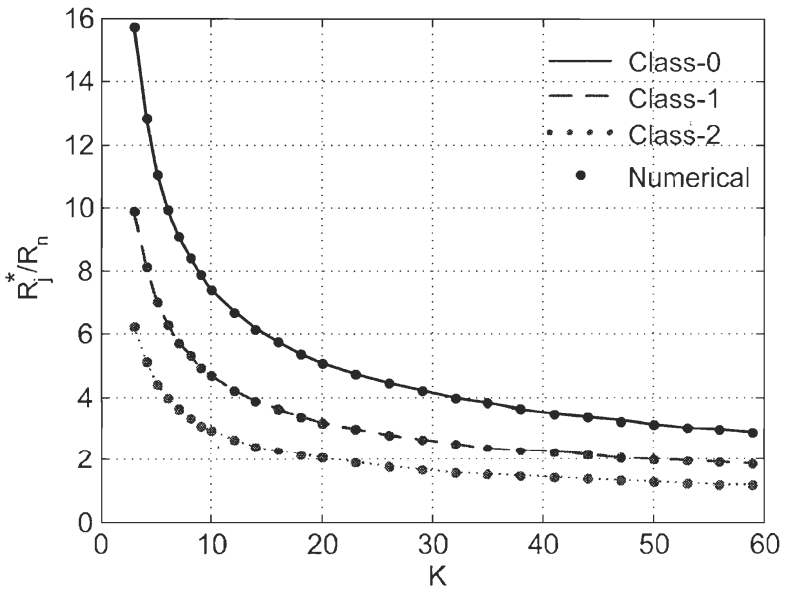

Fig. 4.6: The normalized optimal transmission rate of class-*j* users versus the total number of users.

The proposed controlling scheme adjusts the transmission rate of class-1 as β_1 varies to fit the requirements as illustrated in Fig. 4.7, while R_0^* and R_2^* are constant. The highest transmission rate is allocated when a poor QoS is required. Then, whether more users become active or a stringent QoS is demanded, R_1^* decreases toward the nominal rate. The decrease in the transmission rate results from lowering the number of overlapped bits per time slot in order to reduce the induced MAI level. When $\beta_1 > \beta^{(u)}$, we remark that high QoS's are no more tolerable since they force the transmission rate to go below the nominal rate. This in turn validates the analytical result presented in Lemma 4.3.

The power control versus the rate allocation of class-1 is revealed in Fig. 4.8. Low rate users are illuminated with high power since they transmit at a high QoS. As the allotted transmission rate increases, the corresponding supplied power decays rapidly because the QoS has been relaxed. Moreover, when K increases, less power is allowed per user and the maximum allowable increase in the transmission rate above the nominal rate is smaller.

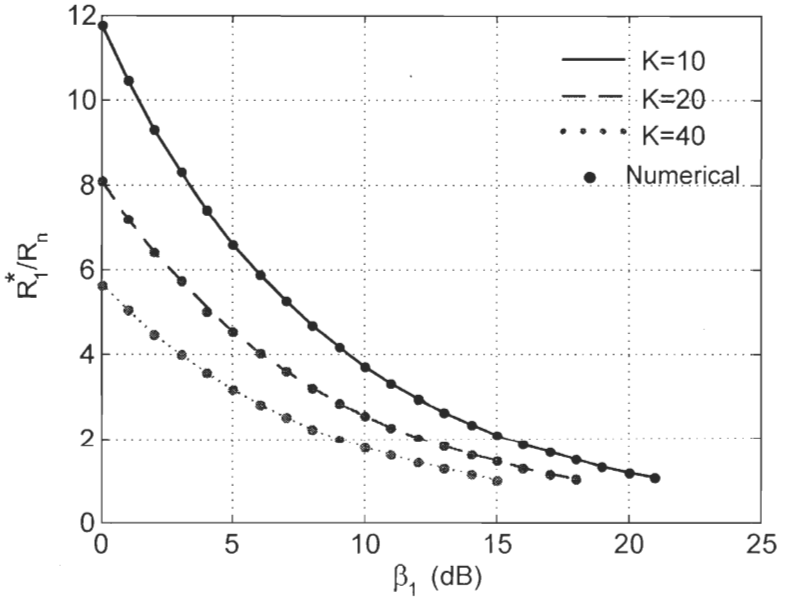

Fig. 4.7: The normalized optimal transmission rate of class-1 users versus QoS.

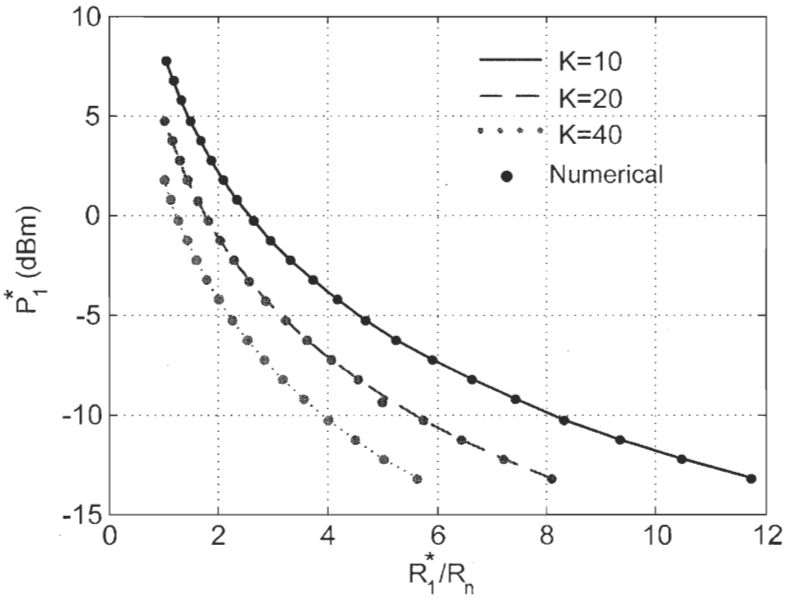

Fig. 4.8: The optimal transmission power allocation as a function of the normalized optimal transmission rate of class-1 users.

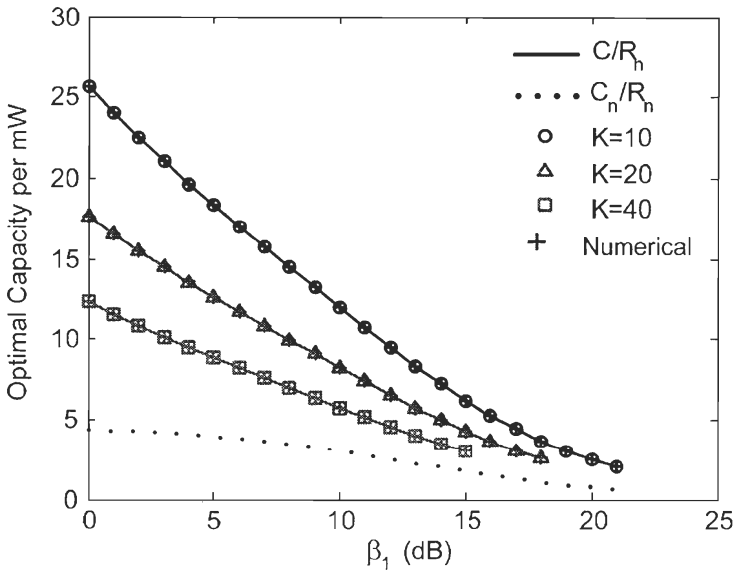

Fig. 4.9: The normalized optimal user's capacity versus the QoS variation of class-1.

The normalized optimal network capacity per user is depicted in Fig. 4.9. The improvement of the capacity with respect to the nominal capacity is obvious for different network conditions. For example, in the presence of 20 active users, six of which are in class-1 transmitting at a target QoS $\beta_1 = 0$ dB, the maximum achievable capacity is 17.7 times R_n per mW, which is around four times the nominal capacity. Such an improvement diminishes when the number of active users increases, and/or when the demand on QoS increases. The fast capacity decay is due to the fact that the controlling scheme tends to guarantee high QoS requirements rather than to increase the transmission rate of users by reducing the MAI effect in the network.

4.7.2 The Delay-Constraint Optimization Assessment

A numerical evaluation has been performed for $(\mathcal{O}p2)$ in three different situations. The first one is when all users transmit successfully all their packets, and we refer to this situation as an ideal case $(P_{tr} = 1)$. The second and the third situations are those when the proposed MAC protocol is S-ALOHA/OV-CDMA protocol and, R^3T/OV-CDMA,

respectively $(P_{tr} < 1)$, using EPA in both cases (Appendix C). The upper limit transmission latency is $d = 3$ slots. For R^3T/OV-CDMA protocol, the packet generation probability is 0.6, the two-way propagation delay is 2 time slots, and the timeout duration is one time slot. For S-ALOHA/OV-CDMA protocol, the packet generation probability is also 0.6, the retransmission probability is 0.9 and the number of retransmission attempts is 2. The other design parameters are similar to the previous section.

In Fig. 4.10, the throughput of the MAC, normalized to the nominal transmission rate, is evaluated. Notice that the MAC throughputs under both protocols are comparable with a slight superiority for the S-ALOHA/OV-CDMA. This means that the latter can stimulate the optical channel to tolerate more transmitted bits per second. However, both protocols offer much lower throughput compared against the ideal case; a fact which is obvious in a non-ideal channel where the average number of correctly transmitted packets is restrained by MAI induced by the overlapping process and the non-perfect orthogonality of the codewords. On the other hand, the MAC throughputs of the three situations decay and approach each other as a high QoS is required since now the optical overlapped system reduces the number of overlapping bit during the transmission.

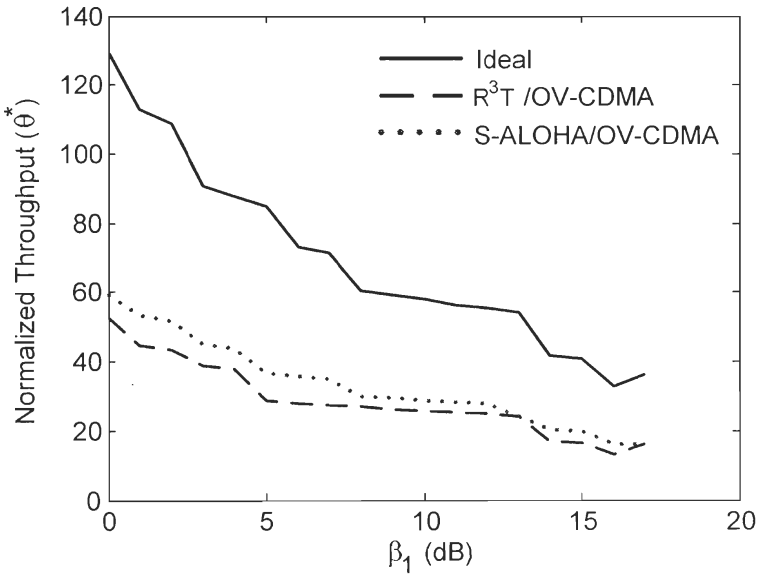

Fig. 4.10: The normalized throughput of the MAC for three different cases versus the QoS of class-1.

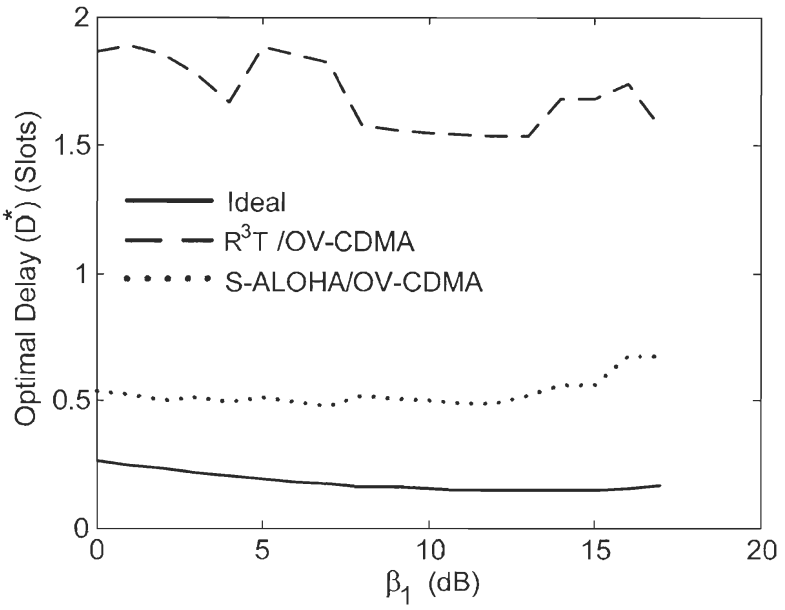

Fig. 4.11: The delay faced by the MAC in the three different cases versus the QoS of class-1.

Fig. 4.11 depicts the delay faced by the MAC when undergoing the different situations. S-ALOHA/OV-CDMA offers low delay compared to the R^3T/OV-CDMA for several reasons. First, it is the presence of signaling mode, in the latter protocol, which in case of failure can raise the number of retransmissions, and hence the delay time. Second, it is the presence of the propagation delay. Third, the average delay increases with packet generation and transmission probability (equals to 0.6). However, due to the joint optimization of the MAC and the PHY layers, the average delay of R^3T/OV-CDMA is smaller than the defined two-way propagation delay. Hence it is inherently satisfying the delay constraint $(d = 3)$. For S-ALOHA/OV-CDMA, the average delay is solely depending on the retransmission probability, so that raising this probability decreases the delay. In addition, even in the ideal case the average delay is persistent in the MAC. This means that a packet may face collision especially at higher transmission rate (high load) before it successfully reaches the destination. By the proposed MAC design, the average delay in all cases is always respecting the delay requirement.

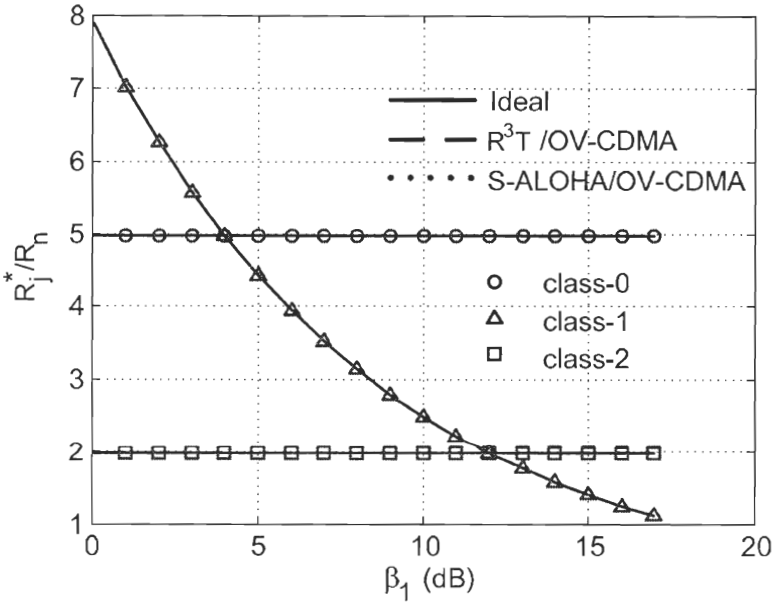

Fig. 4.12: The transmission rate allocations of the three classes through the MAC optimization.

The transmission rate allocations of the three classes of users are revealed in Fig. 4.12. Note that the transmission rates are allotted by the MAC optimization undergoing both protocols are equal to that of the ideal case although the performance of the latter at the MAC layer is much higher. This means that the proposed MAC design guarantees an optimal allocation of the transmission rate of all the classes. Since both protocols provide comparable performance at the link layer, their transmission rates are similar. In addition, the transmission rate of class-0 and class-2 are constant while that of class-1 decays as QoS increases. This happens since the solitary SIR's always satisfy the constraint (4.67) with equality, which is QoS-dependent, hence, the transmission rate. Furthermore, class-1 transmission rate diminishes as β_1 increases until it reaches the nominal rate at the upper bound QoS, which is in this case 18 dB.

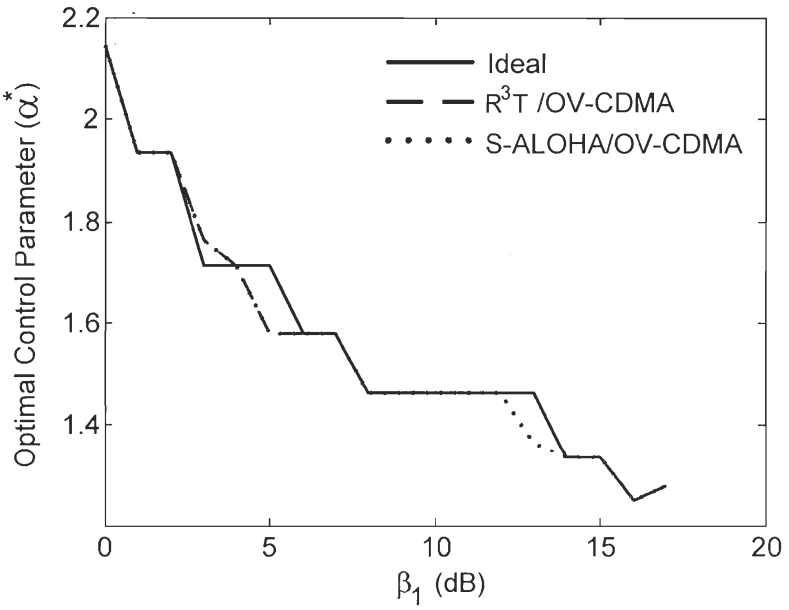

Fig. 4.13: The optimal control paramter obtained through the MAC optimization undergoing the three situations.

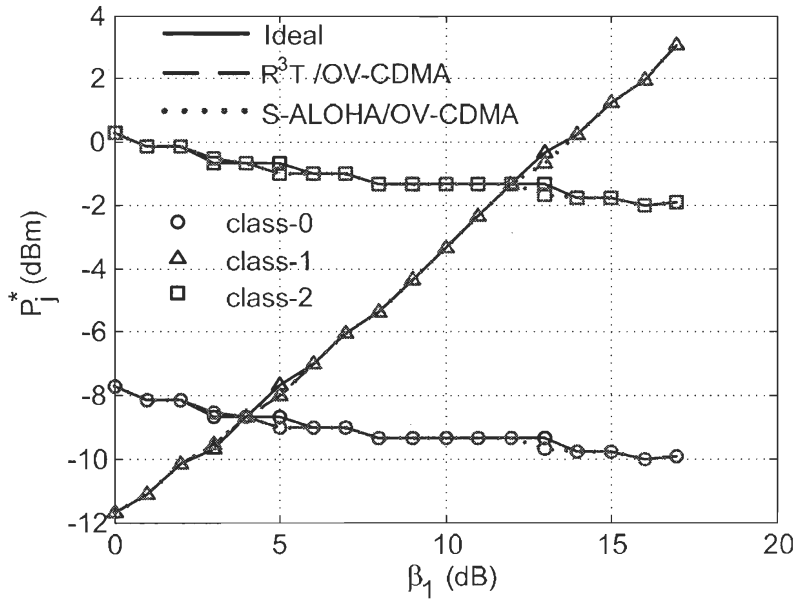

Fig. 4.14: The transmission power allocations of the three classes through the MAC optimization.

In Fig. 4.13, a similar scenario can be observed in terms of the optimal control parameter of the three MAC situations. That is, the optimal control parameters assigned to both protocols are almost identical to that of the ideal case and they are reduced with the increase of β_1. This denotes that the MAC assigns almost the same optical power for the different protocols regardless of their performances, a situation which is undesired. The reason behind this is that in a non-ideal optical channel more power is required per transmission to combat the collision factor, which is considered in both protocols. Also, it is certified that low transmission rate consumes less optical power. The optical power allotted to the users under different MAC protocols are quantitatively illustrated in Fig. 4.14.

The throughput variations in terms of the total offered load is represented in Fig. 4.15. The results assert that both protocols provide almost the same performance with nearly equal load, while the optimal throughput of the ideal case forms the upper bound that can be achieved.

According to the comparison between the two protocols, it seems logical to have comparable performance in general. However, S-ALOHA provides slight improvement over R^3T especially when all other parameters are optimized.

In our previous analyses, we have seen that the performance of former protocol moderately outperforms the latter one at low rates, and the latter also moderately surpasses the former one at higher rates, while both are competitive at moderate rates. The delay-constraint fair resource allocation always tends to allocate low to moderate overlapping transmission rate. This transmission rate is still higher than the nominal rate, and hence the existence of this performance comparability of both protocols. However, S-ALOHA/OV-CDMA is better serving the higher offered load than the other protocol. On the other hand, Fig. 4.16 indicates that with equal QoS-proportional transmission power S-ALOHA/OV-CDMA performs better than R^3T/OV-CDMA, while both of them are around 50% less than the ideal performance.

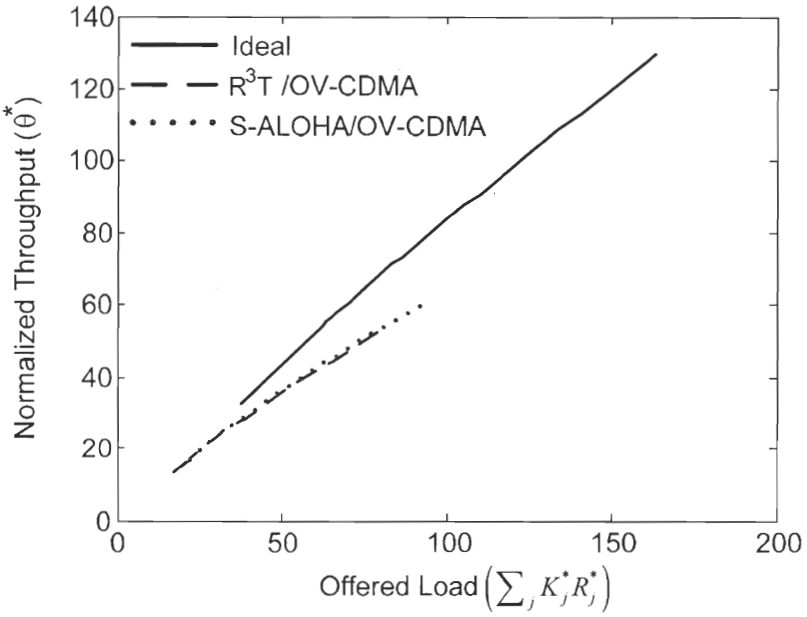

Fig. 4.15: The throughput of the MAC versus the offered load, both normalized to R_n,

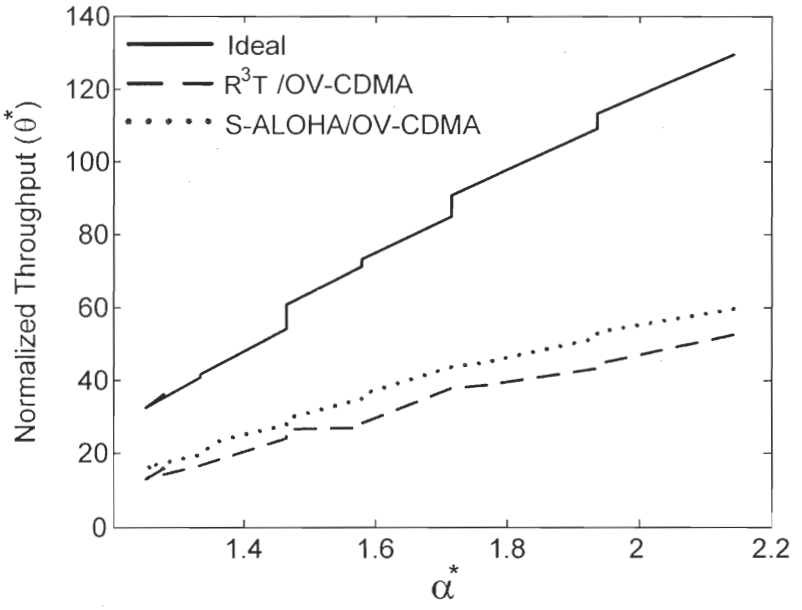

Fig. 4.16: The normalized throughput of the MAC versus the optimal control paramter.

4.8 Conclusion

We proposed a fair resource allocation scheme for multi-class time-slotted optical OV-CDMA-based packet networks. This scheme is fair as it is based on the QoS requirements of the users. In addition, no class of users can dominate the other classes. The Sherman-Morrison's matrix inversion lemma was used to solve the power allocation problem in a closed form. A rate-characteristic polynomial has been derived and solved for the optimal transmission rate allocation. The resources are optimally allocated as functions of a single control parameter, which helps to reduce the search space into one dimensional space. Our approach is unified since it is independent from the shape of the network capacity. Then, we proposed a delay-constraint fair resource allocation optimization for OV-CDMA-based packet networks that uses the fair resource allocation scheme at the PHY layer with QoS-adaptive BER to maximize the MAC throughput with some delay requirements. S-ALOHA/OV-CDMA and R^3T/OV-CDMA are compared to using EPA with binomial arrival distribution. A numerical search method was employed to validate the analytical results. Both numerical and analytical results proved that our resource allocation scheme is simple to implement and offers a substantial improvement to the system capacity. In addition, the comparison assessment shows that the performances of both protocols are almost comparable while their optimal delay is always respecting the MAC layer requirement. The fairness and the optimality of the resource allocation are also preserved.

Chapter 5

Conclusion and Future Perspective

We close our thesis by stating concisely the main contributions of our work as follows:

1) We analyzed the performance of the OV-CDMA system for a single class of transmission rate with unity power for all users at the link layer of a time-slotted packet access network. We compared the performance of the proposed system to that of the classical VPG CDMA system for multirate applications. Having derived the correct packet probability, the performances of both systems were investigated in terms of throughput, delay and stability under S-ALOHA protocol. Further, we derived a comparison of performances undergoing two MAC protocols – a simple S-ALOHA and a more advanced R^3T protocol, originally proposed for optical packet networks. The comparison investigates the influence of varying the offered load on the throughput and the average delay of both protocols. The original results of this study revealed that the proposed overlapped system outperforms the variable processing gain system despite the MAC protocol used. Concerning the efficiency of the MAC protocols, S-ALOHA/FFH-CDMA performs better than R^3T/FFH-CDMA at relatively high offered load. On the other hand, the latter protocol is more effective at low and medium offered load. While, at moderate channel load conditions, both protocols can offer comparable performances. The results are basically related to the size of the optical network whether of large or of small scale. In small scale networks, example of which is the local area network, the number of users is almost limited to orders of tens. The originated traffic load in this case can be within the MAI-limited capacity of the OV-CDMA channel especially at medium transmission rate. R^3T performs better than S-ALOHA. In large scale networks, examples of which are the metropolitan networks, the originated traffic load is heavier. S-ALOHA is more efficient is this case.

2) Thus, the first step of our study was carried at the link layer with a random selection of the physical parameters such as the overlapping coefficient (which is equivalent to the transmission rate) with no consideration to the optical transmission power. For this reason, we developed a new resource allocation strategy for the OV-CDMA system at the PHY layer of the network to optimally allocate the transmission rate and the transmission power to users spread out over different classes of the QoS. That was our second contribution which gave us a useful insight on the optimal distribution of the physical resources of the overlapped system. We remarked that the resources are unfairly distributed among the users of different QoS's so that at high QoS only one class of users can achieve relatively high transmission rate through the overlapping process while other classes transmit at nominal rate (i.e. with no overlapping process). Also, at low and medium QoS only one class can transmit at intermediate rate, while the others either transmit at a rate with full overlapping process or at the nominal rate. Albeit this unfairness, the results reported a possibility of achieving an optimal resource allocation and impelled us to seek more fair and realistic strategy to improve the system performance.
3) Consequently, our third general contribution was manifested by designing a fair resource allocation strategy for the overlapped system taking into concern its possible integration into the packet access network. Thus, we proposed a fair resources allocation scheme whereby which the allocation is based on the QoS demanded by each class of users in a time-slotted optical packet network. The key characteristic of this scheme is its application of a unified approach which maximizes any form of the objection function, solely depending on a control parameter, also known as the fairness parameter. Also, it is simple to implement in the ultra-fast optical networks. By this strategy, first the average capacity per user has been improved, second more classes can simultaneously have their transmission rates allotted at higher values above the nominal one and third they can achieve their transmissions at upper-bound power levels still lower than that of the previous strategy.
4) Finally, we combined the analysis performed at the link layer with the fair QoS-based resource allocation strategy at the PHY layer as a delay-constraint optimization. This

aimed at optimizing the performance of the time-slotted OV-CDMA-based packet network while at the same time optimizing the resource allocation at the PHY layer for different classes of QoS's. We assessed the performance in terms of the network throughput, and the average delay under S-ALOHA and R^3T at the MAC layer, and the fairness and the optimality of the resource allocation at the PHY layer, using OOK channel modulation scheme. The results were compared to an ideal situation where all users successfully transmit their packets, simultaneously. Indeed, the proposed design hits our objectives. First, it allocates the transmission rate for users in different classes as high as that of the ideal case under both protocols. Second, the transmission power is fairly low compared to the ideal case and relative to the transmission capacity that the users can handle. Third, the network throughput is around half of that of the ideal case under both MAC protocols. Finally, the network delay constraint is always respected. Concerning the efficiency of both protocols, S-ALOHA/OV-CDMA shows a modest dominance over R^3T/OV-CDMA. The reason is that the former protocol was proved to handle heavy traffic load and high transmission rate better than the latter one.

The results of our contributions validate our choice of the S-ALOHA as a simple protocol to control the arrival of packets at the link layer of the OV-CDMA-based packet network against the R^3T or any other complex protocol like reservation ALOHA (R-ALOHA) [29], [82], while we can achieve a relatively good throughput with less management.

Future Perspective

To consolidate the potential efficiency of optical networks, synergy among different communication layers will be suggested as a new approach of optimality control of the QoS and the resource utilization. This approach is prevalently known as cross-layer optimization [77]-[81]. The cross-layer design violates the reference architecture of the protocol stack to impose direct communication and collaboration among the different layers. This is achieved by creating new interface layers whose roles are to share parameters dynamically during the

runtime. The major objective of the cross-layer is to optimize the network performance where a strict layered architecture is incompetent to realize.

Consequently, simpler resource allocation schemes which are analytically more tractable will be foreseeable. Also, more advanced MAC protocols can be tested and selected opportunistically. Beside S-ALOHA and R^3T, CSMA-like protocols [28], [32]-[37] will be nominated to control the OV-CDMA traffic load at the MAC layer or even at the cross-layer.

In our thesis, the beat noise is considered mitigated, and the main source of noise is the multiple access interference. However, although advanced scenarios have been developed to mitigate the beat noise effect or to reduce it [72]-[74], those scenarios are still restricted to some particular optical systems' architectures, spread spectrum patterns or channel coding schemes. To date, there is no mature canonical methodology that can be practically applied to optical communication systems to alleviate the beat noise impairment. Hence, the suggestion of analyzing the performance of the OV-CDMA system taking into account the beat noise effect will be considered prospectively. Consequently, we expect that this accurate analysis will render the optical overlapped system more viable for practical implementation as it can provide more realistic insight on the systems' behavior.

Appendix A

Proof of Lemma 3.2

Consider that $\mathbf{R}^* = \left(R_i^*, R_j^*\right)^T$ solves the optimization problem $\left(\Pi_2\right)$ for any two-class subsystem, *class-i* and *class-j* $\forall i \neq j \in \{0,1,\ldots,S-1\}$. Satisfying the KT conditions, the solution of $\left(\Pi_2\right)$ is represented by twelve possible cases. For each one of them, the transmission rates are feasible by satisfying the system constraints (3.17) to (3.20) and have unique solution in finite intervals of the QoS β_i and β_j for *class-i* and *class-j*, respectively. Consequently, the solution is given as follows:

Case 1:

$$\beta_i \in \left(\beta_j, \frac{1}{M_0 R^{(\ell)}}\right) \text{ and } \beta_j \in \left(0, \frac{1-2M_i R^{(\ell)}\beta_i - \sqrt{\left(1-2M_i R^{(\ell)}\beta_i\right)^2 - \left(2M_j R^{(u)}\beta_i\right)^2}}{2M_j R^{(u)}}\right)$$

if the second term has a positive real value; otherwise,

$$\beta_j \in \left(0, \frac{-M_j R^{(u)}\beta_i + \sqrt{\left(M_j R^{(u)}\beta_i\right)^2 + M_i R^{(\ell)}\left(\beta_i - M_i R^{(\ell)}\beta_i^2\right)}}{M_i R^{(\ell)}}\right)$$

The optimal solution is given by

$$R_i^* = R^{(\ell)} \tag{A.1}$$

$$R_j^* = R^{(u)} \tag{A.2}$$

The Lagrange multipliers are

$$\lambda_1^* = SNR_n M_i \left(2M_i R^{(\ell)} + \left(\frac{\beta_i}{\beta_j} + \frac{\beta_j}{\beta_i} \right) M_j R^{(u)} - \frac{1}{\beta_i} \right) \tag{A.3}$$

$$\lambda_4^* = SNR_n M_j \left(-2M_j R^{(u)} - \left(\frac{\beta_i}{\beta_j} + \frac{\beta_j}{\beta_i} \right) M_i R^{(\ell)} + \frac{1}{\beta_j} \right) \tag{A.4}$$

$$\lambda_2^* = \lambda_3^* = \lambda_5^* = 0 \tag{A.5}$$

By checking the interval of β_i and β_j, we can easily recognize that $\beta_i > \beta_j$. In addition, the optimal solution in (A.1) and (A.2) shows clearly that $R_i^* < R_j^*$, which satisfies Lemma 3.2.

Case 2:

$$\beta_i \in \left(0, \frac{1}{2M_i R^{(u)} + 2M_j R^{(\ell)}} \right)$$

$$\text{and } \beta_j \in \left(\begin{array}{l} \max\left(\beta_i, \dfrac{-M_j R^{(\ell)} \beta_i + \sqrt{\left(M_j R^{(\ell)} \beta_i \right)^2 + M_i R^{(u)} \left(\beta_i - M_i R^{(u)} \beta_i^2 \right)}}{M_i R^{(u)}} \right), \\ \dfrac{1 - 2M_i R^{(u)} \beta_i + \sqrt{\left(1 - 2M_i R^{(u)} \beta_i \right)^2 - \left(2M_j R^{(\ell)} \beta_i \right)^2}}{2M_j R^{(\ell)}} \end{array} \right)$$

$$R_i^* = R^{(u)} \tag{A.6}$$

$$R_j^* = R^{(\ell)} \tag{A.7}$$

$$\lambda_2^* = SNR_n M_j \left(2M_j R^{(\ell)} + \left(\frac{\beta_i}{\beta_j} + \frac{\beta_j}{\beta_i} \right) M_i R^{(u)} - \frac{1}{\beta_j} \right) \tag{A.8}$$

$$\lambda_3^* = SNR_n M_i \left(-2M_i R^{(u)} - \left(\frac{\beta_i}{\beta_j} + \frac{\beta_j}{\beta_i} \right) M_j R^{(\ell)} + \frac{1}{\beta_i} \right) \tag{A.9}$$

$$\lambda_1^* = \lambda_4^* = \lambda_5^* = 0 \tag{A.10}$$

In this case, $\beta_j > \beta_i$ and $R_j^* < R_i^*$.

Case 3:

$$\beta_i \in \left(\beta_j, \frac{1}{M_i R^{(\ell)}} \right)$$

$$\text{and } \beta_j \in \left(\frac{-M_j R^{(u)} \beta_i + \sqrt{\left(M_j R^{(u)} \beta_i \right)^2 + M_i R^{(\ell)} \left(\beta_i - M_i R^{(\ell)} \beta_i^2 \right)}}{M_i R^{(\ell)}}, \min \left(\beta_i, \frac{-M_j R^{(\ell)} \beta_i + \sqrt{\left(M_j R^{(\ell)} \beta_i \right)^2 + M_i R^{(\ell)} \left(\beta_i - M_i R^{(\ell)} \beta_i^2 \right)}}{M_i R^{(\ell)}} \right) \right)$$

$$R_i^* = R^{(\ell)} \tag{A.11}$$

$$R_j^* = \frac{1}{2M_j \beta_j} - \frac{M_i}{2M_j} \left(\frac{\beta_i}{\beta_j} + \frac{\beta_j}{\beta_i} \right) R^{(\ell)} \tag{A.12}$$

$$\lambda_1^* = SNR_n M_i \frac{\left(\beta_i^2 - \beta_j^2 \right)}{2\beta_i^2 \beta_j^2} \left(\beta_i - M_i R^{(\ell)} \left(\beta_i^2 - \beta_j^2 \right) \right) \tag{A.13}$$

$$\lambda_2^* = \lambda_3^* = \lambda_4^* = \lambda_5^* = 0 \tag{A.14}$$

Note that $\beta_j < \beta_i$, $R_i^* = R^{(\ell)}$ and $R_j^* \neq \left\{R^{(\ell)}, R^{(u)}\right\}$. In addition, since R_i^* and R_j^* are feasible solutions and satisfying Lemma 3.1, R_j^* should satisfy $R^{(\ell)} \le R_j^* \le R^{(u)}$. This implies that $R_j^* > R_i^*$.

Case 4:

$$\beta_i \in \left(0, \frac{1}{2M_i R^{(\ell)} + 2M_j R^{(\ell)}}\right)$$

and $\beta_j \in$

$$\left(\max\left(\beta_i, \frac{1-2M_i R^{(u)}\beta_i + \sqrt{\left(1-2M_i R^{(u)}\beta_i\right)^2 - \left(2M_j R^{(\ell)}\beta_i\right)^2}}{2M_j R^{(\ell)}}\right), \frac{1-2M_i R^{(\ell)}\beta_i + \sqrt{\left(1-2M_i R^{(\ell)}\beta_i\right)^2 - \left(2M_j R^{(\ell)}\beta_i\right)^2}}{2M_j R^{(\ell)}}\right)$$

$$R_i^* = \frac{1}{2M_i\beta_i} - \frac{M_j}{2M_i}\left(\frac{\beta_i}{\beta_j} + \frac{\beta_j}{\beta_i}\right)R^{(\ell)} \tag{A.15}$$

$$R_j^* = R^{(\ell)} \tag{A.16}$$

$$\lambda_2^* = SNR_n M_j \frac{\left(\beta_j^2 - \beta_i^2\right)}{2\beta_i^2\beta_j^2}\left(\beta_i - M_j R^{(\ell)}\left(\beta_j^2 - \beta_i^2\right)\right) \tag{A.17}$$

$$\lambda_1^* = \lambda_3^* = \lambda_4^* = \lambda_5^* = 0 \tag{A.18}$$

Using the same analysis in Case 3 we can show that $\beta_j > \beta_i$ and $R_j^* < R_i^*$.

Case 5:

$$\beta_i \in \left(0, \frac{1}{2M_i R^{(u)}}\right)$$

$$\text{and } \beta_j \in \left(\begin{array}{l} \max\left(\beta_i, \dfrac{-M_j R^{(u)}\beta_i + \sqrt{\left(M_j R^{(u)}\beta_i\right)^2 + M_i R^{(u)}\left(\beta_i - M_i R^{(u)}\beta_i^2\right)}}{M_i R^{(u)}}\right), \\ \dfrac{-M_j R^{(\ell)}\beta_i + \sqrt{\left(M_j R^{(\ell)}\beta_i\right)^2 + M_i R^{(u)}\left(\beta_i - M_i R^{(u)}\beta_i^2\right)}}{M_i R^{(u)}} \end{array} \right)$$

$$R_i^* = R^{(u)} \tag{A.19}$$

$$R_j^* = \frac{1}{2M_j\beta_j} - \frac{M_i}{2M_j}\left(\frac{\beta_i}{\beta_j} + \frac{\beta_j}{\beta_i}\right)R^{(u)} \tag{A.20}$$

$$\lambda_3^* = SNR_n M_i \frac{\left(\beta_j^2 - \beta_i^2\right)}{2\beta_i^2\beta_j^2}\left(\beta_i + M_i R^{(u)}\left(\beta_j^2 - \beta_i^2\right)\right) \tag{A.21}$$

$$\lambda_1^* = \lambda_2^* = \lambda_4^* = \lambda_5^* = 0 \tag{A.22}$$

Also using the same analysis in Case 3 we can show that $\beta_j > \beta_i$ and $R_j^* < R_i^*$.

Case 6:

$$\beta_i \in \left(0, \frac{1}{2M_i R^{(\ell)} + 2M_j R^{(u)}}\right) \text{ and}$$

$$\beta_j \in \left(\frac{1-2M_iR^{(\ell)}\beta_i - \sqrt{\left(1-2M_iR^{(\ell)}\beta_i\right)^2 - \left(2M_jR^{(u)}\beta_i\right)^2}}{2M_jR^{(u)}}, \frac{1-2M_iR^{(u)}\beta_i - \sqrt{\left(1-2M_iR^{(u)}\beta_i\right)^2 - \left(2M_jR^{(u)}\beta_i\right)^2}}{2M_jR^{(u)}} \right) \cup$$

$$\left(\max\left(\frac{1-2M_iR^{(\ell)}\beta_i - \sqrt{\left(1-2M_iR^{(\ell)}\beta_i\right)^2 - \left(2M_jR^{(u)}\beta_i\right)^2}}{2M_jR^{(u)}}, \frac{1-2M_iR^{(u)}\beta_i + \sqrt{\left(1-2M_iR^{(u)}\beta_i\right)^2 - \left(2M_jR^{(u)}\beta_i\right)^2}}{2M_jR^{(u)}} \right), \min\left(\beta_i, \frac{1-2M_iR^{(\ell)}\beta_i + \sqrt{\left(1-2M_iR^{(\ell)}\beta_i\right)^2 - \left(2M_jR^{(u)}\beta_i\right)^2}}{2M_jR^{(u)}} \right) \right)$$

$$R_i^* = \frac{1}{2M_i\beta_i} - \frac{M_j}{2M_i}\left(\frac{\beta_i}{\beta_j} + \frac{\beta_j}{\beta_i}\right)R^{(u)} \tag{A.23}$$

$$R_j^* = R^{(u)} \tag{A.24}$$

$$\lambda_4^* = SNR_nM_j\frac{\left(\beta_i^2 - \beta_j^2\right)}{2\beta_i^2\beta_j^2}\left(\beta_i + M_jR^{(u)}\left(\beta_i^2 - \beta_j^2\right)\right) \tag{A.25}$$

$$\lambda_1^* = \lambda_2^* = \lambda_3^* = \lambda_5^* = 0 \tag{A.26}$$

The same interpretation as in Case 3 leads to $\beta_j < \beta_i$ and $R_j^* > R_i^*$.

Case 7:

$$\beta_i \in \left(0, \max\left(\frac{1}{2M_iR^{(\ell)} + 2M_jR^{(\ell)}}, \frac{M_i}{M_i^2R^{(\ell)} - M_j^2R^{(\ell)}}, \frac{1}{M_iR^{(\ell)}}\right)\right)$$

and $\beta_j \in \left(\max \left(\dfrac{1-2M_iR^{(\ell)}\beta_i + \sqrt{\left(1-2M_iR^{(\ell)}\beta_i\right)^2 - \left(2M_jR^{(\ell)}\beta_i\right)^2}}{2M_jR^{(\ell)}}, \dfrac{-M_jR^{(\ell)}\beta_i + \sqrt{\left(M_jR^{(\ell)}\beta_i\right)^2 + M_iR^{(\ell)}\left(\beta_i - M_iR^{(\ell)}\beta_i^2\right)}}{M_iR^{(\ell)}} \right), \dfrac{1-M_iR^{(\ell)}\beta_i}{M_jR^{(\ell)}} \right)$

$$R_i^* = R_j^* = R^{(\ell)} \tag{A.27}$$

$$\lambda_1^* = SNR_n M_i \left(2M_iR^{(\ell)} + \left(\frac{\beta_i}{\beta_j} + \frac{\beta_j}{\beta_i} \right) M_jR^{(\ell)} - \frac{1}{\beta_i} \right) \tag{A.28}$$

$$\lambda_2^* = SNR_n M_j \left(2M_jR^{(\ell)} + \left(\frac{\beta_i}{\beta_j} + \frac{\beta_j}{\beta_i} \right) M_iR^{(\ell)} - \frac{1}{\beta_j} \right) \tag{A.29}$$

$$\lambda_3^* = \lambda_4^* = \lambda_5^* = 0 \tag{A.30}$$

In this case, since $R_j^* = R_i^*$, whether $\beta_j < \beta_i$ or $\beta_j > \beta_i$, then the condition $R_j^* = R_i^*$ is always satisfied.

Case 8:

$\beta_i \in \left(0, \dfrac{1}{2M_iR^{(u)} + 2M_jR^{(u)}} \right)$ and

$\beta_j \in \left(\dfrac{1-2M_iR^{(u)}\beta_i - \sqrt{\left(1-2M_iR^{(u)}\beta_i\right)^2 - \left(2M_jR^{(u)}\beta_i\right)^2}}{2M_jR^{(u)}}, \dfrac{-M_jR^{(u)}\beta_i + \sqrt{\left(M_jR^{(u)}\beta_i\right)^2 + M_iR^{(u)}\left(\beta_i - M_iR^{(u)}\beta_i^2\right)}}{M_iR^{(u)}} \right)$

$$R_i^* = R_j^* = R^{(u)} \tag{A.31}$$

$$\lambda_3^* = SNR_n M_i \left(-2M_i R^{(u)} - \left(\frac{\beta_i}{\beta_j} + \frac{\beta_j}{\beta_i} \right) M_j R^{(u)} + \frac{1}{\beta_i} \right) \tag{A.32}$$

$$\lambda_4^* = SNR_n M_j \left(-2M_j R^{(u)} - \left(\frac{\beta_i}{\beta_j} + \frac{\beta_j}{\beta_i} \right) M_i R^{(u)} + \frac{1}{\beta_j} \right) \tag{A.33}$$

$$\lambda_1^* = \lambda_2^* = \lambda_5^* = 0 \tag{A.34}$$

The same interpretation is used as in Case 8.

Case 9:

$\beta_i \in \left(P_{\max} SNR_n / 2, P_{\max} SNR_n \Big/ \left(P_{\max} SNR_n M_i R^{(\ell)} + 1 \right) \right)$, and

$$\beta_j \in \left(\begin{array}{l} \max \left(\dfrac{1 - 2\beta_i / \left(P_{\max} SNR_n \right) + \sqrt{\left(1 - 2\beta_i / \left(P_{\max} SNR_n \right) \right)^2 + \left(2M_j R^{(u)} \beta_i \right)^2}}{2M_j R^{(u)}}, \right. \\ \left. \dfrac{1}{M_j R^{(u)}} \left(1 - \beta_i \left(M_i R^{(u)} + 1 / \left(P_{\max} SNR_n \right) \right) \right) \right), \\ \min \left(\beta_i, \dfrac{1}{M_j R^{(u)}} \left(1 - \beta_i \left(M_i R^{(\ell)} + 1 / \left(P_{\max} SNR_n \right) \right) \right) \right) \end{array} \right)$$

$$R_i^* = \frac{1}{M_i \beta_i} \left(1 - \beta_i / \left(P_{\max} SNR_n \right) - M_j R^{(u)} \beta_j \right) \tag{A.35}$$

$$R_j^* = R^{(u)} \tag{A.36}$$

$$\lambda_4^* = \frac{M_j}{\beta_0 \beta_j P_{\max}} \left(\beta_i^2 - \beta_j^2 \right) \tag{A.37}$$

$$\lambda_5^* = \frac{SNR_n}{\beta_i^2 \beta_j}\left(\beta_j^2 M_j R^{(u)} + \beta_j\left(2\beta_i/\left(P_{\max} SNR_n\right) - 1\right) - M_j R^{(u)} \beta_i^2\right) \tag{A.38}$$

$$\lambda_1^* = \lambda_2^* = \lambda_3^* = 0 \tag{A.39}$$

Notice that $\beta_i > \beta_j$ is imposed on the solution so that λ_4^* in (A.37) should satisfy the KT condition, $\lambda_4^* \geq 0$. In addition, $R_i^* < R_j^*$ using the analysis used in Case 3. The same reasoning will be applied to the remaining cases.

Case 10:

$\beta_i \in \left(0, \min\left(\beta_j, 1/\left(M_i R^{(\ell)}\right)\right)\right)$ and

$$\beta_j \in \left(\max\left(\beta_i, \frac{1+\sqrt{1+4M_j R^{(\ell)} \beta_i^2 \left(M_j R^{(\ell)} + 2/\left(P_{\max} SNR_n\right)\right)}}{2M_j R^{(\ell)} + 4/\left(P_{\max} SNR_n\right)}, \frac{1 - M_i R^{(u)} \beta_i}{M_j R^{(\ell)} + 1/\left(P_{\max} SNR_n\right)} \right), \frac{1 - M_i R^{(\ell)} \beta_i}{M_j R^{(\ell)} + 1/\left(P_{\max} SNR_n\right)} \right)$$

$$R_i^* = \frac{1}{M_i \beta_i}\left(1 - \beta_j\left(M_j R^{(\ell)} + 1/\left(P_{\max} SNR_n\right)\right)\right) \tag{A.40}$$

$$R_j^* = R^{(\ell)} \tag{A.41}$$

$$\lambda_2^* = \frac{M_j}{\beta_i^2 P_{\max}}\left(\beta_j^2 - \beta_i^2\right) \tag{A.42}$$

$$\lambda_5^* = \frac{SNR_n}{\beta_i^2 \beta_j}\left(\beta_j^2\left(M_j R^{(\ell)} + 2/\left(P_{\max} SNR_n\right)\right) - \beta_j - M_i R^{(\ell)} \beta_i^2\right) \tag{A.43}$$

$$\lambda_1^* = \lambda_3^* = \lambda_4^* = 0 \tag{A.44}$$

In this case, $\beta_j > \beta_i$ and $R_j^* < R_i^*$.

Case 11:

$\beta_i \in \left(1/\left(M_i R^{(\ell)} + 2/\left(P_{\max} SNR_n\right)\right), 1/\left(M_i R^{(\ell)} + 1/\left(P_{\max} SNR_n\right)\right)\right)$ and

$$\beta_j \in \left(\begin{array}{l} \max\left(0, \dfrac{1-\beta_i\left(M_i R^{(\ell)} + 1/\left(P_{\max} SNR_n\right)\right)}{M_j R^{(u)}}\right), \\ \min\left(\beta_i, \dfrac{1-\beta_i\left(M_i R^{(\ell)} + 1/\left(P_{\max} SNR_n\right)\right)}{M_j R^{(\ell)}}, \sqrt{\dfrac{\beta_i^2\left(M_i R^{(\ell)} + 2/\left(P_{\max} SNR_n\right)\right) - \beta_i}{M_i R^{(\ell)}}}\right) \end{array} \right)$$

$$R_i^* = R^{(\ell)} \tag{A.45}$$

$$R_j^* = \frac{1}{M_j \beta_j}\left(1 - \beta_i\left(M_i R^{(\ell)} + 1/\left(P_{\max} SNR_n\right)\right)\right) \tag{A.46}$$

$$\lambda_1^* = \frac{M_i}{\beta_j^2 P_{\max}}\left(\beta_i^2 - \beta_j^2\right) \tag{A.47}$$

$$\lambda_5^* = \frac{SNR_n}{\beta_i \beta_j^2}\left(-\beta_j^2 M_j R^{(\ell)} + \beta_i^2\left(M_i R^{(\ell)} + 2/\left(P_{\max} SNR_n\right)\right) - \beta_i\right) \tag{A.48}$$

$$\lambda_2^* = \lambda_3^* = \lambda_4^* = 0 \tag{A.49}$$

In this case, $\beta_i > \beta_j$ and $R_j^* > R_i^*$.

Case 12:

$$\beta_i = \left(\frac{M_i R^{(u)}}{\left(M_i R^{(u)}\right)^2 + 1/\left(P_{\max} SNR_n\right)^2}, \min\left(\beta_j, \frac{1}{M_i R^{(u)}}\right) \right), \text{ and}$$

$$\beta_j = \left(\begin{array}{l} \max\left(\beta_i, \dfrac{1 - M_i R^{(u)} \beta_i}{M_j R^{(u)} + 1/\left(P_{\max} SNR_n\right)}, \right. \\ \left. \dfrac{\beta_i / \left(P_{\max} SNR_n\right) - \sqrt{\beta_i^2 / \left(P_{\max} SNR_n\right)^2 + M_i R^{(u)} \left(M_i R^{(u)} \beta_i^2 - \beta_i\right)}}{M_i R^{(u)}} \right), \\ \dfrac{1 - M_i R^{(u)} \beta_i}{M_j R^{(\ell)} + 1/\left(P_{\max} SNR_n\right)} \end{array} \right)$$

$$R_i^* = R^{(u)} \tag{A.50}$$

$$R_j^* = \frac{1}{M_j \beta_j} \left(1 - \beta_j / \left(P_{\max} SNR_n\right) - M_i R^{(u)} \beta_i\right) \tag{A.51}$$

$$\lambda_3^* = \frac{M_i}{\beta_0 \beta_j P_{\max}} \left(\beta_j^2 - \beta_i^2\right) \tag{A.52}$$

$$\lambda_5^* = \frac{SNR_n}{\beta_i \beta_j^2} \left(-\beta_j^2 M_i R^{(u)} + 2\beta_j \beta_i / \left(P_{\max} SNR_n\right) + M_i R^{(u)} \beta_i^2 - \beta_i\right) \tag{A.53}$$

$$\lambda_1^* = \lambda_2^* = \lambda_4^* = 0 \tag{A.54}$$

In this case, $\beta_j > \beta_i$ and $R_j^* < R_i^*$.

As a result, it is clear that for all possible solutions of a two-class subsystem when $\beta_i > \beta_j$, $R_i^* \le R_j^*$ and vice versa, which proves the lemma for the two subclasses. To generalize this result to the *S*-class system, consider a third class, class-*k*, with a QoS β_k. Applying the previous derivation to the two-class subsystem *class-j* and *class-k*, we can

prove that when $\beta_j > \beta_k$, $R_j^* \leq R_k^*$ and vice versa. Therefore if $\beta_i > \beta_j > \beta_k$, then $R_i \leq R_j \leq R_k$ is always true. Following the same recurrence for S classes, we can easily show that if $\beta_0 > \beta_1 > \cdots > \beta_{S-1}$, then $R_0 \leq R_1 \leq \cdots \leq R_{S-1}$, which completes the proof. ■

Appendix B

The constant coefficients of the polynomials that form the average interference variance over all bit-positions in a packet time-slot in (4.8) section 4.3 are given as follows.

$$A_4 = GL^4 - 12GL^3 + 51GL^2 - 90GL + 54G$$

$$A_3 = 5GL^4 - (42G + 6F)L^3 + (102G + 30F)L^2 - (54G + 48F)L - 27G + 24F$$

$$A_2 = 8GL^4 - (34G + 6F)L^3 - (G - 6F)L^2 + (60G + 24F)L - 9G - 24F$$

$$A_1 = 4GL^4 + (8G + 6F)L^3 - (40G + 30F)L^2 + (12G + 24F)L$$

$$A_0 = (8G + 6F)L^3 - (4G + 6F)L^2$$

$$B_3 = GL^2 - 6GL + 9G$$

$$B_2 = 3GL^2 - (6G - 2F)L - 9G - 2F$$

$$B_1 = -4FL^2 + (12G + 4F)L$$

$$B_0 = 2FL^3 - (4G + 2F)L^2$$

Appendix C

In both protocols, it is assumed that packets arrive following a binomial distribution with a transmission probability P_{tr}. Then the throughput functions of OV-CDMA-based network undergoing both protocols can be rearranged to be of the form $\theta_j = K_j P_{tr} P_{c,j}$.

When we consider the ideal situation, we meant the situation when the utmost number of available packets in the network are transmitted and correctly received, that is, K_j packets engendered by K_j users and hence $P_{tr} = 1$. However, in S-ALOHA and R^3T only $(P_{tr} < 1)$ percent out of the available K_j packets are transmitted and correctly received due to collision consideration. Thus, the ideal case provides an insight into how much the protocol efficiencies are far from the boundary limit.

I. A Simplified Model of S-ALOHA/OV-CDMA Protocol using EPA

Consider a finite number of users, K, available in the system. Each user generates a new message at the beginning of the time slot with probability P_o once a previous message is completely transmitted. The message is divided into a number of packets geometrically distributed with mean ℓ. The message is stored in a queue, which it cannot accept any new message unless the current message is completely transmitted. The channel propagation delay is assumed negligible.

Initially, a user is in state m; it sends its packet with probability $P_o(1-\sigma)$, receives with probability σ or stays idle otherwise as illustrated in Fig. C.1 That is, either a user transmits, receives packets or does nothing. In the transmission mode (states s_i), a user proceeds with transmitting the next packet if the current packet is successfully sent with a correct packet probability P_c. Otherwise, errors may occur with probability $(1-P_c)$, and hence collisions.

The user then enters the backlogged mode (states d_l^i). Unsuccessfully transmitted packets are backlogged, and then retransmitted at the next time slot with a probability P_r. After t unsuccessful retransmission attempts, the backlogged packet is assumed to be immediately retransmitted (i.e. $P_r = 1$). In the reception mode (states r_l), a packet is considered correctly received if it is successfully transmitted over the channel. Finally, if all packets are correctly received, the user returns to its initial state.

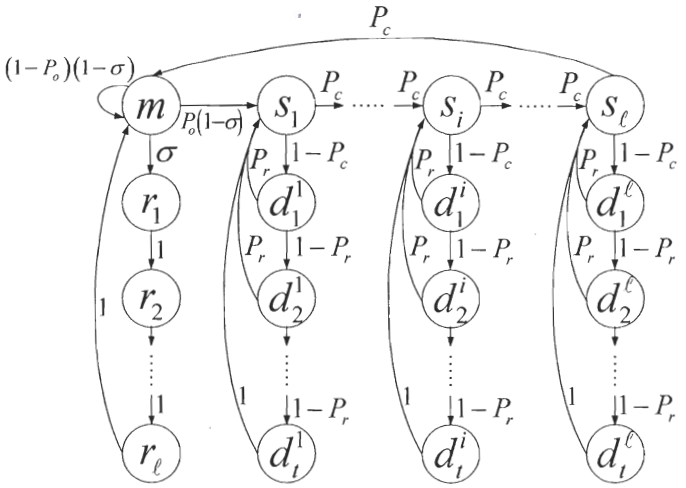

Fig. C.1: Simplified S-ALOHA/OV-CDMA model using EPA approximation.

We define s, d and r as the total number of packets in the transmission mode, the backlogged mode and the reception mode at equilibrium, respectively, and the flow equations are given as follows:

$$s_i = P_c^{i-1} s_1 \Rightarrow s \triangleq \sum_{i=1}^{\ell} s_i = \frac{1-P_c^{\ell}}{1-P_c} s_1 \tag{C.1}$$

$$d_l^i = \left(1-P_r\right)^{l-1} d_1^i \tag{C.2}$$

$$s_1\left(1-P_c\right) = P_r \sum_{l=1}^{t-1} d_l^i + d_t^i = d_1^i \tag{C.3}$$

$$d \triangleq \sum_{i=1}^{\ell} \sum_{l=1}^{i} d_l^i = \frac{1}{P_r}\left(1-\left(1-P_r\right)^l\right)\left(1-P_c\right)s \tag{C.4}$$

$$m\sigma = r_1 = \cdots = r_\ell \Rightarrow r \triangleq \sum_{i=1}^{\ell} r_i = \ell r_1 \tag{C.5}$$

The last packet received is equal to the last packet transmitted, so that

$$mP_o\left(1-\sigma\right) = s_\ell P_c \tag{C.6}$$

At equilibrium, the received packets in state i are equal to those transmitted. This gives

$$r_i = P_c\left(s_i + P_r \sum_{l=1}^{i-1} d_l^i + d_i^i\right) = P_c\left(2-P_c\right)s_i \tag{C.7}$$

Thus, (C.5) - (C.7) yield the reception probability at equilibrium

$$\sigma = \frac{P_o\left(2-P_c\right)\left(1-P_c^\ell\right)}{\ell\left(1-P_c\right)P_c^{\ell-1} + P_o\left(2-P_c\right)\left(1-P_c^\ell\right)}.$$

The number of packets in all states should be equal to the total number of packets offered for transmission. $K = m+s+d+r$ and $s_o \triangleq s+d$ is defined as the total number of packets attempting transmission. This implies

$$\frac{K}{s_o} = 1 + \frac{\left(\ell\sigma+1\right)\left(1-P_c\right)P_c^\ell}{P_o\left(1-\sigma\right)\left(1-P_c^\ell\right)\left(1+P_r^{-1}\left(1-\left(1-P_r\right)^l\right)\left(1-P_c\right)\right)} \tag{C.8}$$

Note that, since in OV-CDMA system P_c is independent of the number of users, (C.8) represents the relationship between K and s_o.

The EPA model of S-ALOHA/CDMA is applied to every class-j of users, $\forall j \in \{0,...,S-1\}$. The throughput of each class-j users is then given by

$$\begin{aligned}\theta_j &= s_j P_{c,j} \\ &= s_{o,j}\left(1+P_r^{-1}\left(1-\left(1-P_r\right)^{\ell}\right)\left(1-P_{c,j}\right)\right)^{-1} P_{c,j} \\ &= K_j \frac{P_o\left(1-\sigma_j\right)\left(1-P_{c,j}^{\ell}\right)}{P_o\left(1-\sigma_j\right)\left(1-P_{c,j}^{\ell}\right)\left(1+P_r^{-1}\left(1-\left(1-P_r\right)^{\ell}\right)\left(1-P_{c,j}\right)\right)+\left(\ell\sigma_j+1\right)\left(1-P_{c,j}\right)P_{c,j}^{\ell}} P_{c,j}\end{aligned} \tag{C.9}$$

The average number of backlogged users of class-j is $\bar{n}_j = 1+d_j$, hence the delay is given by Little's theorem. P_{tr} is represented by the fraction term. K_j, P_{tr} and $P_{c,j}$ are all optimized through the optimization problem $(\mathcal{OP}2)$.

II. R^3T/OV-CDMA

From Chapter 2, we know that the system throughput under the R^3T is computed as [25]

$$\theta_j\left(K_j, A, t, \tau_o, L\right) = r_{o,j}\left(K_j\right)\frac{L}{L+\left(1-P_{c,j}\right)\left(\min\{t,L\}-1\right)\left(L-\min\{t,L/2\}\right)} P_{c,j} \tag{C.10}$$

where $r_{o,j}\left(K_j\right)$ can be obtained such that the following condition is satisfied:

$$\begin{aligned}&K_j\left[L+\left(1-P_{c,j}\right)\left(\min\{t,L\}-1\right)\left(L-\min\{t,L/2\}\right)\right] = \\ &r_{o,j}\left[2tL\left(1-P_{c,j}\right)+\left(2t+2L-1\right)P_{c,j}+\frac{P_{c,j}}{\rho_j}+A\left(t-1\right)\frac{1-\rho_j}{\rho_j}P_{c,j}+\left\{1-\left[1-\frac{\rho_j}{A\left(1-\rho_j\right)}\right]^{\frac{1}{\tau_o}}\right\}^{-1} P_{c,j}\right]\end{aligned} \tag{C.11}$$

where $$\rho_j = \rho\left(r_{o,j}\right) = 0.5\left[\sqrt{u_j^2 + 4u_j} - u_j\right]$$

and $$u_j = \frac{AP_{c,j} \cdot \tau_o \cdot r_{o,j}}{K_j\left[L + \left(1 - P_{c,j}\right)\left(\min\{t, L\} - 1\right)\left(L - \min\{t, L/2\}\right)\right]}.$$

The delay is given by

$$D_j = \frac{K_j \cdot A}{\theta_j\left(K_j, A, t, \tau_o, L\right)} \tag{C.12}$$

where $\left(K_j \cdot A\right)$ is the average offered traffic of class-*j*.

Notice that, in this case the average transmission probability is complex to represent explicitly. However, having optimized K_j, satisfying (C.11), (C.10) is equivalent to

$$\theta_j = \overbrace{K_j}^{r_{o,j}(K_j)} \times \underbrace{\left(a\ certain\ factor\right) \times \frac{L}{L + \left(1 - P_{c,j}\right)\left(\min\{t, L\} - 1\right)\left(L - \min\{t, L/2\}\right)} P_{c,j}}_{P_{tr}} \tag{C.13}$$

Bibliography

[1] K. Fouli and M. Maier, "OCDMA and Optical Coding: Principles, Applications and Challenges," *IEEE Communication Magazine*, pp. 27 – 34, August 2007.

[2] A. Stok and E. H. Sargent, "The Role of Optical CDMA in Access Networks", *IEEE Comm. Magazine*, vol 40, no 9, pp. 83 – 87, September 2002.

[3] A. Stok and E. H. Sargent, "Lighting ther local network: optical code division multiple access and quality of servise provisioning," *IEEE Network*, vol. 14, no. 6, pp. 42 – 46, November/December 2002.

[4] S. Goldberg and P. Prucnal, "On the teletraffic capacity of the optical CDMA," *IEEE Trans. On Communications*, vol. 55, no. 7, pp. 1334 – 1343, July 2007.

[5] J. G. Zhang, "Novel Optical Fiber Code-Division Multiple Access Networks Supporting Real-Time Multichannel Variable-Bit-Rate (VBR) Video Distributions," *IEEE Trans. on Broadcasting*, vol. 43, pp. 339 – 349, September 1997.

[6] J. G. Zhang, "Design of a Special Family of Optical CDMA Address Codes for Fully Asynchronous Data Communications," *IEEE Trans. on Communications*, vol. 47, pp. 967 – 973, July 1999.

[7] E. Inaty, L. A. Rusch, and P. Fortier, "SIR Performance Evaluation of a Multirate OFFH-CDMA System," *IEEE Communication Letters*, vol.5, no.5, pp.254 – 226, Apr 2001.

[8] E. Inaty, H. M. H. Shalaby, and P. Fortier, "On the Cutoff Rate of a Multi-rate, Multi-class Overlapped OFFH-CDMA System," *IEEE Trans. on Communications*, Vol. 53, No 2, pp. 323 – 334, February 2005.

[9] E. Inaty, H. M. H. Shalaby, and P. Fortier, "A New Transmitter-Receiver Architecture for Nonchoherent Multirate OFFH-CDMA System With Fixed Optimal Detection Threshold," *IEEE J. of Lightwave Technology*, vol. 20, pp. 1885 – 1894, November 2002.

[10] F. R. K. Chung, J. A. Salehi, and V. K. Wei, "Optical orthogonal codes: Design, analysis, and applications," IEEE Trans. *Inform. Theory*, vol. 35, pp. 595 – 604, May 1989.

[11] L. D. Wronski, R. Hossain, and A. Albicki, "Extended Hyperbolic Congruencial Frequency Hop Code: Generation and Bounds for Cross- and Auto-Ambiguity Function," *IEEE Trans. on Communications*, vol.44, no.3, pp. 301 – 305, April 1996.

[12] G.-C. Yang and,W. C. Kwong, "Prime codes with applications to CDMA optical and wirless networks" Archatec House Mobile communication series,2002.

[13] H. Fathallah, L. A. Rusch and S. LaRochelle, "Passive optical fast frequency-hop CDMA communications system," *IEEE J Lightwave Technol.*, vol. 17, pp. 397-405, March 1999.

[14] W. C. Kwong, and G.-C. Yang, "Extended carrier-hopping prime codes for wavelength-time optical code-division multiple access," *IEEE Trans. Commun.*, vol. 52, pp. 1084 – 1091, July 2004.

[15] J. A. Salehi, C. A. Brackett, "Code division multiple-user techniques in optical fiber networks - Part I," *IEEE Trans. on Communications*, vol. 37, no. 8, pp. 824 – 833, August 1989.

[16] H. Ben Jaafar, S. LaRochelle, P. -Y. Cortes, and H. Fathallah, "1.25 Gbit/s transmission of optical FFH-OCDMA signals over 80 km with 16 users," *OFC*, vol. 2, pp TuV3.1 – TuV3.3, 2001.

[17] H. M. H. Shalaby, "Complexities, error probabilities, and capacities of optical OOK-CDMA communication systems," *IEEE Trans. on Communications*, vol. 50, No. 12, pp. 2009 – 2017, December 2002.

[18] A. Stok and E. H. Sargent, "Comparison of diverse optical CDMA codes using a normalized throughput metric," *IEEE Comm. Letters*, vol. 7, pp. 242 – 244, May 2003.

[19] A. Stok and E. H. Sargent, "System performance comparison of optical CDMA and WDMA in a broadcast local area network," *IEEE Comm. Letters*, vol. 6, pp. 409-411, September 2002.

[20] G. N. M. Sudhakar, N. D. Georganas, and M. Kavehrad, "Slotted Aloha and Reservation Aloha Protocols for Very High-Speed Optical Fiber Local Area Networks Using Passive Star Topology," *IEEE/OSA J. Lightwave Technology*, vol. LT-9, pp. 1411 – 1422, October 1991.

[21] H. M. H. Shalaby, "Optical CDMA Random Access Protocols With and Without Pretransmission Coordination," *IEEE/OSA J. Lightwave Technology*, vol.21, pp.2455 – 2462, November 2003.

[22] S. Zahedi, and J. A. Salehi, "Analytical comparison of various fiber-optic CDMA receiver structures," *IEEE J. Lightwave Technol.*, vol. 18, pp. 1718 – 1727, December 2000.

[23] F. Xue, Zhi Ding, and S. J. Ben Yoo, "Performance Analysis for Optical CDMA Networks with Random Access Schemes," *IEEE Globecom 2004*, pp.1883 – 1887, November 2004.

[24] F. Xue, S. J. Ben Yoo, and Zhi Ding, "Design and analysis of coordinated access schemes for code-limited optical-CDMA networks," *IEEE Globecom 2005 proc.*, pp.1930 – 1935, 2005.

[25] H. M. H. Shalaby, "Performance analysis of an optical CDMA random access protocol," *IEEE J Lightwave Technol.*, vol. 22, pp. 1233 – 1241, May 2004.

[26] C.-S. Hsu and V. O. K. Li, "Performance analysis of slotted fiber-optic code-division multiple-access (CDMA) packet networks," *IEEE Trans. Commun.*, vol. 45, pp. 819 – 828, July 1997.

[27] R. Murali, and B. L. Hughes, "Random access with large propagation delay," *IEEE/ACM Trans. On Communications*, vol. 5, no. 6, pp. 924-935, December 1997.

[28] P. Kamath, J. D. Touch and A. J. Bannister, "The need for media access control in optical CDMA networks," *IEEE INFOCOM*, vol. 4, pp 2208 – 2219, March 2004.

[29] D. Bertsekas and R. Gallager, "Data networks," *Printice Hall*, second edition, pp. 17 – 32, 1992.

[30] L. Litwin, "The Medium Access Control," *IEEE Potential*, vol. 20, no. 4, pp. 30 – 34, October/November 2001.

[31] N. Abramson, " The Aloha System – Another Alternative for Computer Communications," in *Proc. Fall Joint Comput. Amer. Red Inf. Rocess. Soc. (AFIPS) Conf.*, Montvale, NJ, vol. 44, pp. 281 – 285, 1970.

[32] F. L. Lo, T. Sang Ng, and T. T. Yuk, "Performance Analysis of a Fully-Connected Full-Duplex CDMA ALOHA Network With Channel Sensing and Collision Detection," *IEEE J. Select. Areas Communications*, vol.14, no.9, pp.1708-1716, December 1996.

[33] F. L. Lo, T. Sang Ng, and T. T. Yuk, "Performance Analysis of a CDMA ALOHA Network With Channel Sensing," *IEEE/ISSSTA*, vol.3 , pp.1188-1192, September 1996.

[34] S. Tasaka, "Dynamic behavior of a CDMA-CD System with a finiste population of buffered users," *IEEE Tans. on Communications*, vol. Com-34, no. 6, pp. 576 – 586, June 1986.

[35] W. Yue and Y. Matsumoto, "Performance analysis of multi-channel and multi-traffic on wirkless communicatioon networks," Kluwer Acadamic Publisher, 2002.

[36] S. Glisic and J. Vikstedt, "Effect of wireless link charactreistics on packet-level QoS in CDMA/CSMA networks," *IEEE Select. Areas In Communications*, vol. 16, no. 6, pp. 875 – 889, August 1998.

[37] P. Kamath, J. D. Touch and J. A. Bannister, "Algorithms for interference sensing in optical CDMA networks," *IEEE Comm. Society*, pp. 1720 – 1724, 2004.

[38] A. B. Carleial, and M. E. Hellman, "Bistable Behavior of ALOHA-Type Systems," *IEEE Trans. on Communications*, vol. COM-23, no. 4, pp.401-410, April 1975.

[39] L. Kleinrock and S. S. Lam, "Packet Switching in a Multiaccess Broadcast Channel: Performance Evaluation," *IEEE Trans. on Communications*, vol. COM-23, no. 4, pp.410-422, April 1975.

[40] D. Raychaudhuri, "Performance analysis of random access packet-switched code division multiple access systems", *IEEE Trans. on Communications*, vol. 29, no.6, pp. 895-901, June 1981.

[41] A. Polydoros and J. Silvester, "Slotted random access spread-spectrum networks: and analytical framework," *IEEE J. Select. Erea On Communications*, vol. SAC.5, no. 6, pp. 989-998, July 1987.

[42] J. Mayer, and J. Schlee, "Protocol ascpects of evolutionary CDMA schemes," *IEEE ISSSTA* vol. 3, pp.1172 – 1177, September 1996

[43] P. W de Graaf, and J. S. Lehnert, "Performance Comparison of a Slotted ALOHA DS/SSMA Network and a Multichannel Narrow-Band Slotted ALOHA Network," *IEEE Trans. on Communications*, vol. COM-46, no. 4, pp.544-552, April 1998.

[44] O. Sallent and R. Agusti, "A proposal for an adaptive S-ALOHA access system for a mobile CDMA environment," *IEEE Trans. on Vehicular Technol.*, vol. 47, no. 3, pp. 977-986, August 1998.

[45] O. Sallent and R. Agusti, "Adapticve S-ALOHA CDMA as an alternative way of integrating services in mobile CDMA environment," *IEEE Trans. On Vehicular Technol.*, vol. 49, no. 3, pp. 936-947, May 2000.

[46] R. Raad, E. Inaty, P. Fortier, H.M.H. Shalaby, "Optical S-ALOHA/CDMA system for multirate applications: architecture, performance evaluation, and system stability," *IEEE J. Lightwave Technol.*, vol. 24, no. 5, pp. 1968 – 1977, May 2006.

[47] R. Raad, E. Inaty, P. Fortier, H.M.H. Shalaby, "Optical S-ALOHA/CDMA system for multirate applications: system architecture and performance evaluation," *IEEE Globecom 2005*, pp. 1936 – 1941, November/December 2005.

[48] R. Raad, E. Inaty, "A MAC protocol based on an S-ALOHA/overlapped CDMA system supporting multirate applications," *IEEE VETECH*, pp. 2073 – 2076, September 2005.

[49] E. Inaty, R. Raad, P. Fortier, H. M. H. Shalaby, "Performance comparison between S-ALOHA and R3T protocols for multirate OFFH-CDMA systems in optical packet networks," *OSA J. Optical Networks*, vol. 5, pp 927 – 936, November 2006.

[50] R. Raad, E. Inaty, P. Fortier, H. M. H. Shalaby, "Optimal resource allocation scheme in multirate overlapped optical CDMA system," *IEEE J. Lightwave Technol*, vol. 25, no. 8, pp. 2044 – 2053, August 2007.

[51] R. Raad, E. Inaty, P. Fortier, H. M. H. Shalaby, "Hybrid Power/Overlap Allocation Scheme for a Multirate Overlapped Optical CDMA System," *IEEE ICC*, pp. 2115 – 2121, June 2007.

[52] E. Inaty, R. Raad, P. Fortier, H. M. H. Shalaby, "A Fair QoS-Based Resource Allocation Scheme for a Time-Slotted Optical OV-CDMA Network: a Unified Approach," *IEEE J. Lightwave Technol*. Under review.

[53] R. Raad, E. Inaty, P. Fortier, H. M. H. Shalaby, "Time-Slotted Optical OV-CDMA Network Using a Fair QoS-Based Resource Management Algorithm," *IEEE Globecom 2008*, November/December 2008.

[54] S. Maric, O. Moreno, and C. J. Corrada, "Multimedia Transmission in Fiber Optical LAN's Using Optical CDMA," *IEEE/OSA J. on Lightwave Technology*, Vol. 14, pp. 2149-2153, October 1996.

[55] I. M. I. Habbab, M. Kavehrad, and C. W. Sundberg, "Protocols for Very High-Speed Optical Fiber Local Area Network Using a Passive Star Topology," *IEEE/OSA J. Lightwave Technology*, vol. LT-5, pp. 1782—1794, December 1987.

[56] L. Wang, M. Ma and M. Hamdi, "Efficient protocols for multimedia streams on WDMA networks,",*IEEE J. Lightwave Techonl.*, vol. 21, no. 10, pp. 2133 – 2144, October 2003.

[57] W. J. Tomlinson, "Evolution of passive optical component technologies for fiber-optic communication systems," *IEEE J. Lightwave Technol.*, vol. 26, no. 9, pp. 1046 – 1062, May 2008.

[58] E. Inaty, H. M. H. Shalaby, P. Fortier, and L. A. Rusch "Multirate optical fast frequency hopping CDMA system using power control," IEEE J. Lightwave Technol., vol. 20, pp. 166-177, February 2002.

[59] H. Yashima, and T. Kobayashi "Optical CDMA with time hopping and power control for multirate networks," *IEEE J. Lightwave Technol.*, vol. 21, pp. 695-702, March 2003.

[60] T. Miyazawa, and I. Sasase "Multi-rate and multi-quality transmission scheme using adaptive overlapping pulse-position modulator and power controller in optical network," *IEEE ICON*, vol. 1, pp. 127 – 131, November 2004.

[61] N. G. Tarhuni, M. S. Elmusrati, T. O. Korhonen, and E. Mutafungwa "Multi-access-interference mitigation using power control in optical-CDMA star networks," *IEEE ICC*, vol. 3, pp. 1593 – 1597, May 2005.

[62] L. C. Yun and D. G. Messerschmitt, "Variable quality of service in CDMA systems by statistical power control," *IEEE ICC*, Seattle, WA, pp. 713 – 719, 1995.

[63] M. L. Honig and J. B. Kim, "Resource allocation for packet data transmission in DS-CDMA," in proc. of 33rd Allerton Conf. on Communication, Control, and Computing, Urbana, IL, pp. 925 – 934, 1995.

[64] S. Ramakrishna, and J. M. Holtzman, "A scheme for throughput maximization in a dual class CDMA system," *IEEE J. Select. Areas Communications*, vol.16, pp.830-844, Aug. 1998.

[65] E. K. P. Chong and S. H. Zak, "An introduction to optimization," *Wiley Interscience*, 2001.

[66] Leon Cooper. "Applied Nonlinear Programming for Engineers and Scientists," Aloray, Englewood, New Jersey 07631, 1974.

[67] L. G. Kazovsky, W. Shaw, D. Gutierrez, N. Cheng, and S. Wong, "Next-generation Optical access networks," *IEEE J. of Lightwave Technolgy.*, vol. 25, no. 11, pp. 3426 – 3442, Nov. 2007.

[68] C. W. Sung and W. S. Wong, "Power control and rate management for wireless multimedia CDMA systems," *IEEE Transactions on Comm.*, vol. 49, no. 7, pp. 1215-1226, July 2001.

[69] A. Kwasinski and N. Farvardin, "Resource allocation for CDMA networks based on real-time source rate adaptation," *IEEE ICC CNF*, vol. 5, pp. 3307-3311, May 2003.

[70] S. Oh, D. Zhang, and K. M. Wasserman, "Optimal resource allocation in multiservice CDMA networks," *IEEE Transactions on Wireless Comm.*, vol. 2, no. 4, pp. 811-821, July 2003.

[71] D. Zhang, S. Oh, and N. T. Sindhushayana, "Optimal resource allocation for data service in CDMA reversed link," *IEEE Transactions on Wireless Comm.*, vol. 6, no. 10, pp. 3648-3656, October 2007.

[72] T. M. Bazan, D. Harle and I. Andonovic, "Mitigaton of beat noise in time-wavelength opitcal code-division multiple-access systems." *IEEE J. Lightwave Technol.*, Vol. 24, No. 11, pp. 4215 – 4222, November 2006.

[73] M. Yoshino, S. Kaneko, T. Taniguchi, N. Miki, K. Kumozaki, T. Imai, N. Yoshimoto and M. Tsubokawa, "Beat Noise mitigation of spectaral amplitude coding OCDMA using heterodyne detection," *IEEE J. Lightwave Technol.*, vol. 26, no. 8, pp. 962 – 970, April 2008.

[74] M. M. Rad, H. Fathallah, and L. A. Rusch, "Beat noise mitigation via hybrid 1D/2D-OCDM: application to monitoring of high capacity PONs," *OFC/NFOEC*, 2008.

[75] G. Keiser, "Optical fiber communication," McGraw Hill, 3rd ed., 2000.

[76] J. Sherman and W. J. Morrison, "Adjustment of an Inverse Matrix Corresponding to a Change in One Element of a Given Matrix," *Annals of Mathematical Statistics*, vol. 21, no. 1, pp. 124-127, 1950.

[77] V. Srivastava and M. Motani, "Cross-layer design: a survey and the road ahead," *IEEE Comm. Magazin*, vol. 43, no. 12, pp. 112 – 119, December 2005.

[78] Q. Zhang and Y.Q. Zhang, "Cross-layer design for QoS support in multihop wireless networks," *IEEE Proceedings*, vol. 96, no. 1, pp. 64 – 76, January 2008.

[79] T. Khattab and H. Alnweiri, "Cross-layer throughput analysis for optical code labelled GMPLS networks," *IEEE ICBN*, vol. 1, pp. 323 – 326, October 2005.

[80] A. Kimas, H. Overby, S. Bjornstad and V. L. Tuft, "A cross layer study of packet loss in all-optical networks," *IEEE AICT/ICIW*, pp. 65 – 65, February 2006.

[81] H. Chen, H. C. B. Chan and V. C. M. Leung, "Two cross-layer optimization methods for transporting multimedea traffic over multicode CDMA networks," *IEEE WCNC*, pp. 288 – 293, March 2007.

[82] G. N. M. Sudhakar, N. D. Georganas and M. Kavehrad, "Slotted ALOHA and reservation ALOHA protocols for very high-speed optical fiber local area networks using passive star Topology," IEEE J. Lightwave Technol., vol. 9, no. 10, pp 1411 – 1422, October 1991.